Medizinische Fakultät der Martin-Luther-Universität Halle-Wittenberg

The GID-complex is a Novel Ubiquitin Ligase involved in the Regulation of Adenosine monophosphate-activated protein kinase (AMPK) and the Function of the Primary Cilium

Dissertation
Zur Erlangung des akademischen Grades
Doktor rerum medicarum (Dr. rer. medic.)
für das Fachgebiet Molekulare Medizin

vorgelegt
der Medizinischen Fakultät
der Martin Luther Universität Halle-Wittenberg

von Huaize Liu

geboren am Feb. 26 1990 in HEILONGJIANG CHINA

Betreuer: PD. Dr. rer. nat. Pfirrmann

Gutachterin/Gutachter: Prof. Dr. Regine Heller

Prof. Dr. rer. nat. Rüdiger Horstkorte

03.12.2019

03.09.2020

Summary

The AMP-activated protein kinase (AMPK) regulates cellular energy homeostasis by sensing the metabolic status of the cell. AMPK is regulated by phosphorylation and dephosphorylation as a result of changing ADP/ATP and AMP/ATP levels and by removal of inhibitory ubiquitin residues by USP10. In this context, we identified the GID-complex, an evolutionarily conserved ubiquitin-ligase-complex (E3), as a negative regulator of AMPK activity. Our data show that the GID-complex targets AMPK for ubiquitination thereby altering its activity. Cells depleted of GID-subunits mimic a state of starvation as shown by increased AMPK activity and the downstream autophagic flux. Consistently, *gid*-genes knockdown in *C. elegans* results in increased organismal lifespan. This study may contribute to understand metabolic disorders like type 2 diabetes mellitus and morbid obesity and implements alternative therapeutic approaches to alter AMPK activity. In addition, we found that the GID-complex partially localizes at the basal body of primary cilia. Loss-of-function of the GID-complex attenuates the response of Sonic Hedgehog signaling pathway, giving us a novel idea about the potential mechanism of SHH signal related ciliopathies.

Zusammenfassung

Die AMP-aktivierte Proteinkinase (AMPK) reguliert die zelluläre Energiehomöostase, indem der metabolische Status der Zelle erfasst wird. AMPK wird durch Phosphorylierung und Dephosphorylierung als Ergebnis der Änderung der ADP/ATP- und AMP/ATP-Spiegel und durch Entfernung von inhibierenden Ubiquitinresten durch USP10 reguliert. In diesem Zusammenhang haben wir den GID-Komplex, einen evolutionär konservierten Ubiquitin-Ligase-Komplex (E3), als negativen Regulator der AMPK-Aktivität identifiziert. Unsere Daten zeigen, dass der GID-Komplex die AMPK ubiquitiniert und dadurch ihre Aktivität verändert. Zellen, die in GID-Untereinheiten depletiert sind, ahmen einen Zustand des Hungerns nach, was durch erhöhte AMPK-Aktivität und autophagischen Fluss sowie eine verringerte mTOR-Aktivierung gezeigt wird. In *C. elegans* führt der Knockdown von *gid*-Genen zu einer erhöhten Lebensdauer von Organismen. Diese Studie kann zum Verständnis von Stoffwechselstörungen wie Diabetes mellitus Typ 2 und krankhafter Fettleibigkeit beitragen und trägt alternative therapeutische Ansätze zur Änderung der AMPK-Aktivität bei. Zusätzlich fanden wir, dass sich der GID-Komplex teilweise am Basalkörper des primären Ziliums befindet. Funktionsverlust des GID-Komplex schwächt die Reaktion des Sonic Hedgehog Signalwegs ab und gibt uns eine neue Vorstellung über einen möglichen Mechanismus der SHH-Signal-Ziliopathien.

1. Contents

List of Figures and Tables

2. Preface

This cumulative thesis, containing two publications, represents my doctoral work from 2016 to 2019. The first publication is a review, which comprehensively summarizes the past and present of the GID-complex, including its research background, related genes, structures, the vast majority of discovered functions (all we knew) and the functional outlooks. It allows the reader to fully grasp the basic knowledge of this area. The second publication is a novel discovery of the function of the mammalian GID-complex. It is an important breakthrough, linking the GID-complex with autophagy and aging. This knowledge helps to understand the physiological significance of this evolutionary conserved ubiquitin ligase complex. In addition, this thesis contains a brief introduction and discussion to get the reader started and to make the underlying hypothesis more understandable.

A few words to the gene and protein nomenclature: due to the research background, historic custom and different emphasis, one gene often has many names which is often confusing. Aliases make academic exchanges very difficult. Even using the same name, there is also an issue with the upper- or lower- case in writing. In order to solve this problem, we followed the recommendations of the HUGO gene nomenclature committee (HGNC), and use the standard writing format. For example (please focus on the format of "gid4", gene in front, protein in the back), yeast *GID4* and Gid4, worm *gid4* and gid4, mouse *Gid4* and GID4, human *GID4* and GID4.

3. Abbreviations

ACTB actin, beta

AMP adenosine monophosphate

AMPK AMP-activated protein kinase

CAMKK2 calcium/calmodulin dependent protein kinase kinase 2

E1 ubiquitin-activating enzyme

E2 ubiquitin-conjugating enzyme

E3 ubiquitin ligase

FBP1 fructose-bisphosphatase 1

GID glucose induced degradation deficient

LC3 microtubule-associated protein 1 light chain 3

LCA5 Leber congenital amaurosis 5

mRNA messenger RNA

MTOR mechanistic target of rapamycin

qPCR quantitative polymerase chain reaction

RING really interesting new gene

RMND5A required for meiotic nuclear division5 homolog A

RPS6 ribosomal protein S6

RPTOR regulatory associated protein of MTOR

SQSTM1 sequestosome 1

Thr threonine

Ub ubiquitin

UPS ubiquitin proteasome system

4. Introduction

4.1. Ubiquitination

Ubiquitin is a small protein of only 76 amino acids and is a very well described post-translational modifier. Protein modification with ubiquitin requires the help of a ubiquitin-activating enzyme (E1), a ubiquitin-conjugating enzyme (E2), and a ubiquitin ligase (E3). In the canonical pathway, the C-terminus of ubiquitin forms an isopeptide bond with the amino group of an internal lysine residue of the substrate or it concomitantly forms an isopeptide bond with one of 7 lysine residues within ubiquitin giving rise to various substrate ubiquitination patterns like mono-, multi-mono-, poly-, multi-poly- ubiquitination (Swatek and Komander 2016) (**Figure 1**). These different topologies of ubiquitination have a wide range of physiological functions including the rapid and selective degradation of K48 polyubiquitinated proteins by the 26S proteasome (Oh, Akopian et al. 2018). In addition, ubiquitination can also regulate lysosome-dependent degradation, cell signaling and protein cellular distribution (Akutsu, Dikic et al. 2016). Substrate specificity of the ubiquitination machinery is mostly dependent on the ubiquitin ligase involved in the processes, hence ubiquitin ligases form the largest group of E3s with more than 600 in humans (Zheng and Shabek 2017). To form the so-called ternary complex consisting of the E2 that covalently binds ubiquitin via a high energy thioester bond, the substrate and the ubiquitin ligase, special domains within the E3 are required. One of these typical functional structures, is the RING (really interesting new gene) finger domain. These domains consist of a stretch of conserved cysteine and histidine residues which are essential for the binding of two zinc ions (Zheng and Shabek 2017). This process is essential for structural integrity of the RING domain and thus mutations in the zinc complexing cysteine/histidine residues often result in loss-of-function of the corresponding E3 (Zheng and Shabek 2017).
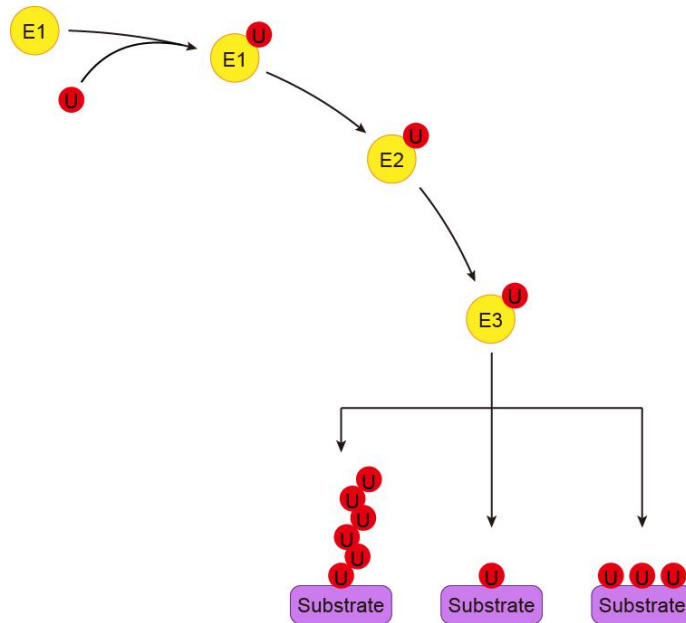
Figure 1: Ubiquitination. Abbreviations: U, ubiquitin; E1, ubiquitin-activating enzyme; E2, ubiquitin-conjugating enzyme; E3, ubiquitin ligase.

4.2. The GID-complex

Glucose is an essential energy source and is important to provide building blocks for anabolic pathways, such as glycerol for lipid synthesis. When glucose is deprived, cells synthesize glucose from precursor molecules *e.g.* glycerol, lactate or alanine *de novo* in a process called gluconeogenesis. In principle, this pathway can be considered as the antagonistic pathway of glycolysis and most chemical reactions in glycolysis and gluconeogenesis share the same set of enzymes. However, some thermodynamically irreversible reactions require specific enzymes that are specific for gluconeogenesis, *e.g.* fructose-1,6-bisphosphatase (Fbp1) catalyzes the dephosphorylation of fructose-1,6-bisphosphate. Gluconeogenesis in higher vertebrates is mostly restricted to the liver and the kidney and the process is highly regulated dependent on the energy status of the organism. Similarly, the single cell eukaryotic organism *S. cerevisiae* can precisely regulate the activity of key gluconeogenic enzymes to regulate gluconeogenesis. As a prominent example, Fbp1 is rapidly degraded by the ubiquitin-proteasome-system when

yeast cells starved for glucose are replenished with glucose. The degradation of key gluconeogenic enzymes results in an irreversible shut-off gluconeogenesis and was named catabolite degradation (Chiang and Schekman 1991). In a yeast genetic screen designed to find genes important for this process nine *GID* (glucose induced degradation deficient) genes were identified. Seven of these proteins are part of the GID-complex, which functions as an ubiquitin ligase that binds Fbp1 for subsequent polyubiquitination and proteasomal degradation (Menssen, Schweiggert et al. 2012). It is worth to note that both Gid2 and Gid9 subunits contain a RING domain, suggesting that they are required for the ubiquitin ligase function of the whole complex (Santt, Pfirrmann et al. 2008, Braun, Pfirrmann et al. 2011). All *S. cerevisiae GID* genes are evolutionary highly conserved and even in *homo sapiens* the orthologous proteins constitute a protein-complex called the GID/CTLH-complex. A set of protein domains that are conserved in different species, the yeast gene IDs and names as well as the corresponding human orthologs are shown in **Table 1**. Due to the fact that almost all GID-proteins contain the conserved C-terminal to LisH (CTLH) domain, the complex is now also called CTLH-complex. Recently published data and our own results suggest, that similar to the yeast GID-complex also the GID-complex of higher vertebrates is involved in the regulation of metabolism (Liu and Pfirrmann 2019). There is also evidence that the process of catabolite degradation is not evolutionary conserved and *e.g.* FBP1 and phosphoenolpyruvate carboxykinase (PCK1) are not directly degraded by the GID-complex in a nutrient dependent manner (Lampert and Stafa 2018). Our own data however suggests that the metabolic switch to different nutritional stimuli is still regulated by the GID-complex, however, via regulation of AMPK and not by direct degradation of key enzymes. The function of the mammalian GID-complex will be discussed in the following publications.

Table 1: Proteins of the GID-complex with accession numbers and protein domains.

S. cerevisiae	*H. sapiens*	Domains	Accession Nr.	*C. elegans*
Gid1	RANBP9 RANBP10	SPRY, LisH, CTLH, CRA	NM_005493	y54e5a.7
Gid2/Rmd5	RMND5A RMND5B	LisH, CTLH, RING	NM_022780	t07d1.2
Gid4	GID4	-	NM_024052	-
Gid5	ARMC8	ARM	NM_213654	-
Gid7	MKLN1	LisH, CTLH, WD40 or Kelch	NM_013225	y39h10a.6 (y39h10a_224b)
Gid8	GID8	LisH, CTLH, CRA	NM_017896	f53e2.1
Gid9	MAEA	LisH, CTLH	BC001225	-

4.3. Autophagy

Autophagy, as the name suggests, means "eating itself". Autophagy and lysosomes together constitute another cellular degradation system, the autophagy-lysosome-system (ALS). As another UPS independent intracellular protein degradation system, ALS recently gained a lot of attention in the scientific community partly because of the recently awarded Nobel Prize (Tooze and Dikic 2016). A basal level of autophagy degrades macromolecules, organelles, membrane structures and endocytic components to get rid of proteinogenic intracellular waste. On the other hand, autophagy induced by starvation or some other signaling pathways can selectively or unselectively degrade cellular components to provide the starving cell with energy and

4

emergency materials for material synthesis by providing *e.g.* free amino acids, lipids, sugars and nucleotides. This function is usually used to help cells to survive under hard nutritional conditions (Morishita and Mizushima 2019).

In the autophagy process, as a first step of cargo engulfment, a bilayer membrane has to enclose the cargoes that later forms a vesicle called the autophagosome. There are many coating proteins on the inner and outer membranes of autophagosomes that are required for transporting and factor recruiting (Tanida, Ueno et al. 2004). Among them microtubule associated protein 1 light chain 3 (MAP1LC3, hereinafter referred to as LC3) is phosphatidylethanolamine modified (LC3-II) before it localizes to the inner and outer membranes of autophagosomes. LC3-II correlates with the number of autophagosomes and is therefore a common marker protein to assess autophagic flux measured by Western blot quantification or by immunochemistry and subsequent quantification of autophagosomes. The autophagosome that contains the cargo can later fuse with the lysosome and utilize its multiple hydrolases to digest the cargoes. In this process, a cargo-carrying protein Sequestosome 1 (SQSTM1) binds to the inner-membrane located LC3-II and is degraded together with the cargoes. SQSTM1 is always continuously degraded during autophagy, and conversely accumulates when autophagy is blocked (Figure 2, yellow area).

4.4. AMPK

Adenosine monophosphate-activated protein kinase (AMPK), is a heterologous trimeric kinase, composed of a catalytic α-subunit (α1 or α2), a regulatory β-subunit (β1 or β2), and an adenosyl nucleotide-binding γ-subunit (γ1, γ2 or γ3). AMPK activity is directly regulated by the intracellular AMP/ATP ratio. The binding of AMP exposes the Thr172 site of AMPK α-subunit (nomenclature: PRKAA), where AMPK can be phosphorylated by the upstream serine/threonine kinase 11 (STK11, also known as liver kinase B1, LKB1). This

phosphorylation directly regulates the kinase activity of AMPK. In addition, other post-translational modifications may also indirectly regulate its kinase activity. For instance, ubiquitination of AMPK inhibits its activity by blocking its interaction with LKB1, and conversely deubiquitination mediated by ubiquitin specific peptidase 10 (USP10) is described to remove this AMPK inhibitory modification. On the other hand, several AMP-independent AMPK regulatory mechanisms are described in the literature. Firstly, another upstream kinase of AMPK, calcium/calmodulin-dependent kinase kinase 2 (CAMKK2) phosphorylates Thr172 site of AMPK upon increasing intracellular Ca^{2+} concentrations. Indeed, this Ca^{2+}-mediated regulation is a frequent mechanism by which metabolically relevant hormones induce transient activation of AMPK (Garcia and Shaw 2017). Secondly, the concentration of fructose-1,6-bisphosphate is described to be an allosteric regulator of AMPK activity (Zhang, Hawley et al. 2017).

As a kinase, AMPK has a broad protein interaction network and a large number of substrates. In general, activated AMPK promotes cellular catabolic processes (*e.g.* fatty acid oxidation, glucose uptake, glycolysis, autophagy) and simultaneously inhibits cellular anabolic processes (*e.g.* protein synthesis, fatty acid synthesis, glycogen synthesis and gluconeogenesis). Focusing on the substrates related to autophagy, AMPK can directly regulate autophagy via phosphorylating some autophagy initiation factors for example Unc-51 like autophagy activating kinase 1 (ULK1), Beclin1 (BECN1) and autophagy-related protein 9 (ATG9) (Garcia and Shaw 2017). In addition, AMPK also indirectly influences autophagy by regulating autophagy upstream inhibitors, for example, mechanistic target of rapamycin complex 1 (MTORC1) (**Figure 2**).
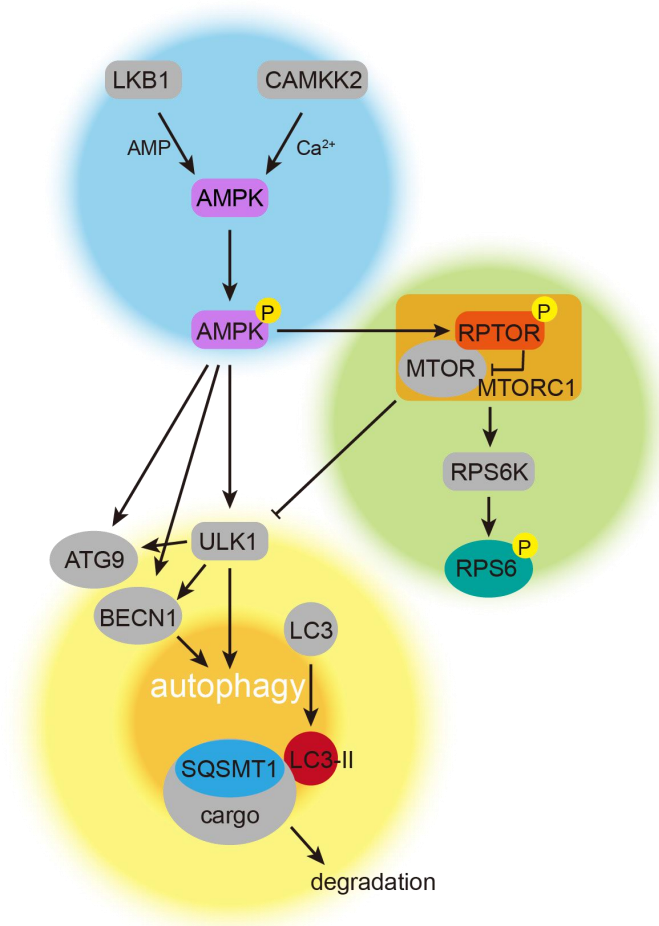
Figure 2: Network of the AMPK-MTORC1-autophagy pathway. Induction of AMPK activity results in an increased protein level of p-AMPK (blue area). Activated AMPK directly activates autophagy by phosphorylating ULK1, ATG9, BECN1 (yellow area) and indirectly via MTORC1 (green area). In the process of autophagy, inner-membrane-located LC3-II recruits the cargo-carrying protein SQSMT1 and bound cargoes that results in the degradation of all of them via lysosome-dependent degradation.

5. Aims of the thesis

The GID-complex is an evolutionary conserved ubiquitin-ligase complex. Our lab focused on this complex for a long time and revealed a few functions of it in yeast and *Xenopus Laevis*. In this work, we want to investigate the function of the GID-complex in mammalian cells, and the mechanism behind its function.

6. Discussion

GID genes were discovered and named for the first time in a yeast screen designed to discover proteins involved in the regulation of the metabolic switch from gluconeogenesis to glycolysis (Regelmann, Schule et al. 2003). In ongoing studies, several additional yeast *GID* genes were described. Work from the same group and others discovered that seven Gid proteins are part of a protein complex that was named the yeast GID-complex. At the same time the CTLH protein complex was discovered in higher vertebrates (Kobayashi, Yang et al. 2007). Interestingly, later studies confirmed that the CTLH/GID-complex is composed of proteins encoded by the evolutionary conserved mammalian homologous *GID* genes. This suggested that the function of the GID-complex as an ubiquitin ligase is also evolutionary conserved. Indeed, several studies have shown, that the CTLH/GID-complex also functions as an ubiquitin ligase (Pfirrmann, Villavicencio-Lorini et al. 2015, Lampert and Stafa 2018, Maitland, Onea et al. 2019). Therefore, it is an intriguing hypothesis that the mammalian GID-complex also regulates the key enzymes in the process of gluconeogenesis by polyubiquitination and degradation. The yeast substrates Fbp1 and Pck1 are also evolutionary conserved and have their homologous enzymes in mammalian cells. At the moment, the existing data indicates that the process of catabolite degradation is not conserved and both enzymes are not targeted for proteasomal degradation directly (Lampert and Stafa 2018). However, other recent data suggests, that the GID/CTLH complex is involved in the regulation of renal gluconeogenesis via the protein BICC1 (Leal-Esteban and Rothe 2018). In mammals the process of gluconeogenesis is restricted to the liver and the kidney (Weber, Lea et al. 1967). To get further insights in the place of action of the human GID-complex, we decided to measure mRNA levels of the GID2/RMND5A subunit by qPCR in different human tissues. Interestingly, the *GID* genes are expressed in most tissues and not only restricted to liver and kidney (**Figure 3**). This suggests a much broader more complex function of the GID-complex in humans.
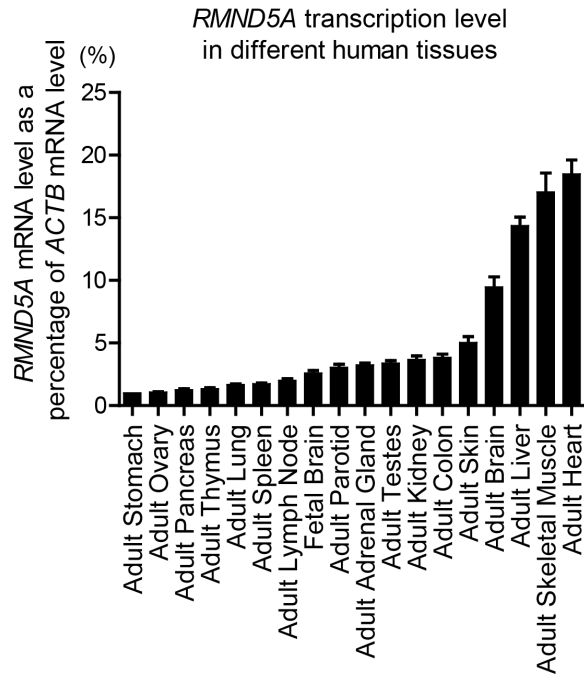
Figure 3. ***RMND5A/GID2* transcription pattern in different human tissues.** cDNAs were reverse transcribed from the RNA samples as labeled. *ACTB* levels were used as the qPCR internal control. *RMND5A* mRNA of different tissues is compared to its own corresponding housekeeping gene (*ACTB*) in percent. In most tissues, *RMND5A* is expressed in an amount equivalent to more than 5% of housekeeping gene.

The highlight of this work is the finding that the mammalian GID-complex is also involved in the regulation of metabolism, particularly in switching metabolic pathways. Interestingly, AMPK is responsible for the metabolic switch from catabolic to anabolic pathways in mammals, including the switch from glycolysis to gluconeogenesis and *vice versa*. We showed that AMPK activity is directly affected by the GID-complex. The most striking differences between AMPK activity were observed when GID-complex deficient cells (KO cells) and wild-type control cells were starved for relatively short periods of time (after 2 hours of starvation) (see **Figure 4A**).

This phenotype turned out to be independent of phosphorylation or dephosphorylation because short-term starvation resulted in rapid and comparable phosphorylation and activation of AMPK in both KO and WT cells. Similarly, refeeding starved cells with glucose led to rapid dephosphorylation of AMPK. This experiment suggests that the GID-complex does not affect the function of AMPK upstream kinases or phosphatases (**Figure 4B**). Under starvation

condition AMPK is activated and further promotes cellular catabolic processes, and simultaneously inhibits cellular anabolic processes (Garcia and Shaw 2017) to provide a constant supply of various small cellular molecular compounds. This metabolic switch helps the cells to overcome hard nutritional times by providing these building blocks. Normally, AMPK activity is reduced upon long-term starvation in WT cells (**Figure 4D**, black curve), however, AMPK activity in GID-complex deficient cells maintained a high level of AMPK activity over a long time (**Figure 4D**, red curve). This abnormal attenuated adaptation of AMPK activity to starvation is specifically dependent on the ubiquitin ligase function of the GID-complex (**Figure 4E**). We thus hypothesize that the mammalian GID-complex negatively regulates AMPK activity especially at long-time starvation conditions, probably as a result of adaptation to strong starvation conditions.
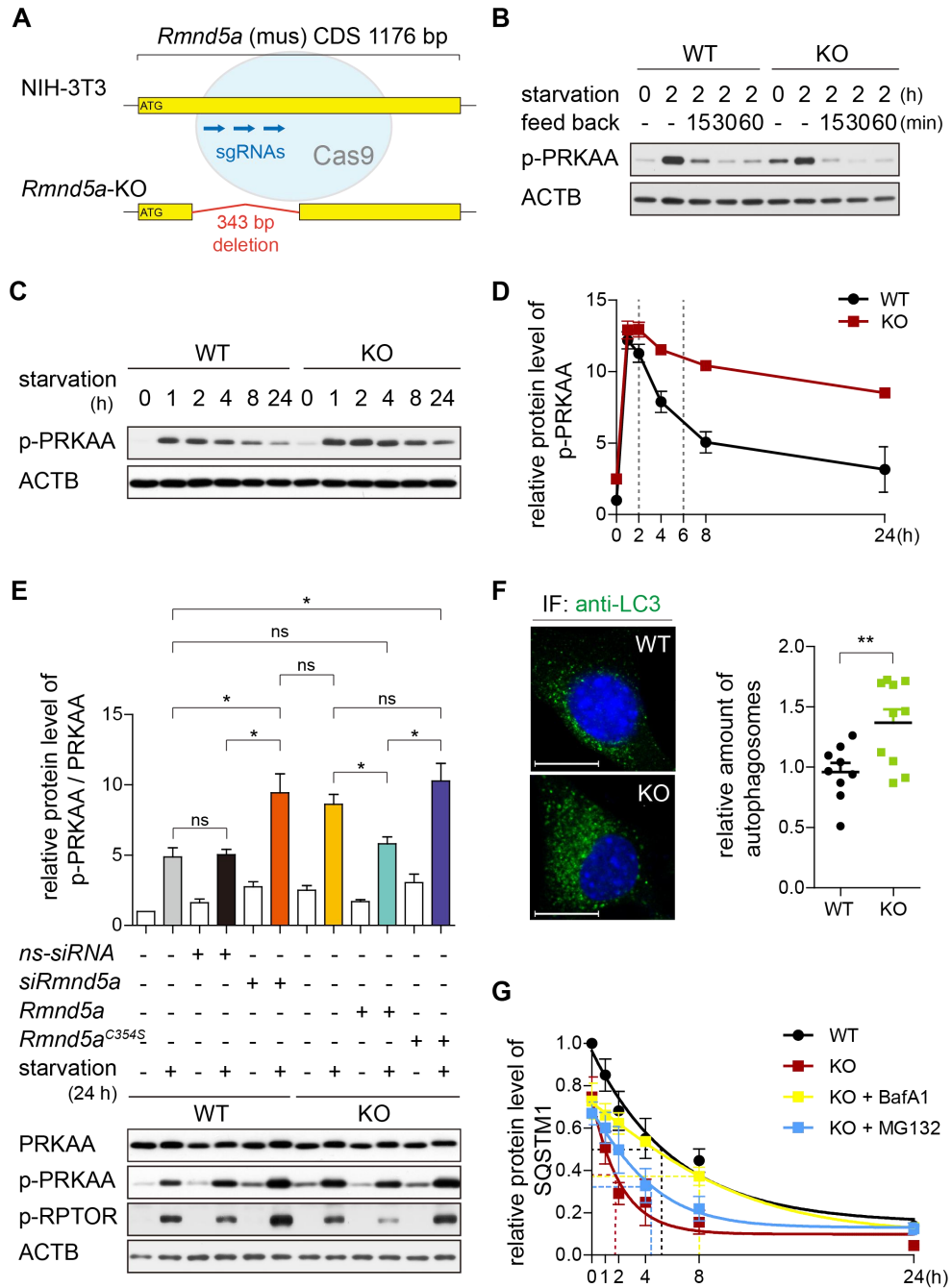
Figure 4: The GID-complex regulates AMPK activity and downstream autophagy. (**A**) Schematic representation of CRISPR-CAS9 generated *Rmnd5a* (NCBI Reference Sequence: NM_024288.2) knockout mutant (*Rmnd5a*-KO, hereinafter referred to as KO) in NIH-3T3 cells (hereinafter referred to as WT). (**B**) Cells were cultured in nutrient-rich medium (high-glucose DMEM with 10% serum) and shifted into starvation medium (DMEM without glucose and serum) for 2 h. After 2 hours' starvation cells were fed back with nutrient-rich medium (high-glucose DMEM with 10% serum) and samples taken at the indicated time points (15 min, 30 min, or 60 min). ACTB/β-actin as loading control. The results show that, p-PRKAA/p-AMPKα is rapidly phosphorylated after starvation, and also rapidly dephosphorylated after supplementation with nutrient-rich medium cells in WT and KO. (**C** and **D**) Western blot and quantifications of p-PRKAA. Cells were starved (DMEM without glucose and serum)

12

for 24 h and samples were taken at indicated time points. ACTB as loading control. WT cells at 0 h are set to 1. (**E**) Western blot of AMPK activity markers. WT cells were transfected with siRNA against *Rmnd5a*. KO cells were transfected with plasmid encoding mouse *Rmnd5a* or *Rmnd5a* RING domain C354S mutant (*Rmnd5a^{C354S}*, which has no ubiquitin ligase function). After 24 h (for plasmid) or 48 h (for siRNA) of transfection, cells were subsequently starved (DMEM without glucose and serum) for additional 24 h. ACTB as loading control. Quantification showing relative protein level of p-PRKAA compared with PRKAA. Both two AMPK activity markers (p-PRKAA and p-PRTOR) show that the unusually elevated AMPK activity in KO cells can be rescued by overexpression with *Rmnd5a*, but not with *Rmnd5a^{C354S}*. It suggests that, the ubiquitin ligase function of the GID-complex is required for the regulation of AMPK activity. Unpaired t-test n = 3. *, P < 0.05. (**F**) Representative confocal microscope images and quantifications of autophagosomes (green). Cells were treated with Bafilomycin A1 (BafA1, 100 nM) for 4 h to block autophagosomes fusion with lysosomes. Autophagosomes were stained with anti-LC3 antibody. Scale bars, 10 μm. Quantification showing relative amount of autophagosomes (relative fluorescence area, left). Average values of WT are set to 1. Unpaired t-test n = 15. **, P < 0.01. (**G**) Quantification showing relative protein level of SQSTM1 (compared with loading control) during its turnover. Cells were treated with cycloheximide (CHX, 100 μg/ml, protein synthesis inhibitor) for 24 h. The half-life of SQSTM1 in WT cells (black), KO cells (red), KO cells treated with BafA1 (yellow) and KO cells treated with MG132 (blue) shown by dotted line. WT cells at 0 h are set to 1. From the curves we can see that, the half-life of SQSTM1 in KO cells (red, about 1.8 h) is quite shorter than the WT (black, about 5.5 h). It suggests that KO cells have an obvious increased autophagic flux. In addition, this accelerated turnover of SQSTM1 in KO cells can be slowed by BafA1 (yellow), but not by proteosome inhibitor MG132 (blue).

All our experiments support a hypothesis that GID-complex dependent regulation of AMPK further affects downstream autophagy, because increases in AMPK activity correlated with an enhanced level of autophagic flux (**Figure 4F** and **4G**). This gives rise to an interesting thought about the real function and physiological significance of the GID-complex in vertebrates. The function of GID proteins may be neither limited to regulating the ubiquitination-dependent degradation nor to regulating some vesicular degradation pathways as in autophagy. Instead it is possible that it functions as a monitor that measures the dynamic balance of either a common intracellular small molecular pool or of some specific molecules. When cells cannot get the necessary compounds from the environment, they will initiate processes to degrade macromolecules or organelles to get access to some crucial chemical compounds (*e.g.* amino acids) necessary for the synthesis of macromolecules (*e.g.* proteins) and thus cell survival. In this way, cells are able to further synthesize macromolecules and energy required for their survival even under hard times of low nutrition. However, in order to avoid unnecessary waste

caused by excessive degradation of macromolecules, a monitor is required to regulate these degradation processes in a negative feedback loop. We speculate, that the GID-complex monitors the level of at least one compound that is released by autophagy degradation processes (**Figure 5**).
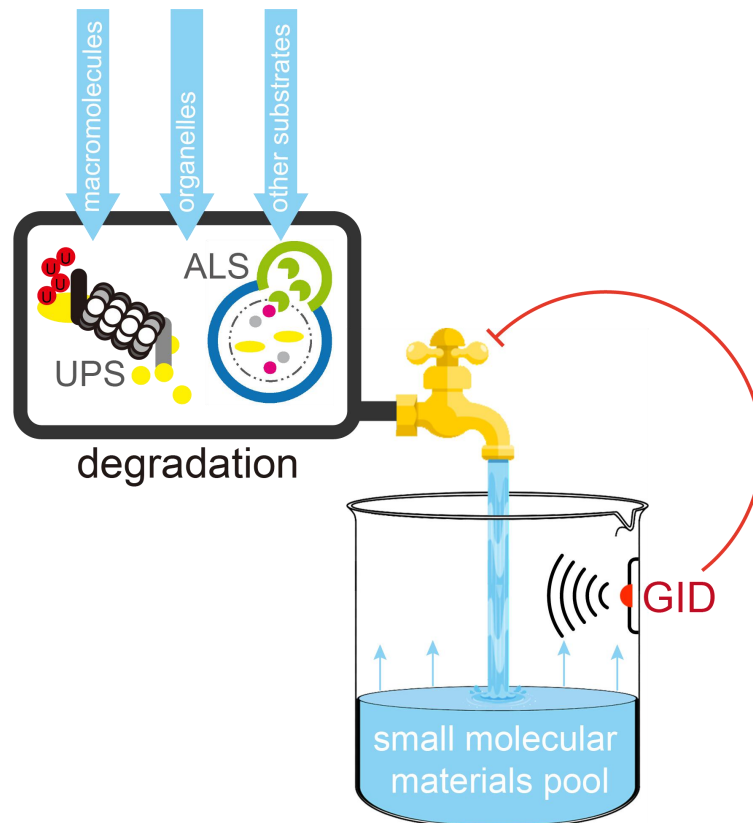

Figure 5: The function and physiological significance of the evolutionary conserved GID-complex. As a sensor, the GID-complex is monitoring the cellular small molecular compound pool. Once these specific compounds reach a proper concentration, it will immediately inhibit the upstream degradation pathways and reduce the degradation capacity in a negative feedback loop.

Stimulated by starvation, AMPK is normally activated by upstream kinases that induce downstream autophagy within one hour (**Figure 4D**, from 0 h to 1 h). During this time enhanced autophagy results in the degradation of macromolecules and the release of small compounds and as a result, cells no longer require high levels of autophagy (in fact, a long time of high-intensity autophagy is harmful to cells). At these time points, the GID-complex can

14

sensitively capture the presence of some small molecules in the cell and inactivate AMPK by ubiquitination and degradation. Therefore, we speculate that especially under long-term starvation conditions, the GID-complex functions as a negative feedback regulator that attenuates autophagic flux and avoids excessive autophagy once the pool of compounds or the pool of a single signaling compound is replenished.

To me, two further questions were of particular interest: is there a specific small molecule that triggers GID-dependent ubiquitination of AMPK and where in the cell does the process of AMPK degradation happen? Some interesting unpublished results will give unexpected answers. To discover putative chemical compounds that can trigger GID-complex activity or AMPK degradation we performed targeted quantitative metabolomics of WT and KO cells together with the company Human Metabolome Technologies Inc. (Tokyo, Japan). The company measured and quantified the cellular concentration of 116 metabolites involved in different pathways like *e.g.* glycolysis, pentose phosphate pathway, tricarboxylic acid (TCA) cycle, urea cycle and amino acid metabolism. Among many compounds that were unchanged in WT and KO cells, acetyl-coenzyme A (acetyl-CoA) was significantly reduced (around 40%) in KO cells (**Figure 6A**). Additionally, our extended analysis showed that all three branched-chain amino acids (leucine, isoleucine, and valine) were significantly reduced in KO cells (**Figure 6B**). It is known that, acetyl-CoA is a major integrator of the nutritional status at the crossroad of fat, sugar, and protein catabolism (Marino, Pietrocola et al. 2014) and thus an interesting allosteric regulator. Acetyl-CoA is continuously consumed by catabolic processes, most of which are induced by activated AMPK. It is reported that, acetyl-CoA can regulate autophagy, for example via acetyltransferase EP300 (Zhao, Xu et al. 2010, Marino, Pietrocola et al. 2014, Pietrocola, Lachkar et al. 2015). And the activity of MTORC1 can also be affected by the branched-chain amino acids (Ijichi, Matsumura et al. 2003, Nie, He et al. 2018). On the other hand, acetyl-CoA also provides the acetyl group for a universal and important post-translational modification, acetylation, that like ubiquitination targets lysine residues (Scott 2012). Interestingly, the level of acetylation is described to correlate with the concentration of acetylated proteins (Drazic, Myklebust et al. 2016). We thus speculate, that acetylation and ubiquitination can compete for the same lysine residues of particular metabolic key enzymes like AMPK and that low

acetyl-CoA levels might induce ubiquitination of sites that are normally blocked by acetylation. This intriguing idea is supported by our finding, that PRKAA is acetylated and ubiquitinated at several sites. Some of these modification sites are even shared by both ubiquitination and acetylation (Wagner, Beli et al. 2011, Sol, Wagner et al. 2012, Weinert, Schölz et al. 2013, Elia, Boardman et al. 2015, Svinkina, Gu et al. 2015) (**Figure 6C**). In such a situation, starvation-activated AMPK induces downstream catabolic processes, simultaneously consuming a huge number of acetyl-CoA; a reduction of acetylated AMPK can subsequently be ubiquitinated by the GID-complex. Ubiquitination and further proteasomal degradation attenuate AMPK activity, giving rise to a perfect negative feedback regulation of AMPK. When this negative feedback is blocked by deficiencies in the GID-complex, activated AMPK cannot be degraded, resulting in a continuously high level of AMPK activity and downstream autophagy in KO cells (**Figure 6D**). This scenario is consistent with our observations and will be further studied in the future.
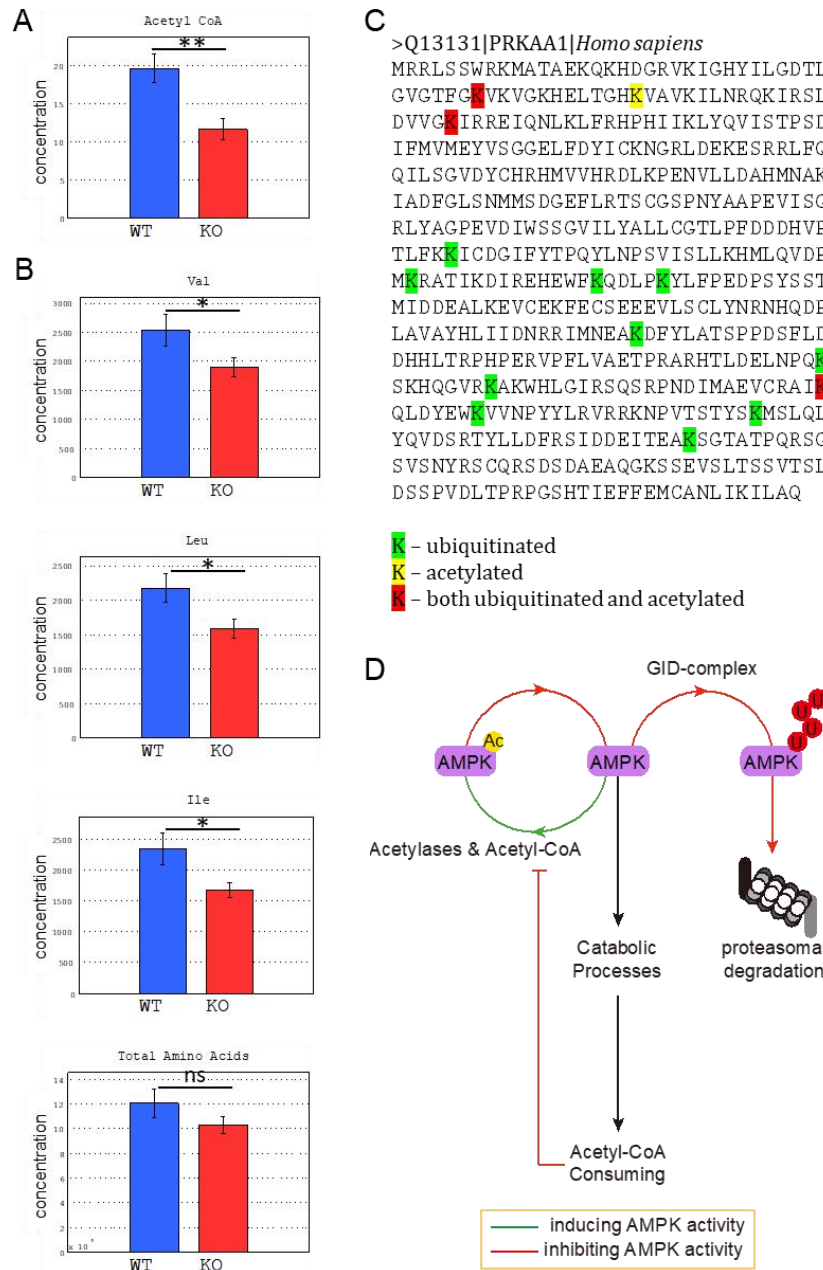
Figure 6: Acetyl-CoA as a potential regulator of GID-complex dependent AMPK activity.
(**A** and **B**) Quantitative metabolomics analysis of WT and KO cells performed by Human Metabolome Technologies Inc. (HMT, Tokyo, Japan) shows that acetyl-CoA is 40% reduced in KO cells. Hierarchical cluster analysis (HCA) and principal component analysis (PCA) were performed by statistical analysis software (developed at HMT). The p-value is computed by Welch's t-test. (*<0.05, **<0.01). Cell number of each sample: 1×10^6. (**C**) Amino acid sequence of PRKAA (*homo sapiens*) shows post-translational modification sites, ubiquitination (green) (Wagner, Beli et al. 2011) and acetylation (yellow) (Sol, Wagner et al. 2012, Weinert, Schölz et al. 2013, Elia, Boardman et al. 2015, Svinkina, Gu et al. 2015). Lysine sites modified by both ubiquitination and acetylation are labeled in red. (**D**) Hypothesis of the regulation of AMPK by the GID-complex and acetyl-CoA.

Concerning the second question, where GID-dependent regulation of AMPK happens our data strongly leads to an amazing organelle, the primary cilium. Cilia are highly evolutionary conserved organelles in the eukaryotic kingdom that can be found on the surface of the majority of cells of many organisms (Praetorius and Spring 2005). Cilia are hair-like structures that are similar to bacterial flagella and can be divided into motile and non-motile cilia. Non-motile cilia, or primary cilia, are sensors of external signals such as odor, tastes and light. In addition, they also respond to fluid flow, Sonic Hedgehog (SHH) signaling, Wnt signaling, growth factors and many more (Singla and Reiter 2006). Primary cilia consist of a nine-duplet microtubular filament ring (called "9 + 0" axoneme) that arises from the basal body, which is derived from the mother centriole, and covered by the ciliary membrane to form the cilium structure (**Figure 7A**). Cilia are involved in diverse cellular functions, such as cell proliferation, differentiation and polarity, and can act as signaling hubs. Therefore, cilia dysfunction always leads to different hereditary organ-specific or syndromic diseases, summarized as ciliopathies. Several recent publications link primary cilium function with cellular and organismal energy homeostasis, *e.g.* to the basal body localized AMPK and other autophagy factors (Aznar and Billaud 2010, Boehlke, Kotsis et al. 2010, Pampliega and Cuervo 2016). Furthermore, some ciliopathies (*e.g.* Bardet-Biedl-syndrome and Almström-syndrome) are accompanied with morbid obesity and type 2 diabetes mellitus, suggesting disorganized energy sensing and signaling (Girard and Petrovsky 2011, Forsythe, Kenny et al. 2018).

Recently, it was reported that some GID-subunits interact with basal body proteins (*e.g.* with LCA5 and RAB8), suggesting a close relationship between the GID-complex and primary cilia (Boldt and van Reeuwijk 2016). To monitor the cellular localization of GID-complex, we expressed a GFP fused human RMND5A/GID2 protein in NIH-3T3 cells. Interestingly, the GFP-RMND5A fusion protein partially accumulated at the basal body of primary cilium, as demonstrated by co-staining and the overlapping signal (**Figure 7B** and **7C**). We thus suspect that the GID-complex plays a role in ciliogenesis or the function of primary cilium. Our data support this idea: Firstly, we showed that, loss of function of GID-complex elongates primary cilium length by enhancing autophagic flux (in the second following publication). Next, we tested the function of primary cilia in GID-complex functional deficient cells by measuring the

SHH signaling pathway, which is known as a primary cilium dependent signaling pathway. SHH signaling can be activated by Smoothed Agonist (SAG), and results in transcriptional up-regulation of downstream genes, such as *Gli1* and *Ptch1* (**Figure 7D**). In contrast to the WT, the SHH signaling response was severely reduced in KO cells (**Figure 7E** and **7F**) and in *Rmnd5a* knockdown cells (**Figure 7G**).
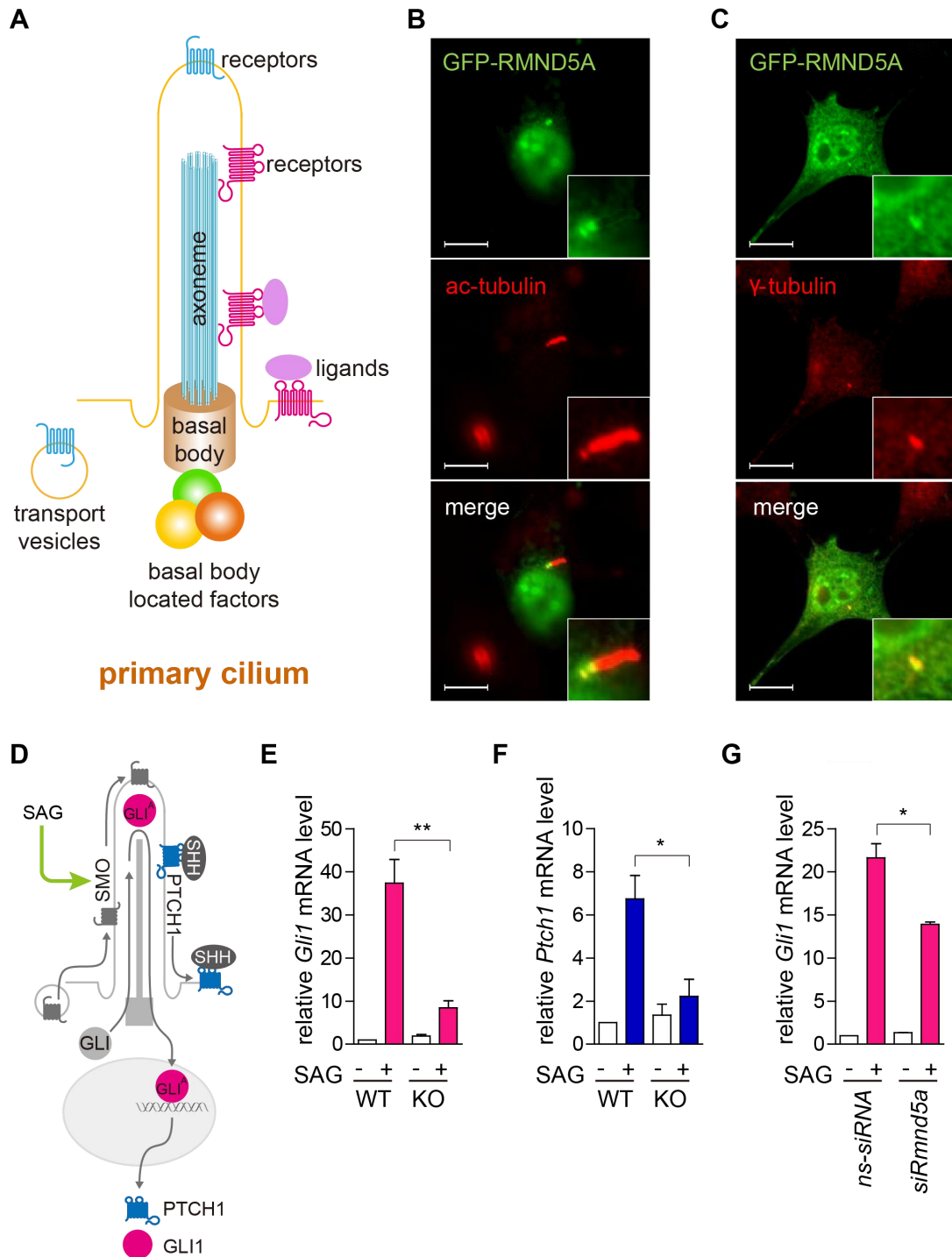
Figure 7: GID-dependent regulation of the primary cilium. (A) Schematic model of the primary cilium, composed of a basal body, axoneme and ciliary membrane. A large number of transporters, structure proteins, membrane receptors and basal body located factors are working in the primary cilium. (B-C) RMND5A localizes to the basal body of the primary cilium in NIH-3T3 cells. Cells were transfected with plasmids encoding GFP-RMND5A (human) for 24 h and further serum starved (high glucose DMEM, 0.5% FCS) for additional 24 h to induce ciliogenesis. After fixation, cells were stained with acetylated tubulin (ac-tubulin) or γ-tubulin antibody to visualize the axoneme or the basal body of the primary cilium respectively. Images were merged to identify overlapping signals

(merge, yellow). Scale bars, 10 μm. (D) Schematic representation of primary cilium dependent Sonic Hedgehog (SHH) signaling in the "on state". After binding with SHH ligand, PTCH1 relieves the inhibition of SMO. Then the transcription factor GLI is activated, turning on downstream gene expression, such as *Gli1* and *Ptch1*. Abbreviations: PTCH1, Patched1; SMO, Smoothened; GLI^A, GLI active form. (E-G) qPCR of two SHH signaling markers (*Gli1* and *Ptch1*) during *Rmnd5a* knockout and knockdown. Cells were cultured under cilia-induced condition (high glucose DMEM, 0.5% FCS) with or without SAG (100 nM) treatment for 24 h and harvested for further analyzing. Unpaired t test n = 3. *, P < 0.05; **, P < 0.01.

Several recent observations link primary cilia function with cellular and organismal energy homeostasis and suggest a function of the primary cilium as a nutrient sensor with the basal body as a control center (Oh, Vasanth et al. 2015). Exemplary, AMPK is directly activated at the basal body of the primary cilium of kidney cells by LKB1-dependent phosphorylation to regulate cell size (Boehlke, Kotsis et al. 2010). Additionally, several proteins involved in autophagy are integral parts of the basal body or the primary cilium integrating energy homeostasis and cilia function (Orhon, Dupont et al. 2015). Together with our published data, we consider that GID-dependent regulation of AMPK might very well be at the basal body of primary cilium. In addition, we show that GID-dependent induction of autophagy can influence primary cilium length. Some aspects that will be considered in the future will be to study whether the attenuation of SHH signaling response is also affected by GID-induced autophagy.

7. References

Akutsu, M., I. Dikic and A. Bremm (2016). "Ubiquitin chain diversity at a glance." Journal of Cell Science **129**(5): 875-880.

Aznar, N. and M. Billaud (2010). "Primary cilia bend LKB1 and mTOR to their will." Dev Cell **19**(6): 792-794.

Boehlke, C., F. Kotsis, V. Patel, S. Braeg, H. Voelker, S. Bredt, T. Beyer, H. Janusch, C. Hamann, M. Godel, K. Muller, M. Herbst, M. Hornung, M. Doerken, M. Kottgen, R. Nitschke, P. Igarashi, G. Walz and E. W. Kuehn (2010). "Primary cilia regulate mTORC1 activity and cell size through Lkb1." Nat Cell Biol **12**(11): 1115-1122.

Boldt, K. and J. van Reeuwijk (2016). "An organelle-specific protein landscape identifies novel diseases and molecular mechanisms." **7**: 11491.

Braun, B., T. Pfirrmann, R. Menssen, K. Hofmann, H. Scheel and D. H. Wolf (2011). "Gid9, a second RING finger protein contributes to the ubiquitin ligase activity of the Gid complex required for catabolite degradation." FEBS Lett **585**(24): 3856-3861.

Chiang, H.-L. and R. Schekman (1991). "Regulated import and degradation of a cytosolic protein in the yeast vacuole." Nature **350**(6316): 313-318.

Drazic, A., L. M. Myklebust, R. Ree and T. Arnesen (2016). "The world of protein acetylation." Biochimica et Biophysica Acta (BBA) - Proteins and Proteomics **1864**(10): 1372-1401.

Elia, Andrew E. H., Alexander P. Boardman, David C. Wang, Edward L. Huttlin, Robert A. Everley, N. Dephoure, C. Zhou, I. Koren, Steven P. Gygi and Stephen J. Elledge (2015). "Quantitative Proteomic Atlas of Ubiquitination and Acetylation in the DNA Damage Response." Molecular Cell **59**(5): 867-881.

Forsythe, E., J. Kenny, C. Bacchelli and P. L. Beales (2018). "Managing Bardet-Biedl Syndrome-Now and in the Future." Front Pediatr **6**: 23.

Garcia, D. and R. J. Shaw (2017). "AMPK: Mechanisms of Cellular Energy Sensing and Restoration of Metabolic Balance." Mol Cell **66**(6): 789-800.

Girard, D. and N. Petrovsky (2011). "Alstrom syndrome: insights into the pathogenesis of metabolic disorders." Nat Rev Endocrinol **7**(2): 77-88.

Ijichi, C., T. Matsumura, T. Tsuji and Y. Eto (2003). "Branched-chain amino acids promote albumin synthesis in rat primary hepatocytes through the mTOR signal transduction system." Biochemical and Biophysical Research Communications **303**(1): 59-64.

Kobayashi, N., J. Yang, A. Ueda, T. Suzuki, K. Tomaru, M. Takeno, K. Okuda and Y. Ishigatsubo (2007). "RanBPM, Muskelin, p48EMLP, p44CTLH, and the armadillo-repeat proteins ARMC8alpha and ARMC8beta are components of the CTLH complex." Gene **396**(2): 236-247.

Lampert, F. and D. Stafa (2018). "The multi-subunit GID/CTLH E3 ubiquitin ligase promotes cell proliferation and targets the transcription factor Hbp1 for degradation."   **7**.

Leal-Esteban, L. C. and B. Rothe (2018). "Role of Bicaudal C1 in renal gluconeogenesis and its novel interaction with the CTLH complex."   **14**(7): e1007487.

Liu, H. and T. Pfirrmann (2019). "The Gid-complex: an emerging player in the ubiquitin ligase league."   **400**(11): 1429-1441.

Maitland, M. E. R., G. Onea, C. A. Chiasson, X. Wang, J. Ma, S. E. Moor, K. R. Barber, G. A. Lajoie and G. S. Shaw (2019). "The mammalian CTLH complex is an E3 ubiquitin ligase that targets its subunit muskelin for degradation."   **9**(1): 9864.

Marino, G., F. Pietrocola, T. Eisenberg, Y. Kong, S. A. Malik, A. Andryushkova, S. Schroeder, T. Pendl, A. Harger, M. Niso-Santano, N. Zamzami, M. Scoazec, S. Durand, D. P. Enot, A. F. Fernandez, I. Martins, O. Kepp, L. Senovilla, C. Bauvy, E. Morselli, E. Vacchelli, M. Bennetzen, C. Magnes, F. Sinner, T. Pieber, C. Lopez-Otin, M. C. Maiuri, P. Codogno, J. S. Andersen, J. A. Hill, F. Madeo and G. Kroemer (2014). "Regulation of autophagy by cytosolic acetyl-coenzyme A." Mol Cell **53**(5): 710-725.

Menssen, R., J. Schweiggert, J. Schreiner, D. Kusevic, J. Reuther, B. Braun and D. H. Wolf (2012). "Exploring the topology of the Gid complex, the E3 ubiquitin ligase involved in catabolite-induced degradation of gluconeogenic enzymes." J Biol Chem **287**(30): 25602-25614.

Morishita, H. and N. Mizushima (2019). "Diverse Cellular Roles of Autophagy." Annu Rev Cell Dev Biol **35**: 453-475.

Nie, C., T. He, W. Zhang, G. Zhang and X. Ma (2018). "Branched Chain Amino Acids: Beyond Nutrition Metabolism." International Journal of Molecular Sciences **19**(4): 954.

Oh, E., D. Akopian and M. Rape (2018). "Principles of Ubiquitin-Dependent Signaling." Annual Review of Cell and Developmental Biology **34**(1): 137-162.

Oh, E. C., S. Vasanth and N. Katsanis (2015). "Metabolic regulation and energy homeostasis through the primary Cilium." Cell Metab **21**(1): 21-31.

Orhon, I., N. Dupont, O. Pampliega, A. M. Cuervo and P. Codogno (2015). "Autophagy and regulation of cilia function and assembly." Cell Death Differ **22**(3): 389-397.

Pampliega, O. and A. M. Cuervo (2016). "Autophagy and primary cilia: dual interplay." Curr Opin Cell Biol **39**: 1-7.

Pfirrmann, T., P. Villavicencio-Lorini, A. K. Subudhi, R. Menssen, D. H. Wolf and T. Hollemann (2015). "RMND5 from Xenopus laevis is an E3 ubiquitin-ligase and functions in early embryonic forebrain development." PLoS One **10**(3): e0120342.

Pietrocola, F., S. Lachkar, D. P. Enot, M. Niso-Santano, J. M. Bravo-San Pedro, V. Sica, V. Izzo, M. C. Maiuri, F. Madeo, G. Marino and G. Kroemer (2015). "Spermidine induces autophagy by inhibiting the acetyltransferase EP300." Cell Death Differ **22**(3): 509-516.

Praetorius, H. A. and K. R. Spring (2005). "A physiological view of the primary cilium." Annu Rev Physiol **67**: 515-529.

Regelmann, J., T. Schule, F. S. Josupeit, J. Horak, M. Rose, K. D. Entian, M. Thumm and D. H. Wolf (2003). "Catabolite degradation of fructose-1,6-bisphosphatase in the yeast Saccharomyces cerevisiae: a genome-wide screen identifies eight novel GID genes and indicates the existence of two degradation pathways." Mol Biol Cell **14**(4): 1652-1663.

Santt, O., T. Pfirrmann, B. Braun, J. Juretschke, P. Kimmig, H. Scheel, K. Hofmann, M. Thumm and D. H. Wolf (2008). "The yeast GID complex, a novel ubiquitin ligase (E3) involved in the regulation of carbohydrate metabolism." Mol Biol Cell **19**(8): 3323-3333.

Scott, I. (2012). "Regulation of cellular homoeostasis by reversible lysine acetylation." Essays Biochem **52**: 13-22.

Singla, V. and J. F. Reiter (2006). "The primary cilium as the cell's antenna: signaling at a sensory organelle." Science **313**(5787): 629-633.

Sol, E. M., S. A. Wagner, B. T. Weinert, A. Kumar, H.-S. Kim, C.-X. Deng and C. Choudhary (2012). "Proteomic Investigations of Lysine Acetylation Identify Diverse Substrates of Mitochondrial Deacetylase Sirt3." PLOS ONE **7**(12): e50545.

Svinkina, T., H. Gu, J. C. Silva, P. Mertins, J. Qiao, S. Fereshetian, J. D. Jaffe, E. Kuhn, N. D. Udeshi and S. A. Carr (2015). "Deep, Quantitative Coverage of the Lysine Acetylome Using Novel Anti-acetyl-lysine Antibodies and an Optimized Proteomic Workflow." Molecular & Cellular Proteomics **14**(9): 2429-2440.

Swatek, K. N. and D. Komander (2016). "Ubiquitin modifications." Cell Research **26**(4): 399-422.

Tanida, I., T. Ueno and E. Kominami (2004). "LC3 conjugation system in mammalian autophagy." Int J Biochem Cell Biol **36**(12): 2503-2518.

Tooze, S. A. and I. Dikic (2016). "Autophagy Captures the Nobel Prize." <u>Cell</u> **167**(6): 1433-1435.

Wagner, S. A., P. Beli, B. T. Weinert, M. L. Nielsen, J. Cox, M. Mann and C. Choudhary (2011). "A Proteome-wide, Quantitative Survey of In Vivo Ubiquitylation Sites Reveals Widespread Regulatory Roles." <u>Molecular & Cellular Proteomics</u> **10**(10): M111.013284.

Weber, G., M. A. Lea, H. J. Convery and N. B. Stamm (1967). "Regulation of gluconeogenesis and glycolysis: studies of mechanisms controlling enzyme activity." <u>Adv Enzyme Regul</u> **5**: 257-300.

Weinert, Brian T., C. Schölz, Sebastian A. Wagner, V. Iesmantavicius, D. Su, Jeremy A. Daniel and C. Choudhary (2013). "Lysine Succinylation Is a Frequently Occurring Modification in Prokaryotes and Eukaryotes and Extensively Overlaps with Acetylation." <u>Cell Reports</u> **4**(4): 842-851.

Zhang, C. S., S. A. Hawley, Y. Zong, M. Li, Z. Wang, A. Gray, T. Ma, J. Cui, J. W. Feng, M. Zhu, Y. Q. Wu, T. Y. Li, Z. Ye, S. Y. Lin, H. Yin, H. L. Piao, D. G. Hardie and S. C. Lin (2017). "Fructose-1,6-bisphosphate and aldolase mediate glucose sensing by AMPK." <u>Nature</u> **548**(7665): 112-116.

Zhao, S., W. Xu, W. Jiang, W. Yu, Y. Lin, T. Zhang, J. Yao, L. Zhou, Y. Zeng, H. Li, Y. Li, J. Shi, W. An, S. M. Hancock, F. He, L. Qin, J. Chin, P. Yang, X. Chen, Q. Lei, Y. Xiong and K.-L. Guan (2010). "Regulation of Cellular Metabolism by Protein Lysine Acetylation." <u>Science</u> **327**(5968): 1000-1004.

Zheng, N. and N. Shabek (2017). "Ubiquitin Ligases: Structure, Function, and Regulation." <u>Annual Review of Biochemistry</u> **86**(1): 129-157.

8. Thesen der Dissertation

Medizinische Fakultät der Martin-Luther-Universität Halle-Wittenberg

1. **The GID-complex is an evolutionary conserved ubiquitin ligase complex.**

2. **The mammalian GID-complex negatively regulates AMPK activity.**

3. **AMPK is polyubiquitinated via K48 by the GID-complex.**

4. **GID-dependent regulation of AMPK mostly happens after a long time of starvation.**

5. **GID-dependent regulation of AMPK further influences downstream autophagy.**

6. **GID-complex functional deficiency increases the basal level of autophagic flux.**

7. **Knockdown of *gid* genes elongates the lifespan of *C. elegans*.**

8. **GID-complex partially localizes at the basal body of primary cilium.**

9. **Loss-of-function of GID-complex attenuates SHH signaling response.**

10. **Acetyl-CoA and branched chain amino acids are significantly reduced in KO cells**

The GID-complex is a Novel Ubiquitin Ligase involved in the Regulation of Adenosine

monophosphate-activated protein kinase (AMPK) and the Function of the Primary Cilium

zur Erlangung des akademischen Grades

Doktor rerum medicarum (Doktor der Medizinischen Wissenschaft)

(Dr. rer. medic.)

für das Fachgebietfür Molekulare Medizin

vorgelegt

der Medizinischen Fakultät

der Martin-Luther-Universität Halle-Wittenberg

von Huaize Liu

geboren am 26.02.1990 in HEILONGJIANG CHINA

9. Published articles relevant for this work

Two first authored publications of Huaize Liu are attached to this thesis:

1. **Huaize Liu** and Thorsten Pfirrmann. The Gid-complex: an emerging player in the ubiquitin ligase league. Biological chemistry. **2019**; 400(11): 1429–1441

2. **Huaize Liu**, Jie Ding, Karl Köhnlein, Nadine Urban, Alessandro Ori, Pablo Villavicencio-Lorini, Peter Walentek, Lars-Oliver Klotz, Thomas Hollemann & Thorsten Pfirrmann. The GID Ubiquitin Ligase Complex is a Regulator of AMPK Activity and Organismal Lifespan. Autophagy. **2019** Dec 3:1-17. doi: 10.1080/15548627.2019.1695399.

10. Eidesstattliche Erklärung

Hiemit versichere ich, dass ich die vorliegende Arbeit „The GID-complex is a Novel Ubiquitin Ligase involved in the Regulation of Adenosine monophosphate-activated protein kinase (AMPK) and the Function of the Primary Cilium" selbstständig und ohne fremde Hilfe angefertigt und keine anderen als die angegebenen Quellen und Hilfsmittel verwendet habe. Die eingereichte schriftliche Fassung der Arbeit entspricht der auf dem elektronischen Speichermedium. Weiterhin versichere ich, dass die vorliegende Arbeit noch nicht als Abschlussarbeit an anderer Stelle eingereicht wurde.
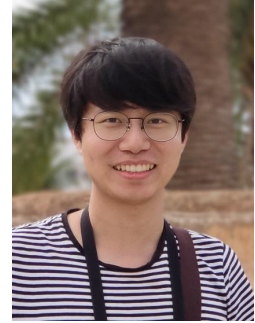
Huaize Liu

Ort   *Halle*

Datum   *30/12/19*

Unterschrift   *Huaize liu*

11. Curriculum Vitae

LIU Huaize 刘怀泽

Date of birth:	Feb. 26th 1990
Place of birth:	HEILONGJIANG CHINA
Nationality:	Chinese
Institutional address:	Institute of Physiological Chemistry
	Hollystr. 1, Halle (Salle) 06114, Germany
E-mail:	liuhuaize@hotmail.com

EDUCATION

2009-2013 Shanghai Ocean University BSc. of Biological Science
2013-2016 Nanjing Medical University MSc. of Developmental Genetics
Supervisor: Prof. PhD. Steven Y. Cheng
2016-2019 Martin-Luther University Halle-Wittenberg Institute of Physiological Chemistry
Supervisor: PD. Dr. rer. nat. Pfirrmann

RESEARCH EXPERIENCE

2014-2016 SENP1 is critical for the activation of Sonic hedgehog signaling
The focus of this project is on whether gli1 can be sumoylated and how sentrin-specific protease 1 (SENP1) regulates its desumoylation. In our research, sumoylation of Gli1 is required for its stability and nuclear-localization, and SENP1 could specifically enhance its desumoylation thereby attenuating Shh signaling activity.

PUBLICATIONS

1. Huaize Liu, Jie Ding, Tingting Yu, Steven Y Cheng. *SENP1-mediated desumoylation of Gli1 attenuates Sonic hedgehog signaling*. Molecular and Cellular Biology, 2017
2. Jie Ding, Huaize Liu, Lie Shao, Lu Xie, Steven Y Cheng. *DGKδ triggers endoplasmic reticulum release of IFT88 positive vesicles destined for supporting the assembly of cilia*. Scientific Reports, 2017
3. Huaize Liu, Thorsten Pfirrmann. *The Gid-complex: an emerging player in the ubiquitin ligase league*. Biological chemistry, 2019
4. Huaize Liu, et al. *The GID Ubiquitin Ligase Complex is a Regulator of AMPK Activity and Organismal Lifespan*. Autophagy, accepted in 2019

12. Acknowledgments

Firstly, I do thank my wife Dr. DING Jie 丁洁 so much. She is always there for me, without her three years of companionship and her help in science I could not have finished my doctoral work. Then I am also grateful to my supervisor PD Dr. Thorsten Pfirrmann. Not only in science, also in the daily life he helped me a lot. He is so clever and good at communication; it is a great honor to work with him. In addition, I would like to thank all the dear colleagues in my lab: Prof. Thomas Hollemann, Juliane Herfurth, Dr. Herbert Neuhaus, Dr. Astrid Vess, Friederike Hantel, Lisa, Danilo and Elisa, we are a big lovely family. Last but not at least, all the buddies from Yong Yuan De Ting Che Peng 永远的停车棚 and Miao Can Ting 喵餐厅 are bringing Jie and me the warmth from the thousands faraway home all the time.

Review

Huaize Liu and Thorsten Pfirrmann*

The Gid-complex: an emerging player in the ubiquitin ligase league

Abstract: The *Saccharomyces cerevisiae* Gid-complex is a highly evolutionary conserved ubiquitin ligase with at least seven protein subunits. Here, we review our knowledge about the yeast Gid-complex as an important regulator of glucose metabolism, specifically targeting key enzymes of gluconeogenesis for degradation. Furthermore, we summarize existing data about the individual subunits, the topology and possible substrate recognition mechanisms and compare the striking similarities, but also differences, between the yeast complex and its vertebrate counterpart. Present data is summarized to give an overview about cellular processes regulated by the vertebrate GID-complex that range from cell cycle regulation, primary cilia function to the regulation of energy homeostasis. In conclusion, the vertebrate GID-complex evolved as a versatile ubiquitin ligase complex with functions beyond the regulation of glucose metabolism.

Keywords: cell cycle; CTLH-complex; energy homeostasis; metabolism; primary cilia; protein degradation.

Introduction: the yeast Gid-complex

Catabolite degradation in *Saccharomyces cerevisiae*

Glucose serves as a high-energy carbon source and its availability is constantly monitored by yeast. Thus, glucose sensing- and signaling-systems are extremely advanced and sensitive. Specialized hexose sensors like Snf3p and Rgt2p react to its presence by affecting metabolism on all layers of control (Celenza et al., 1988; Ozcan et al., 1996), e.g. on transcriptional, posttranscriptional, translational and posttranslational level (Rolland et al., 2002). During glycolysis, glucose is metabolized to pyruvate under aerobic conditions or to ethanol under anaerobic conditions in yeast. Gluconeogenesis is the reciprocally controlled pathway that is required to synthesize glucose *de novo* from precursor molecules when glucose is deprived. To prevent a futile cycle of ATP hydrolysis either of them is active or inactive (Purwin et al., 1982). Both pathways share a major part of their enzymatic equipment, however, some reactions are thermodynamically irreversible and require specific enzymes for gluconeogenesis, e.g. fructose-1,6-bisphosphatase (Fbp1p). In yeast, Fbp1p is expressed when cells are grown on a non-fermentable carbon source, like ethanol or acetate. In a process called catabolite inactivation, gluconeogenesis is shut-off after glucose supplementation in a defined series of events (Figure 1). First, transcription of *FBP1* is repressed by Mig1p (Klein et al., 1998; Rolland et al., 2002) and Fbp1p gets inactivated by Pka1p (protein kinase A) dependent phosphorylation (Funayama et al., 1980). In a next step, the enzyme is degraded by a process called catabolite degradation (Chiang and Schekman, 1991). In their pioneering work, Prof. Schekman and coworkers described a role of vacuolar proteases in Fbp1p degradation due to several observations. By pulse chase analysis they noticed that Fbp1p degradation in response to glucose was slower in *PEP4* deleted cells. *PEP4* encodes for proteinase A, a vacuolar protease that activates all other vacuolar proteases and its deletion leads to impaired vacuolar degradation (Ammerer et al., 1986). By cell fractionation and immunofluorescence microscopy they showed an accumulation of Fbp1p in the cytosol or the vacuole, especially under glucose supplementation. Moreover, they found that vacuolar accumulation of Fbp1p was dependent on components of the secretory pathway. Their data suggested that the catabolite dependent degradation of Fbp1p is taking place by vacuolar degradation processes. Several yeast vacuolar import and degradation (vid) mutants that fail to degrade Fbp1p in response to glucose, were isolated in following work (Hoffman and Chiang, 1996). Some of

*Corresponding author: Thorsten Pfirrmann, Martin Luther University Halle-Wittenberg, Institute of Physiological Chemistry, Hollystr. 1, D-06114 Halle, Germany, e-mail: thorsten.pfirrmann@medizin.uni-halle.de. https://orcid.org/0000-0002-9474-9535
Huaize Liu: Martin Luther University Halle-Wittenberg, Institute of Physiological Chemistry, Hollystr. 1, D-06114 Halle, Germany
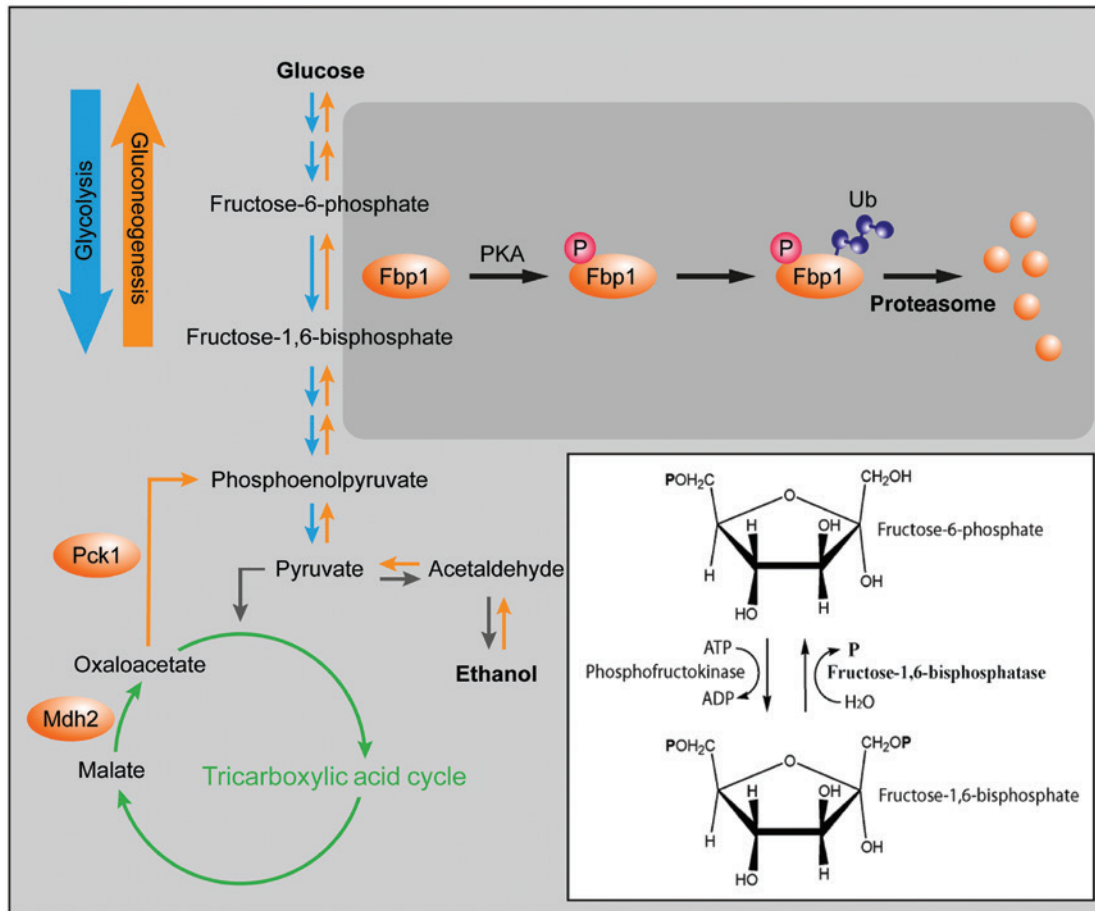
Figure 1: The proteasome mediates the metabolic switch from gluconeogenesis to glycolysis.
Glycolysis (blue) and gluconeogenesis (orange) share a major part of enzymes. Fructose-1,6-bisphosphatase (Fbp1p) catalyzes the dephosphorylation of fructose-1,6-bisphosphate to fructose-6-phosphate (white box). Glucose supplementation results in inactivating phosphorylation (P, red), polyubiquitination (Ub, blue) and proteasomal degradation of Fbp1p. Three enzymes are degraded in this process (malate dehydrogenase, Mdh2p; phosphoenolpyruvate carboxykinase, Pck1p; Fbp1p; orange).

the isolated mutants blocked Fbp1p degradation in the cytosol; others caused accumulation of Fbp1p as small punctate structures within the cytoplasm, suggesting the accumulation in vesicles. Indeed, electron microscopy studies revealed that Fbp1p containing vesicles are distinct from endosomes, vacuoles and other vesicular structures (Huang and Chiang, 1997). The first protein found to be involved in the process of Fbp1p targeting and sequestration into these vesicles is called Vid24p/Gid4p. Vid24p was described to localize to Fbp1p containing vesicles as a peripheral protein. Its deletion led to Fbp1p accumulation in these vesicles that were unable to fuse with the vacuole (Chiang and Chiang, 1998).

Prof. Wolf and colleagues reported on a second mechanism of catabolite degradation. In their experimental setup, catabolite degradation of Fbp1p was dependent on an intact proteasome but not of proteinase A

(Schork et al., 1994a,b). Supporting the idea of a ubiquitin-proteasome dependent degradation, Fbp1p was polyubiquitinated as a response to glucose addition. Additionally, the overexpression of dominant-negative acting ubiquitin variants, which carry a point mutation in lysine 48 (K48R) abolished catabolite degradation (Schork et al., 1995). In a screen with a fusion protein consisting of the amino-terminal part of Fbp1p fused to the marker β-galactosidase, three mutants *GID1*, *GID2* and *GID3* (glucose induced degradation deficient) genes were identified (Hämmerle et al., 1998). Among them, Gid3p was uncovered as the ubiquitin conjugating enzyme Ubc8p (Schüle et al., 2000). Gid1p/Vid30p was previously described to be involved in glucose-induced degradation of Fbp1p in the vacuole (Alibhoy et al., 2012). Differential fractionation of Gid2p demonstrated, that Gid2p and Fbp1p were soluble, which excluded the presence of Gid2p and Fbp1p

in vesicles or the vacuole (Regelmann et al., 2003). In a second genomic approach, a yeast deletion strain collection that represented around 5000 nonessential yeast genes was screened for mutant strains unable to degrade Fbp1p. This screen identified six additional *GID* genes important for glucose induced catabolite degradation. Among them Gid6p turned out to be the deubiquitinating enzyme Ubp14p. Ubp14p is proposed to cleave polyubiquitin chains to single moiety residues. Consequently, the deletion of *UBP14* inhibited the proteasome due to accumulating polyubiquitin chains that competitively inhibit the proteasome (Amerik et al., 1997). This explained the deficiency of an *UBP14* deletion strain to degrade Fbp1p. However, the stability of other proteasomal substrates like the ERAD substrate CPY*-HA (Hiller et al., 1996) was not affected suggesting a more specific function of Ubp14p/Gid6p (Eisele et al., 2006). Among the remaining new proteins, Gid7p, Gid8p and Gid9p were of unknown function, while Gid4p and Gid5p had been described previously to be necessary for vacuolar degradation of Fbp1p (Chiang and Chiang, 1998). The partial functional overlap of Gid and Vid components suggested the existence of two independent degradation pathways that share some components. Interestingly, Prof. Chiang and coworkers showed that Fbp1p degradation shifts from a proteasomal to a vacuolar degradation pathway dependent on the duration of glucose starvation (Hung et al., 2004).

Detailed biochemical analysis of the protein Gid2p demonstrated that it is not present as a monomeric protein within the cell, but rather formed a heterogeneous complex at an approximate molecular mass of 600 kDa. This suggested that it is part of a soluble protein complex, assembled with some of the remaining Gid proteins (Regelmann et al., 2003). Indeed, several proteomic interaction studies in yeast discovered the Gid-proteins Gid1p, Gid2p, Gid4p, Gid5p, Gid7p, Gid8p and Gid9p as parts of a huge protein complex that was named the Gid-complex (Ho et al., 2002; Krogan et al., 2006; Tarassov et al., 2008; Yu et al., 2008; Subbotin and Chait, 2014).

The yeast Gid-complex functions as a ubiquitin ligase

Ubiquitin is a 76 amino acid protein that functions as a posttranslational modifier (Pickart and Eddins, 2004). Posttranslational modifications with ubiquitin regulate processes that include the targeted degradation of modified substrate proteins by the 26S proteasome, the degradation of proteins in the lysosome (vacuole), endocytosis of membrane proteins, intracellular trafficking

and regulation of the secretory pathway, transcriptional regulation and many more (Figure 2). The ubiquitination machinery requires the sequential and hierarchical reaction of a set of three enzyme classes to catalyze mono-ubiquitination, multi-monoubiquitination or polyubiquitination of a substrate (Sadowski et al., 2012). The ubiquitin-activating-enzyme (E1) activates ubiquitin by ATP hydrolysis which is transferred to the ubiquitin-conjugating-enzyme (E2) and finally the substrate specific ubiquitin ligase (E3) transfers ubiquitin onto a lysine residue of the substrate or to one of the seven lysine residues of ubiquitin itself, thus forming polyubiquitin chains (Yau and Rape, 2016). The catalytic specificity for the substrate and for the kind of ubiquitination is dependent on the ubiquitin-ligase and is responsible for the diverse functions regulated by ubiquitination.

In a first attempt to elucidate the function of the yeast Gid-complex, Wolf and colleagues measured protein-protein interactions between the Gid-complex and Fbp1p. The immunoprecipitation of Fbp1p revealed an interaction with members of the Gid-complex following glucose addition. No interaction was detected with the deubiquitinating enzyme Gid6p/Ubp14p (Santt et al., 2008). This suggested a function of the Gid-complex as a Fbp1p specific ubiquitin ligase complex, activated under high glucose conditions, dependent on the energy metabolism of the cell (Figure 3). Indeed, Gid2p/Rmd5p and Gid9p contained degenerated RING domains that were missing some of the eight Cys/His residues important to coordinate the binding of two Zn^{2+}-ions (Santt et al., 2008; Braun et al., 2011). Often the RING domain in ubiquitin-ligases is important for structural integrity and binds the corresponding ubiquitin-conjugating enzyme in the ternary complex (Lorick et al., 1999). However, the presence of a complete cysteine and histidine pattern in a RING domain is not always critical for ubiquitin ligase function. As an extreme example of a degenerated RING domain, so-called U-box ubiquitin ligases share the structure of a classical RING domain but are missing all the cysteine and histidine residues (Hatakeyama and Nakayama, 2003; Ohi et al., 2003). In a canonical RING domain one Zn^{2+} is coordinated by the first, second, fifth and sixth histidine/cysteine residue and the second Zn^{2+} by residues three, four, seven and eight (Freemont, 2000; Deshaies et al., 2009). The RING domain of Gid2p contained all residues necessary to complex the second Zn^{2+} and missed all other residues except for residue one (Santt et al., 2008). Interestingly, another member of the Gid-complex, Gid9p/Fyv10p, carried a similar non-canonical RING domain with even less conserved Zn^{2+} binding residues (Braun et al., 2011). Experimental evidence for the importance of
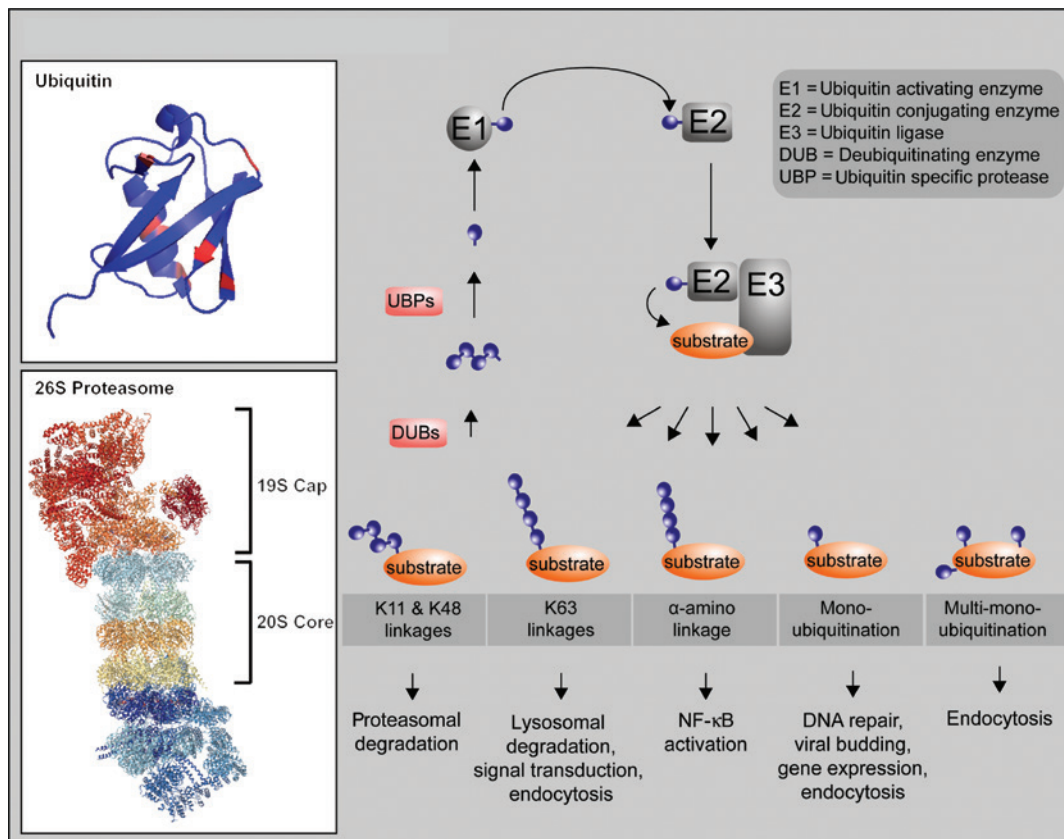
Figure 2: The ubiquitin modification system.
The ubiquitin modification system (UMS) requires the sequential hierarchical reaction of a class of three enzymes to ubiquitinate a substrate protein: E1, E2 and E3. Polyubiquitination, mono-ubiquitination or multi-monoubiquitination regulate different functions. Ubiquitin specific proteases (UBP, DUB) remove ubiquitin from chains or the substrate. Left: 26S proteasome structure with the 20S core and the 19S Cap (pdb: 5GJR); structure of ubiquitin (pdb: 1UBQ).

the non-canonical RING domain in Gid2p and Gid9p in yeast came from several important experiments. *In vivo*, the replacement of a single cysteine residue within the RING domain (C379S) of Gid2p abolished glucose induced Fbp1p polyubiquitination and subsequent degradation (Santt et al., 2008). Similarly, the mutation of a cysteine residue (C434S) within the RING domain of Gid9p blocked polyubiquitination and thus catabolite degradation (Braun et al., 2011). Further experiments showed that the same single point mutation in the RING domain abolished autoubiquitination of Gid2p and polyubiquitination of Fbp1p *in vitro*. Accordingly, Gid9p polyubiquitinated Fbp1p and other gluconeogenic key enzymes and conserved cysteine residues within the non-canonical RING domain were critical for the glucose-induced degradation of Fbp1p, phosphoenolpyruvate carboxykinase (Pck1p) and malate dehydrogenase (Mdh2p) (Figure 1) (Braun et al., 2011). It is thus very likely, that both RING domains are essential binding partners of the respective ubiquitin-conjugating enzyme (E2) and thus recruit Ubc8p to the

ternary complex consisting of the substrate, Ubc8p and the Gid-complex. To the best of our knowledge, a setting in which two non-canonical RING domains in subunits of an E3-ligase-complex are necessary to bind the corresponding E2 is unique to the Gid-complex (Santt et al., 2008; Braun et al., 2011).

The proline N-end rule and the substrate recognition protein Gid4p

Yeast strains expressing chromosomally tagged Gid-proteins under the endogenous promoter revealed, that all Gid-complex subunits are present in gluconeogenic cells and in cells supplemented with glucose (Santt et al., 2008). This suggested the presence of a stable core complex under different growth conditions. In this respect, an unusual subunit of the Gid-complex is Gid4p/Vid24p. It presents the only Gid subunit that is either not expressed under derepressing growth conditions, only in
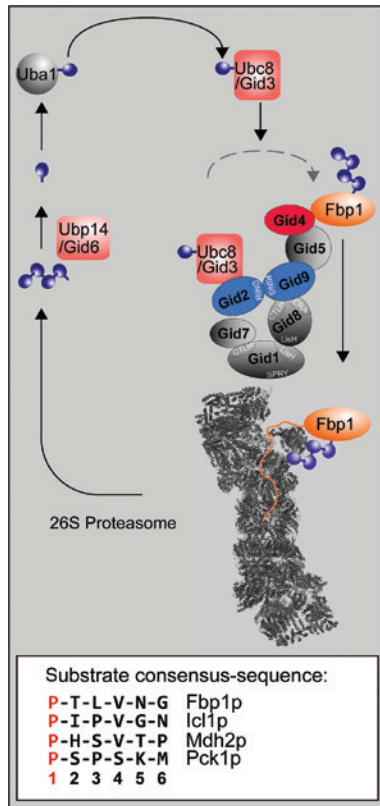
Figure 3: Catabolite degradation of fructose-1,6-bisphosphatase (Fbp1p).
Fbp1p is a key gluconeogenic enzyme. Addition of glucose to gluconeogenic yeast cells induces Gid-complex (ubiquitin ligase complex) dependent Fbp1p (orange) polyubiquitination and degradation. Substrate recognition subunit (Gid4p, red), RING domain bearing subunits (Gid2p, Gid9p, blue), E2 (Gid3p, pink). White box shows N-recognin consensus sequences of substrates.

very low amounts or turned over immediately. Yeast cells grown on rich medium with ethanol as a carbon source did not exhibit measurable amounts of Gid4 protein. In contrast, already 5 min after glucose supplementation a strong signal for Gid4p appeared with a peak around 30 min after glucose addition and thereafter disappeared again. These observations raised the question, whether Gid4 protein levels correlate with Fbp1p degradation, suggesting a Gid4p function in recruiting Fbp1p and other substrates to the Gid-complex for polyubiquitination and subsequent degradation. Several observations support such a hypothesis: First, the addition of the translation-inhibitor cycloheximide (CHX) inhibits Gid4p translation and thus Fbp1p degradation is blocked as a result. Second, all other Gid-complex subunits are expressed and are part of the complex under several growth conditions. Third, Gid4p degradation is dependent on other Gid-components and on a functional proteasome.

Additionally, the ectopic expression of Gid4p under de-repressing conditions can induce Fbp1p degradation (Santt et al., 2008). This suggested, that the inactive core of the Gid-complex is always present and the differential expression of Gid4p mediates complex activity and thus substrate stability. In line with this assumption, a recent report showed that Gid4p directly binds peptides with N-terminal proline residues and at least four adjoining residues (Chen et al., 2017). Indeed, the four known substrates of the yeast Gid-complex contain a proline residue at second position with the exception of Pck1p at the third position (Figure 3, white box). These residues were previously shown to be essential for glucose induced catabolite degradation (Hämmerle et al., 1998). Prof. Varshavsky and coworkers proposed, that the Gid-complex is a novel N-recognin that specifically binds N-terminal proline residues, recruiting substrates to the Gid-complex (Chen et al., 2017). This finding strongly suggests the presence of other Gid-complex substrates that match the proposed consensus sequence. To find these potential novel substrates, we generated a search algorithm that allows screening for proteins that match the proposed consensus site. Two yeast transcription factors Stp1p and Stp2p especially caught our attention because they both matched the proposed consensus sequence and were previously described as proteasomal substrates (Pfirrmann et al., 2010). However, mutation of the N-recognin binding sequence did not substantially affect the turnover of both transcription factors, suggesting that they are not degraded by the Pro-N-end rule pathway (Prof. Ljungdahl personal communication). At this point, substrates that match the suggested consensus site are restricted to the ones previously described, while others need to be discovered (Hämmerle et al., 1998; Chen et al., 2017).

Interestingly, there is evidence that human GID4-mediated recognition of Pro-N-end rule degrons is also evolutionary conserved in *Homo sapiens*. Dong et al. reported on the first crystal structure of human GID4 alone and in complex with various peptides. They showed that the first two N-terminal substrate residues of the Pro-N-degron are anchored inside a narrow cavity of the GID4 β-barrel, while the following two residues rest on a surface groove. Therefore, the substrate binding mechanism of human GID4 is similar to yeast and substrates of the human GID-complex can likely be identified via the first N-terminal four amino acid residues present after removal of the initiator methionine (Dong et al., 2018). However, a recently identified substrate of the human GID-complex, HBP1 did not match the proposed consensus site (Lampert et al., 2018).

Topology of the Gid-complex

The topology of the yeast Gid-complex

Computational protein-protein interaction analysis predicted a core yeast Gid-complex consisting of Gid1p, Gid8p, Gid5p and another protein, Ydl176p (Pitre et al., 2006). To study the topology of the yeast Gid-complex in more detail, Prof. Wolf and colleagues deleted single domains of the predicted core subunits Gid1p and Gid8p and analyzed the composition of the Gid-complex by co-immunoprecipitation experiments. In an elegant set of experiments, which employed *GID*-deletion mutants and mutants lacking individual protein domains, the authors were able to get first insights into the topology of the yeast Gid-complex. They further constructed a yeast deletion strain lacking all seven *GID*-genes and

reconstituted the Gid-complex with individually tagged *GID*-genes. The combination of both approaches ended in an initial model reflecting the topology of the yeast Gid-complex, including the function of particular protein domains (Figure 4, *S. cerevisiae*). Their model suggested that Gid1p directly interacted with Gid7p via its CTLH domain and with Gid8p via its LisH domain (individual domains will be described in Table 1 and later in the text). Gid5p functioned as an adaptor protein for the regulatory subunit Gid4p and additionally bound to Gid9p. Both, Gid9p and Gid2p contain non-canonical RING domains and are connected to the complex via the binding of Gid9p to the CTLH and CRA domain of Gid8p. The authors proposed, that the binding of Gid4p to Gid5p induces a conformational change that allows binding to Gid9p, which activates the ligase complex (Menssen et al., 2012).
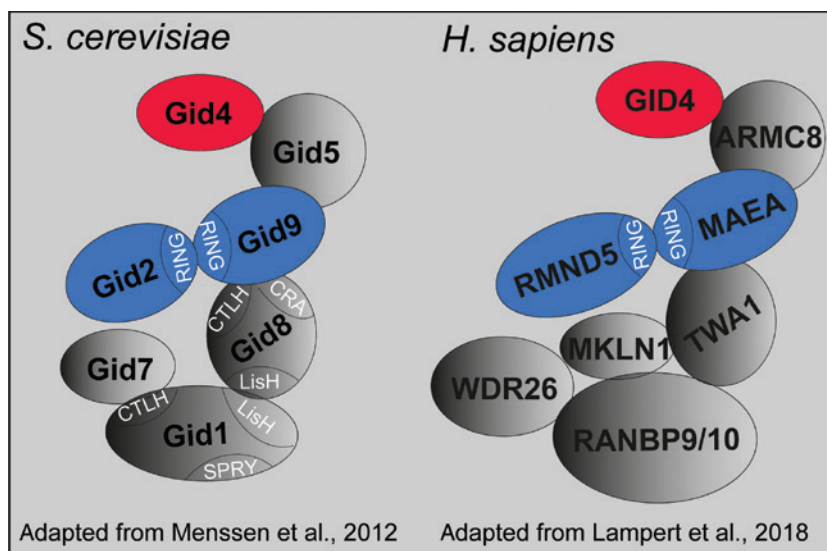

Figure 4: Schematic representation of the yeast and the human GID-complex.

Table 1: The Gid-complex with accession numbers and protein domains.

S. cerevisiae		*H. sapiens*		
Gid-subunits	Accession Nr.	Gid-subunits	Domains	Accession Nr.
Gid1p/Vid30p	NP_011287.1	RANBP10, RANBP9	SPRY, LisH, CTLH, CRA	NM_005493
Gid2p/Rmd5p	NP_010541.3	RMND5A/ RMND5B	LisH, CTLH, RING	NM_022780
Gid4p/Vid24p	NP_009663.1	C17ORF39/GID4	–	NM_024052
Gid5p/Vid28p	NP_012247.3	ARMC8	ARM	NM_213654
Gid7p/Moh2p	NP_009891.1	MKLN1/TWA2	LisH, CTLH, WD40 or Kelch repeat	NM_013225
		WDR26	CTLH, WD40	NM_025160.6
Gid8p/Dcr1p	NP_013854.1	C20orf11/TWA1/GID8	LisH, CTLH, CRA	NM_017896
Gid9p/Fyv10p	NP_012169.1	MAEA/EMP	LisH, CTLH, U-box	NM_001017405.3
Moh1p	NP_009504.1	YPEL5		NM_001127401.1

The topology of the human GID-complex

Individual subunits of the yeast Gid-complex are highly conserved throughout the eukaryotic kingdom and Gid1p/Vid30p, Gid2p/Rmd5p, Gid4p/Vid24p, Gid5p/Vid28p, Gid7p, Gid8p and Gid9p have their closest human counterparts in RANBP9/10, RMND5A/B, GID4/C17ORF39, ARMC8, MKLN1, TWA1/C20ORF11 and MAEA, respectively. All these proteins are subunits of the human GID-complex (Texier et al., 2014) (see Table 1). A recent publication described a first topological arrangement of the human GID-complex (Lampert et al., 2018). The authors used Sf9 insect cells to express combinations of up to 10 full length human GID subunits. They described a similar composition of the human GID-complex compared to yeast, with a stable pentameric core complex containing the RING domain bearing subunits RMND5, MAEA bound to a TWA1 dimer bridging RANBP9 and WDR26 to the complex. The subunit TWA1 was present in a 2:1 molar ratio that is consistent with previous data showing that TWA1 forms dimers (Francis et al., 2017). Similar to the topology of the yeast complex TWA1 was pivotal for efficient MAEA and RMND5A RING dimerization and recruitment of the peripheral members of the complex. Together, TWA1, MAEA, RMND5, RANBP9, WDR26 and MKLN1 form a stable complex and ARMC8 is required for subsequent binding of GID4 (Figure 4).

Members of the yeast Gid-complex contain a series of motifs that are involved in protein-protein interactions (Santt et al., 2008; Table 1), e.g. Gid1p contains a SPRY domain, which is a structural motif that mediates protein-protein interactions (Menon et al., 2004) and a CTLH domain (C-terminal to LisH motif domain) (Gerlitz et al., 2005). CTLH domains are often found in proteins in combination with LisH domains that play a role in microtubule dynamics and cell migration (Emes and Ponting, 2001). The *S. cerevisiae* proteome contains five proteins with a CTLH domain that are all members of the Gid-complex, implicating a specific function within this complex (Santt et al., 2008). In yeast, the CTLH domain of Gid1p was necessary for its association with Gid7p as well as with actin (Alibhoy et al., 2012; Menssen et al., 2012). In mice, the LisH domain in LIS1 protein was described to be important for the formation of homodimers (Cahana et al., 2001; Kim et al., 2004). The CRA domain consists of 100 amino acids at the C-terminus of RANBP9 and forms six helices of the death domain superfamily. Both MKLN1 and its yeast orthologous Gid7p contain an N-terminal CTLH domain and a LisH domain (Kobayashi et al., 2007; Santt et al., 2008). On the one hand, Gid7p contains six WD40 repeats, while MKLN1 contains six Kelch repeats instead. Interestingly, both WD40 repeats and Kelch repeats are

often associated with Cullin ubiquitin ligase complexes and function as substrate adaptors (Angers et al., 2006; Lee et al., 2010; Zou et al., 2016). Both domains differ in the primary sequence but are structurally and functionally related; both form a propeller-like platform for protein-protein interactions (Adams et al., 2000; Li and Roberts, 2001; Hudson and Cooley, 2008).

Function of the vertebrate GID-complex

Function in cell cycle regulation

Recently, Lampert and collegues found that GID-subunit deletion in human cells affected cell proliferation and this defect was accompanied by deregulation of critical cell cycle markers (Lampert et al., 2018). They found the GID-complex as the ubiquitin ligase for the pro-proliferative protein HBP1, which was reported to regulate the expression of cell cycle regulators such as N-MYC, cyclin D1, p16 and p21 (Tevosian et al., 1997; Sampson et al., 2001; Li et al., 2010; Wang et al., 2012). The complex-scaffold subunit GID1/RANBPM was described to interact with citron kinase (CITK), a protein shown to localize to the surface of the lateral ventricles and to be essential for neurogenic mitosis (Chang et al., 2010). RANBPM RNAi decreased the polarization of CITK to the ventricular surface, increased the number of cells in mitosis, and decreased the number of cells in cytokinesis. In addition, RANBPM was also shown to interact with YPEL5 (Hosono et al., 2010) and porphobilinogen deaminase (PBGD) (Greenbaum et al., 2003), which both have a function in cell division. Other subunits, e.g. GID7/WDR26 were identified as presumptive CRL4 adapter proteins, possibly involved in cell cycle regulation (Piwko et al., 2010).

Function of the GID-complex in the regulation of energy homeostasis

In vertebrates, gluconeogenesis is almost exclusively restricted to the liver, but also takes place in the kidney cortex and intestine at a much lower extent (Previs et al., 2009; Mutel et al., 2011). Energy regulation (maintaining blood glucose) in mammals during starvation and/or rigorous exercise is primarily achieved through the breakdown of liver glycogen stocks and gluconeogenesis (Rui, 2014). Though the yeast Gid-complex and its known substrates

are highly evolutionary conserved, a process similar to catabolite degradation of yeast Fbp1p does not seem to exist in vertebrates. Lampert et al. analyzed protein levels of the gluconeogenic enzymes FBP1 and PCK1 in HEK-293 cells and primary mouse hepatocytes under gluconeogenic conditions (glucose-free medium supplemented with pyruvate, lactate and forskolin). They further challenged the system with the knockdown of all GID-subunits by siRNA. Unlike yeast Fbp1p and Pck1p, mouse FBP1 and PCK1 protein levels remained relatively stable over the time-course, independent of the GID knockdown. This suggested that the mammalian GID-complex is dispensable for the degradation of FBP1 and PCK1. Human gluconeogenic enzymes do not harbor N-terminal proline residues and do not match the N-recognin consensus site (Chen et al., 2017). A proteomic screen revealed that the GID-complex interacted with bicaudal C1 (BICC1), a protein required to maintain normoglycemia in kidneys. Here, a decrease in murine *Pepck* mRNA levels was measured specifically in *Bicc1*^{−/−} kidneys but not in liver, resulting in decreased PCK1 and FBP1 protein levels (Leal-Esteban et al., 2018). This suggested a function of the vertebrate GID-complex in the regulation of metabolism. Recent data showed, that human FBP1 was targeted for proteasomal degradation by the MAGE-TRIM28 complex (Jin et al., 2017). Together, GID-complex dependent catabolite degradation processes appear to be absent in vertebrates, however, shows distinct functions in the control of metabolism.

Function in primary cilia

Primary cilia are hair-like structures that are present on almost every mammalian cell. They consist of a ciliary axoneme build-up of a nine-duplet microtubular filament ring that arises from the basal body and that is surrounded by the ciliary membrane (Wheatley, 1995; Wheatley et al., 1996). These organelles are involved in diverse cellular functions, e.g. cell proliferation, differentiation and polarity, and can act as signaling hubs (Berbari et al., 2009; Goetz and Anderson, 2010; Reiter and Leroux, 2017). Primary cilia dysfunction also plays a major role in different hereditary organ-specific or syndromic diseases, summarized as ciliopathies (Pazour et al., 2002; Ansley et al., 2003; Arts et al., 2007; Fliegauf et al., 2007; Reiter and Leroux, 2017). Several recent observations link primary cilia function with cellular and organismal energy homeostasis. Here, the primary cilium may act as a nutrient sensor with the basal body as a control center. Exemplary, AMPK is directly activated at the basal body of the primary cilium of kidney cells upon

LKB1 phosphorylation (Boehlke et al., 2010). Additionally, several proteins involved in autophagy are integral parts of the basal body or the primary cilium and thus link energy homeostasis and cilia function (Pampliega et al., 2013; Wang et al., 2015). In an extensive search for proteins that interact with LCA5 most GID-complex subunits were detected (Boldt et al., 2011). Mutations in LCA5 cause the ciliopathy Leber congenital amaurosis (OMIM#604537) that comprises a group of early-onset childhood retinal dystrophies characterized by vision loss, nystagmus and severe retinal dysfunction (den Hollander et al., 2007; Chung and Traboulsi, 2009). Recently, the GID-complex was identified as an integral part of the primary cilium (Texier et al., 2014; Boldt et al., 2016). The authors found all conserved subunits of the GID-complex at the basal body of the primary cilium, including all the orthologous Gid proteins and additional proteins like YPEL5 (*S. cerevisiae* Moh1 orthologous protein). Moh1p was previously described to be part of the yeast Gid-complex (Ho et al., 2002) with a function other than catabolite degradation (Lampert et al., 2018). An interaction was also found together with the ubiquitin conjugating enzyme UBE2G, suggesting that this E2 is the human *in vivo* partner of the GID-complex at least in this cell type. Notably, several phenotypic effects characteristic of ciliopathies were described as a result of a suppression of GID-complex function. For instance, during *Xenopus laevis* early embryonic development, the expression of *gid2/rmnd5* is strongest in structures derived from the ectoderm, like the prospective brain, eyes and ciliated cells of the skin. The suppression of Rmnd5 function resulted in malformations of the fore- and mid-brain in *Xenopus laevis* (Pfirrmann et al., 2015). An intragenic partial duplication of the *RMND5A* gene in a patient resulted in a giant occipital encephalocele, a malformation reminiscent of the Meckel-Gruber ciliopathy (OMIM#609883) (Vogel et al., 2012). RANBP9 was also found to interact with HDAC6 to inhibit its activity (Salemi et al., 2014). HDAC6 is a tubulin deacetylase that is a component of the aggresome pathway and is involved in the clearance of protein aggregates (Boyault et al., 2007), but also in the disassembly of primary cilia (Gradilone et al., 2013; Smith et al., 2018). All protein-protein interactions and putative functions of the vertebrate GID-complex are summarized in Figure 5.

Outlook and future perspectives

Possible functions of the vertebrate GID-complex include cell cycle regulation, cilia function and the regulation of cellular energy homeostasis (Figure 5). An intriguing
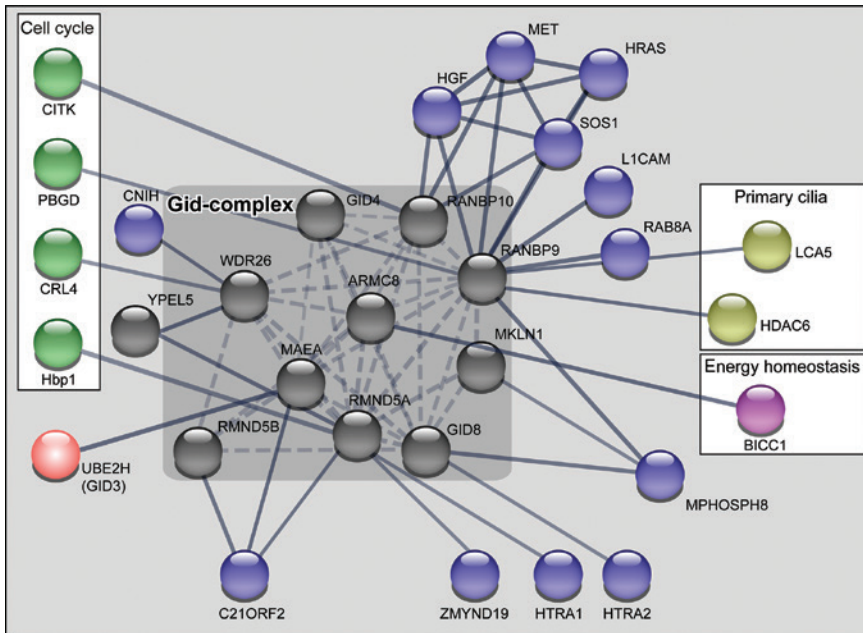
Figure 5: GID-complex interactions and possible functions.
Described protein interactors are classified into functions in cell cycle (green), energy homeostasis (purple), primary cilia (yellow) and others (blue). The GID-complex is colored in gray.

hypothesis is that the vertebrate GID-complex functions similar to the yeast Gid-complex in glucose sensing and energy homeostasis. Newer studies suggest that the primary cilium acts as a sensor to maintain energy homeostasis of the cell. For example, AMPK is phosphorylated at the basal body of the primary cilium (Boehlke et al., 2010). From there it regulates mTOR activity and autophagic flux (Pampliega et al., 2013). It is possible that primary cilia function as nutrient sensors with the GID-complex as an integral player within this process. Intriguingly, primary cilia are formed and disassembled in a cell cycle-dependent manner, suggesting that all three processes are interconnected via the GID-complex. A future challenge will be the identification of novel Gid-complex substrates perhaps with functions at the basal body.

The finding of YPEL5 in the human complex suggests that different evolutionary conserved compositions of the GID-complex exist. It is tempting to speculate that these differentially composed complexes bind and ubiquitinate different substrates and thus modulate substrate specificity. Also, the two paralogous RANBP9 and RANBP10 as well as RMND5A and RMND5B are present in the core GID-complex. The mutual exclusive incorporation of the paralogous proteins RMND5A and RMND5B into the complex might be an elegant mechanism to extend the substrate spectrum of the GID-complex, e.g. by recruiting different ubiquitin conjugating enzymes to the ternary complex.

Together, we speculate that depending on the composition of the GID-complex many more substrates will be identified in the future.

References

Adams, J., Kelso, R., and Cooley, L. (2000). The kelch repeat superfamily of proteins: propellers of cell function. Trends Cell Biol. *10*, 17–24.

Alibhoy, A.A., Giardina, B.J., Dunton, D.D., and Chiang, H.L. (2012). Vid30 is required for the association of Vid vesicles and actin patches in the vacuole import and degradation pathway. Autophagy *8*, 29–46.

Amerik, A., Swaminathan, S., Krantz, B.A., Wilkinson, K.D., and Hochstrasser, M. (1997). In vivo disassembly of free polyubiquitin chains by yeast Ubp14 modulates rates of protein degradation by the proteasome. EMBO J. *16*, 4826–4838.

Ammerer, G., Hunter, C.P., Rothman, J.H., Saari, G.C., Valls, L.A., and Stevens, T.H. (1986). PEP4 gene of *Saccharomyces cerevisiae* encodes proteinase A, a vacuolar enzyme required for processing of vacuolar precursors. Mol. Cell Biol. *6*, 2490–2499.

Angers, S., Thorpe, C.J., Biechele, T.L., Goldenberg, S.J., Zheng, N., MacCoss, M.J., and Moon, R.T. (2006). The KLHL12-Cullin-3 ubiquitin ligase negatively regulates the Wnt-beta-catenin pathway by targeting dishevelled for degradation. Nat. Cell Biol. *8*, 348–357.

Ansley, S.J., Badano, J.L., Blacque, O.E., Hill, J., Hoskins, B.E., Leitch, C.C., Kim, J.C., Ross, A.J., Eichers, E.R., Teslovich, T.M., et al. (2003). Basal body dysfunction is a likely cause of pleiotropic Bardet-Biedl syndrome. Nature *425*, 628–633.

Arts, H.H., Doherty, D., van Beersum, S.E., Parisi, M.A., Letteboer, S.J., Gorden, N.T., Peters, T.A., Marker, T., Voesenek, K., Kartono, A., et al. (2007). Mutations in the gene encoding the basal body protein RPGRIP1L, a nephrocystin-4 interactor, cause Joubert syndrome. Nat. Genet. *39*, 882–888.

Berbari, N.F., O'Connor, A.K., Haycraft, C.J., and Yoder, B.K. (2009). The primary cilium as a complex signaling center. Curr. Biol. *19*, R526–R535.

Boehlke, C., Kotsis, F., Patel, V., Braeg, S., Voelker, H., Bredt, S., Beyer, T., Janusch, H., Hamann, C., Godel, M., et al. (2010). Primary cilia regulate mTORC1 activity and cell size through Lkb1. Nat. Cell Biol. *12*, 1115–1122.

Boldt, K., Mans, D.A., Won, J., van Reeuwijk, J., Vogt, A., Kinkl, N., Letteboer, S.J., Hicks, W.L., Hurd, R.E., Naggert, J.K., et al. (2011). Disruption of intraflagellar protein transport in photoreceptor cilia causes Leber congenital amaurosis in humans and mice. J. Clin. Invest. *121*, 2169–2180.

Boldt, K., van Reeuwijk, J., Lu, Q., Koutroumpas, K., Nguyen, T.M., Texier, Y., van Beersum, S.E., Horn, N., Willer, J.R., Mans, D.A., et al. (2016). An organelle-specific protein landscape identifies novel diseases and molecular mechanisms. Nat. Commun. *7*, 11491.

Boyault, C., Zhang, Y., Fritah, S., Caron, C., Gilquin, B., Kwon, S.H., Garrido, C., Yao, T.P., Vourc'h, C., Matthias, P., et al. (2007). HDAC6 controls major cell response pathways to cytotoxic accumulation of protein aggregates. Genes Dev. *21*, 2172–2181.

Braun, B., Pfirrmann, T., Menssen, R., Hofmann, K., Scheel, H., and Wolf, D.H. (2011). Gid9, a second RING finger protein contributes to the ubiquitin ligase activity of the Gid complex required for catabolite degradation. FEBS Lett. *585*, 3856–3861.

Cahana, A., Escamez, T., Nowakowski, R.S., Hayes, N.L., Giacobini, M., von Holst, A., Shmueli, O., Sapir, T., McConnell, S.K., Wurst, W., et al. (2001). Targeted mutagenesis of Lis1 disrupts cortical development and LIS1 homodimerization. Proc. Natl. Acad. Sci. USA *98*, 6429–6434.

Celenza, J.L., Marshall-Carlson, L., and Carlson, M. (1988). The yeast SNF3 gene encodes a glucose transporter homologous to the mammalian protein. Proc. Natl. Acad. Sci. USA *85*, 2130–2134.

Chang, Y., Paramasivam, M., Girgenti, M.J., Walikonis, R.S., Bianchi, E., and LoTurco, J.J. (2010). RanBPM regulates the progression of neuronal precursors through M-phase at the surface of the neocortical ventricular zone. Dev. Neurobiol. *70*, 1–15.

Chen, S.J., Wu, X., Wadas, B., Oh, J.H., and Varshavsky, A. (2017). An N-end rule pathway that recognizes proline and destroys gluconeogenic enzymes. Science *355*, eaal3655.

Chiang, H.L. and Schekman, R. (1991). Regulated import and degradation of a cytosolic protein in the yeast vacuole. Nature *350*, 313–318.

Chiang, M.C. and Chiang, H.L. (1998). Vid24p, a novel protein localized to the fructose-1, 6-bisphosphatase-containing vesicles, regulates targeting of fructose-1,6-bisphosphatase from the vesicles to the vacuole for degradation. J. Cell Biol. *140*, 1347–1356.

Chung, D.C. and Traboulsi, E.I. (2009). Leber congenital amaurosis: clinical correlations with genotypes, gene therapy trials update, and future directions. J. AAPOS *13*, 587–592.

den Hollander, A.I., Koenekoop, R.K., Mohamed, M.D., Arts, H.H., Boldt, K., Towns, K.V., Sedmak, T., Beer, M., Nagel-Wolfrum, K., McKibbin, M., et al. (2007). Mutations in LCA5, encoding the ciliary protein lebercilin, cause Leber congenital amaurosis. Nat. Genet. *39*, 889–895.

Deshaies, R.J. and Joazeiro, C.A. (2009). RING domain E3 ubiquitin ligases. Annu. Rev Biochem. *78*, 399–434.

Dong, C., Zhang, H., Li, L., Tempel, W., Loppnau, P., and Min, J. (2018). Molecular basis of GID4-mediated recognition of degrons for the Pro/N-end rule pathway. Nat. Chem. Biol. *14*, 466–473.

Eisele, F., Braun, B., Pfirrmann, T., and Wolf, D.H. (2006). Mutants of the deubiquitinating enzyme Ubp14 decipher pathway diversity of ubiquitin-proteasome linked protein degradation. Biochem. Biophys. Res. Commun. *350*, 329–333.

Emes, R.D. and Ponting, C.P. (2001). A new sequence motif linking lissencephaly, Treacher Collins and oral-facial-digital type 1 syndromes, microtubule dynamics and cell migration. Hum. Mol. Genet. *10*, 2813–2820.

Fliegauf, M., Benzing, T., and Omran, H. (2007). When cilia go bad: cilia defects and ciliopathies. Nat. Rev. Mol. Cell Biol. *8*, 880–893.

Francis, O., Baker, G.E., Race, P.R., and Adams, J.C. (2017). Studies of recombinant TWA1 reveal constitutive dimerization. Biosci. Rep. *37*, BSR20160401.

Freemont, P.S. (2000). RING for destruction? Curr. Biol. *10*, R84–R87.

Funayama, S., Gancedo, J.M., and Gancedo, C. (1980). Turnover of yeast fructose-bisphosphatase in different metabolic conditions. Eur. J. Biochem. *109*, 61–66.

Gerlitz, G., Darhin, E., Giorgio, G., Franco, B., and Reiner, O. (2005). Novel functional features of the Lis-H domain: role in protein dimerization, half-life and cellular localization. Cell Cycle 4, 1632–1640.

Goetz, S.C. and Anderson, K.V. (2010). The primary cilium: a signalling centre during vertebrate development. Nat. Rev. Genet. *11*, 331–344.

Gradilone, S.A., Radtke, B.N., Bogert, P.S., Huang, B.Q., Gajdos, G.B., and LaRusso, N.F. (2013). HDAC6 inhibition restores ciliary expression and decreases tumor growth. Cancer Res. *73*, 2259–2270.

Greenbaum, L., Katcoff, D.J., Dou, H., Gozlan, Y., and Malik, Z. (2003). A porphobilinogen deaminase (PBGD) Ran-binding protein interaction is implicated in nuclear trafficking of PBGD in differentiating glioma cells. Oncogene *22*, 5221–5228.

Hämmerle, M., Bauer, J., Rose, M., Szallies, A., Thumm, M., Dusterhus, S., Mecke, D., Entian, K.D., and Wolf, D.H. (1998). Proteins of newly isolated mutants and the amino-terminal proline are essential for ubiquitin-proteasome-catalyzed catabolite degradation of fructose-1,6-bisphosphatase of *Saccharomyces cerevisiae*. J. Biol. Chem. *273*, 25000–25005.

Hatakeyama, S. and Nakayama, K.I. (2003). U-box proteins as a new family of ubiquitin ligases. Biochem. Biophys. Res. Commun. *302*, 635–645.

Hiller, M.M., Finger, A., Schweiger, M., and Wolf, D.H. (1996). ER degradation of a misfolded luminal protein by the cytosolic ubiquitin-proteasome pathway. Science *273*, 1725–1728.

Ho, Y., Gruhler, A., Heilbut, A., Bader, G.D., Moore, L., Adams, S.L., Millar, A., Taylor, P., Bennett, K., Boutilier, K., et al. (2002). Systematic identification of protein complexes in *Saccharomyces cerevisiae* by mass spectrometry. Nature *415*, 180–183.

Hoffman, M. and Chiang, H.L. (1996). Isolation of degradation-deficient mutants defective in the targeting of fructose-1,6-bisphosphatase into the vacuole for degradation in *Saccharomyces cerevisiae*. Genetics *143*, 1555–1566.

Hosono, K., Noda, S., Shimizu, A., Nakanishi, N., Ohtsubo, M., Shimizu, N., and Minoshima, S. (2010). YPEL5 protein of the *YPEL* gene family is involved in the cell cycle progression by interacting with two distinct proteins RanBPM and RanBP10. Genomics *96*, 102–111.

Huang, P.H. and Chiang, H.L. (1997). Identification of novel vesicles in the cytosol to vacuole protein degradation pathway. J. Cell Biol. *136*, 803–810.

Hudson, A.M. and Cooley, L. (2008). Phylogenetic, structural and functional relationships between WD- and Kelch-repeat proteins. Subcell Biochem. *48*, 6–19.

Hung, G.C., Brown, C.R., Wolfe, A.B., Liu, J., and Chiang, H.L. (2004). Degradation of the gluconeogenic enzymes fructose-1,6-bisphosphatase and malate dehydrogenase is mediated by distinct proteolytic pathways and signaling events. J. Biol. Chem. *279*, 49138–49150.

Jin, X., Pan, Y., Wang, L., Zhang, L., Ravichandran, R., Potts, P.R., Jiang, J., Wu, H., and Huang, H. (2017). MAGE-TRIM28 complex promotes the Warburg effect and hepatocellular carcinoma progression by targeting FBP1 for degradation. Oncogenesis *6*, e312.

Kim, M.H., Cooper, D.R., Oleksy, A., Devedjiev, Y., Derewenda, U., Reiner, O., Otlewski, J., and Derewenda, Z.S. (2004). The structure of the N-terminal domain of the product of the lissencephaly gene Lis1 and its functional implications. Structure *12*, 987–998.

Klein, C.J., Olsson, L., and Nielsen, J. (1998). Glucose control in *Saccharomyces cerevisiae*: the role of Mig1 in metabolic functions. Microbiology *144*, 13–24.

Kobayashi, N., Yang, J., Ueda, A., Suzuki, T., Tomaru, K., Takeno, M., Okuda, K., and Ishigatsubo, Y. (2007). RanBPM, Muskelin, p48EMLP, p44CTLH, and the armadillo-repeat proteins ARMC8α and ARMC8β are components of the CTLH complex. Gene *396*, 236–247.

Krogan, N.J., Cagney, G., Yu, H., Zhong, G., Guo, X., Ignatchenko, A., Li, J., Pu, S., Datta, N., Tikuisis, A.P., et al. (2006). Global landscape of protein complexes in the yeast *Saccharomyces cerevisiae*. Nature *440*, 637–643.

Lampert, F., Stafa, D., Goga, A., Soste, M.V., Gilberto, S., Olieric, N., Picotti, P., Stoffel, M., and Peter, M. (2018). The multi-subunit GID/CTLH E3 ubiquitin ligase promotes cell proliferation and targets the transcription factor Hbp1 for degradation. Elife *7*, e35528.

Leal-Esteban, L.C., Rothe, B., Fortier, S., Isenschmid, M., and Constam, D.B. (2018). Role of Bicaudal C1 in renal gluconeogenesis and its novel interaction with the CTLH complex. PLoS Genet. *14*, e1007487.

Lee, Y.R., Yuan, W.C., Ho, H.C., Chen, C.H., Shih, H.M., and Chen, R.H. (2010). The Cullin 3 substrate adaptor KLHL20 mediates DAPK ubiquitination to control interferon responses. EMBO J. *29*, 1748–1761.

Li, D. and Roberts, R. (2001). WD-repeat proteins: structure characteristics, biological function, and their involvement in human diseases. Cell Mol. Life Sci. *58*, 2085–2097.

Li, H., Wang, W., Liu, X., Paulson, K.E., Yee, A.S., and Zhang, X. (2010). Transcription factor HBP1 targets P16(INK4A), upregulating its expression and consequently is involved in Ras-induced premature senescence. Oncogene *29*, 5083–5094.

Lorick, K.L., Jensen, J.P., Fang, S., Ong, A.M., Hatakeyama, S., and Weissman, A.M. (1999). RING fingers mediate ubiquitin-conjugating enzyme (E2)-dependent ubiquitination. Proc. Natl. Acad. Sci. USA *96*, 11364–11369.

Menon, R.P., Gibson, T.J., and Pastore, A. (2004). The C terminus of fragile X mental retardation protein interacts with the multi-domain Ran-binding protein in the microtubule-organising centre. J. Mol. Biol. *343*, 43–53.

Menssen, R., Schweiggert, J., Schreiner, J., Kusevic, D., Reuther, J., Braun, B., and Wolf, D.H. (2012). Exploring the topology of the Gid complex, the E3 ubiquitin ligase involved in catabolite-induced degradation of gluconeogenic enzymes. J. Biol. Chem. *287*, 25602–25614.

Mutel, E., Gautier-Stein, A., Abdul-Wahed, A., Amigo-Correig, M., Zitoun, C., Stefanutti, A., Houberdon, I., Tourette, J.A., Mithieux, G., and Rajas, F. (2011). Control of blood glucose in the absence of hepatic glucose production during prolonged fasting in mice: induction of renal and intestinal gluconeogenesis by glucagon. Diabetes *60*, 3121–3131.

Ohi, M.D., Vander Kooi, C.W., Rosenberg, J.A., Chazin, W.J., and Gould, K.L. (2003). Structural insights into the U-box, a domain associated with multi-ubiquitination. Nat. Struct. Biol. *10*, 250–255.

Ozcan, S., Dover, J., Rosenwald, A.G., Wolfl, S., and Johnston, M. (1996). Two glucose transporters in Saccharomyces cerevisiae are glucose sensors that generate a signal for induction of gene expression. Proc. Natl. Acad. Sci. USA *93*, 12428–12432.

Pampliega, O., Orhon, I., Patel, B., Sridhar, S., Diaz-Carretero, A., Beau, I., Codogno, P., Satir, B.H., Satir, P., and Cuervo, A.M. (2013). Functional interaction between autophagy and ciliogenesis. Nature *502*, 194–200.

Pazour, G.J., San Agustin, J.T., Follit, J.A., Rosenbaum, J.L., and Witman, G.B. (2002). Polycystin-2 localizes to kidney cilia and the ciliary level is elevated in orpk mice with polycystic kidney disease. Curr. Biol. *12*, R378–R380.

Pfirrmann, T., Heessen, S., Omnus, D.J., Andreasson, C., and Ljungdahl, P.O. (2010). The prodomain of Ssy5 protease controls receptor-activated proteolysis of transcription factor Stp1. Mol. Cell Biol. *30*, 3299–3309.

Pfirrmann, T., Villavicencio-Lorini, P., Subudhi, A.K., Menssen, R., Wolf, D.H., and Hollemann, T. (2015). RMND5 from *Xenopus laevis* is an E3 ubiquitin-ligase and functions in early embryonic forebrain development. PLoS One *10*, e0120342.

Pickart, C.M. and Eddins, M.J. (2004). Ubiquitin: structures, functions, mechanisms. Biochim. Biophys. Acta *1695*, 55–72.

Pitre, S., Dehne, F., Chan, A., Cheetham, J., Duong, A., Emili, A., Gebbia, M., Greenblatt, J., Jessulat, M., Krogan, N., et al. (2006). PIPE: a protein-protein interaction prediction engine based on the re-occurring short polypeptide sequences between known interacting protein pairs. BMC Bioinformat. *7*, 365.

Piwko, W., Olma, M.H., Held, M., Bianco, J.N., Pedrioli, P.G., Hofmann, K., Pasero, P., Gerlich, D.W., and Peter, M. (2010). RNAi-based screening identifies the Mms22L-Nfkbil2 complex as a novel regulator of DNA replication in human cells. EMBO J. *29*, 4210–4222.

Previs, S.F., Brunengraber, D.Z., and Brunengraber, H. (2009). Is there glucose production outside of the liver and kidney? Annu. Rev. Nutr. *29*, 43–57.

Purwin, C., Leidig, F., and Holzer, H. (1982). Cyclic AMP-dependent phosphorylation of fructose-1,6-bisphosphatase in yeast. Biochem. Biophys. Res. Commun. *107*, 1482–1489.

Regelmann, J., Schüle, T., Josupeit, F.S., Horak, J., Rose, M., Entian, K.D., Thumm, M., and Wolf, D.H. (2003). Catabolite degradation of fructose-1,6-bisphosphatase in the yeast *Saccharomyces cerevisiae*: a genome-wide screen identifies eight novel *GID* genes and indicates the existence of two degradation pathways. Mol. Biol. Cell. *14*, 1652–1663.

Reiter, J.F. and Leroux, M.R. (2017). Genes and molecular pathways underpinning ciliopathies. Nat. Rev. Mol. Cell Biol. *18*, 533–547.

Rolland, F., Winderickx, J., and Thevelein, J.M. (2002). Glucose-sensing and -signalling mechanisms in yeast. FEMS Yeast Res. *2*, 183–201.

Rui, L. (2014). Energy metabolism in the liver. Compr. Physiol. *4*, 177–197.

Sadowski, M., Suryadinata, R., Tan, A.R., Roesley, S.N., and Sarcevic, B. (2012). Protein monoubiquitination and polyubiquitination generate structural diversity to control distinct biological processes. IUBMB Life *64*, 136–142.

Salemi, L.M., Almawi, A.W., Lefebvre, K.J., and Schild-Poulter, C. (2014). Aggresome formation is regulated by RanBPM through an interaction with HDAC6. Biol. Open *3*, 418–430.

Sampson, E.M., Haque, Z.K., Ku, M.C., Tevosian, S.G., Albanese, C., Pestell, R.G., Paulson, K.E., and Yee, A.S. (2001). Negative regulation of the Wnt-β-catenin pathway by the transcriptional repressor HBP1. EMBO J. *20*, 4500–4511.

Santt, O., Pfirrmann, T., Braun, B., Juretschke, J., Kimmig, P., Scheel, H., Hofmann, K., Thumm, M., and Wolf, D.H. (2008). The yeast GID complex, a novel ubiquitin ligase (E3) involved in the regulation of carbohydrate metabolism. Mol. Biol. Cell *19*, 3323–3333.

Schork, S.M., Bee, G., Thumm, M., and Wolf, D.H. (1994a). Catabolite inactivation of fructose-1,6-bisphosphatase in yeast is mediated by the proteasome. FEBS Lett. *349*, 270–274.

Schork, S.M., Bee, G., Thumm, M., and Wolf, D.H. (1994b). Site of catabolite inactivation. Nature *369*, 283–284.

Schork, S.M., Thumm, M., and Wolf, D.H. (1995). Catabolite inactivation of fructose-1,6-bisphosphatase of *Saccharomyces cerevisiae*. Degradation occurs via the ubiquitin pathway. J. Biol. Chem. *270*, 26446–26450.

Schüle, T., Rose, M., Entian, K.D., Thumm, M., and Wolf, D.H. (2000). Ubc8p functions in catabolite degradation of fructose-1, 6-bisphosphatase in yeast. EMBO J. *19*, 2161–2167.

Smith, Q., Macklin, B., Chan, X.Y., Jones, H., Trempel, M., Yoder, M.C., and Gerecht, S. (2018). Differential HDAC6 activity modulates ciliogenesis and subsequent mechanosensing of endothelial cells derived from pluripotent stem cells. Cell Rep. *24*, 1930.

Subbotin, R.I. and Chait, B.T. (2014). A pipeline for determining protein-protein interactions and proximities in the cellular milieu. Mol. Cell Proteomics. *13*, 2824–2835.

Tarassov, K., Messier, V., Landry, C.R., Radinovic, S., Serna Molina, M.M., Shames, I., Malitskaya, Y., Vogel, J., Bussey, H., and Michnick, S.W. (2008). An *in vivo* map of the yeast protein interactome. Science *320*, 1465–1470.

Tevosian, S.G., Shih, H.H., Mendelson, K.G., Sheppard, K.A., Paulson, K.E., and Yee, A.S. (1997). HBP1: a HMG box transcriptional repressor that is targeted by the retinoblastoma family. Genes Dev. *11*, 383–396.

Texier, Y., Toedt, G., Gorza, M., Mans, D.A., van Reeuwijk, J., Horn, N., Willer, J., Katsanis, N., Roepman, R., Gibson, T.J., et al. (2014). Elution profile analysis of SDS-induced subcomplexes by quantitative mass spectrometry. Mol. Cell Proteomics *13*, 1382–1391.

Vogel, T.W., Manjila, S., and Cohen, A.R. (2012). Novel neurodevelopmental disorder in the case of a giant occipitoparietal meningoencephalocele. J. Neurosurg. Pediatr. *10*, 25–29.

Wang, W., Pan, K., Chen, Y., Huang, C., and Zhang, X. (2012). The acetylation of transcription factor HBP1 by p300/CBP enhances p16INK4A expression. Nucleic Acids Res. *40*, 981–995.

Wang, S., Livingston, M.J., Su, Y., and Dong, Z. (2015). Reciprocal regulation of cilia and autophagy via the MTOR and proteasome pathways. Autophagy *11*, 607–616.

Wheatley, D.N. (1995). Primary cilia in normal and pathological tissues. Pathobiology *63*, 222–238.

Wheatley, D.N., Wang, A.M., and Strugnell, G.E. (1996). Expression of primary cilia in mammalian cells. Cell Biol. Int. *20*, 73–81.

Yau, R. and Rape, M. (2016). The increasing complexity of the ubiquitin code. Nat. Cell Biol. *18*, 579–586.

Yu, H., Braun, P., Yildirim, M.A., Lemmens, I., Venkatesan, K., Sahalie, J., Hirozane-Kishikawa, T., Gebreab, F., Li, N., Simonis, N., et al. (2008). High-quality binary protein interaction map of the yeast interactome network. Science *322*, 104–110.

Zou, X.D., Hu, X.J., Ma, J., Li, T., Ye, Z.Q., and Wu, Y.D. (2016). Genome-wide analysis of WD40 protein family in human. Sci. Rep. *6*, 39262.

Bionotes

Huaize Liu
Martin Luther University Halle-Wittenberg, Institute of Physiological Chemistry, Hollystr. 1, D-06114 Halle, Germany
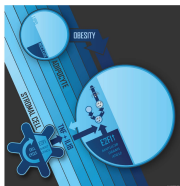
Huaize Liu carried out his Master's thesis on hedgehog signaling and sumoylation at Nanjing Medical University. At present he is a doctoral candidate supported by ProMoAge (GRK 2155) at Martin-Luther University Halle-Wittenberg, Germany. He joined the lab of Dr. Thorsten Pfirrmann and is focusing on GID-complex dependent ubiquitination and energy homeostasis regulation.

Thorsten Pfirrmann
Martin Luther University Halle-Wittenberg,
Institute of Physiological Chemistry,
Hollystr. 1, D-06114 Halle, Germany
thorsten.pfirrmann@medizin.uni-halle.de

Thorsten Pfirrmann studied Technical Biology at the University of Stuttgart, Germany, which spawned his keen and long-term interest in the ubiquitin modification system. He carried out his Master's (Diploma) work examining the *Saccharomyces cerevisiae* specific deubiquitinating enzyme Ubp6 in the laboratory of Rohan Baker at the John Curtin School of Medical Research, Canberra, Australia. In 2002, he returned to Stuttgart to join the laboratory of Dieter Wolf, where as a PhD student he and others discovered the Gid-complex. In 2006, he moved to Stockholm, Sweden for postdoctoral studies, and first worked in the laboratory of Maria Masucci at the Karolinska Institute. In 2008, he joined the laboratory of Per O. Ljungdahl at Stockholm University. Now he is interested in the function of the Gid/CTLH complex in higher vertebrates and runs a research group at the Martin-Luther University Halle-Wittenberg.

The GID ubiquitin ligase complex is a regulator of AMPK activity and organismal lifespan

Huaize Liu, Jie Ding, Karl Köhnlein, Nadine Urban, Alessandro Ori, Pablo Villavicencio-Lorini, Peter Walentek, Lars-Oliver Klotz, Thomas Hollemann & Thorsten Pfirrmann

RESEARCH PAPER

The GID ubiquitin ligase complex is a regulator of AMPK activity and organismal lifespan

Huaize Liu[a], Jie Ding[a], Karl Köhnlein[b], Nadine Urban[b], Alessandro Ori [c], Pablo Villavicencio-Lorini[d], Peter Walentek [e,f,g], Lars-Oliver Klotz[b], Thomas Hollemann[a], and Thorsten Pfirrmann[a]

[a]Institute of Physiological Chemistry, Martin-Luther University Halle-Wittenberg, Halle, Germany; [b]Institute of Nutritional Sciences, Friedrich Schiller University Jena, Jena, Germany; [c]Leibniz Institute on Aging, Fritz Lipmann Institute (FLI), Jena, Germany; [d]Institute of Human Genetics, Martin-Luther University Halle-Wittenberg, Halle, Germany; [e]Division of Genetics, Genomics and Development, Molecular and Cell Biology Department, University of California at Berkeley, Berkeley, USA; [f]Internal Medicine IV, Medical Center – University of Freiburg, Faculty of Medicine, University of Freiburg, Germany; [g]CIBSS – Center for Integrative Biological Signalling Studies, Albert Ludwigs University, Freiburg, Germany

ABSTRACT

The AMP-activated protein kinase (AMPK) regulates cellular energy homeostasis by sensing the metabolic status of the cell. AMPK is regulated by phosphorylation and dephosphorylation as a result of changing AMP/ATP levels and by removal of inhibitory ubiquitin residues by USP10. In this context, we identified the GID-complex, an evolutionarily conserved ubiquitin-ligase-complex (E3), as a negative regulator of AMPK activity. Our data show that the GID-complex targets AMPK for ubiquitination thereby altering its activity. Cells depleted of GID-subunits mimic a state of starvation as shown by increased AMPK activity and macroautophagic/autophagic flux as well as reduced MTOR activation. Consistently, gid-genes knockdown in *C. elegans* results in increased organismal lifespan. This study may contribute to understand metabolic disorders such as type 2 diabetes mellitus and morbid obesity and implements alternative therapeutic approaches to alter AMPK activity.

Abbreviations: ACTB: actin, beta; ADP: adenosine diphosphate; AMP: adenosine monophosphate; AMPK: AMP-activated protein kinase; ARMC8: armadillo repeat containing 8; ATP: adenosine triphosphate; BafA1: bafilomycin A_1; BCAA: branched chain amino acid; BICC1: BicC family RNA binding protein 1; BSA: bovine serum albumin; CAMKK2 kinase: calcium/calmodulin dependent protein kinase kinase 2, beta; CHX: cycloheximide; DMEM: Dulbecco's modified Eagle's medium; E1: ubiquitin-activating enzyme; E2: ubiquitin-conjugating enzyme; E3: ubiquitin ligase; ECAR: extracellular acidification rate; FACS: fluorescent associated cell sorter; FBP1: fructose-bisphosphatase 1; FCCP: carbonyl cyanide-4 (trifluoromethoxy) phenylhydrazone; G6P: glucose-6-phosphate; GDP: guanosine diphosphate; GFP: green fluorescent protein; GID: glucose induced degradation deficient; GMP: guanosine monophosphate; GTP: guanosine triphosphate; HBP1: high mobility group box transcription factor 1; HPRT: hypoxanthine guanine phosphoribosyl transferase; KO: knock out; LE: long exposure; MAEA: macrophage erythroblast attacher; MAP1LC3B/LC3B: microtubule-associated protein 1 light chain 3 beta; MKLN1: muskelin 1; mRNA: messenger RNA; MTOR: mechanistic target of rapamycin; NES: normalized enrichment score; OCR: oxygen consumption rate; PBS: phosphate buffered saline; PCK1: phosphoenolpyruvate carboxykinase 1, cytosolic; PCR: polymerase chain reaction; PFA: paraformaldehyde; RANBP9: RAN binding protein 9; RING: really interesting new gene; RMND5: required for meiotic nuclear division5 homolog; RPS6: ribosomal protein S6; RPTOR: regulatory associated protein of MTOR, complex 1; SE: short exposure; SEM: standard error of the mean; SQSTM1/p62: sequestosome 1; TSC2: tuberous sclerosis complex 2; TUBA4A: tubulin; TUBE: tandem ubiquitin binding entities; Ub: ubiquitin; UPS: ubiquitin proteasome system; WDR26: WD repeat domain 26; WT: wild type.

Introduction

The AMP-activated protein kinase (AMPK) is the key regulator of cellular energy homeostasis. AMPK is composed of a catalytic α-subunit, a regulatory β- and an adenosyl nucleotide-binding γ-subunit [1]. It is activated under energy-deprived conditions, when ATP is depleted and AMP levels are increased [2]. Among many AMPK-substrates, phosphorylation of RPTOR (regulatory associated protein of MTOR, complex 1) and TSC2 (TSC complex subunit 2) inhibit

MTOR signaling and regulate many processes including macroautophagy/autophagy.

Posttranslational modification of proteins with ubiquitin orchestrates a vast number of biological processes, including targeted protein degradation by the ubiquitin-proteasome system (UPS), lysosomal/vacuolar protein degradation, endocytosis, intracellular trafficking, regulation of the secretory pathway and transcriptional regulation [3]. Ubiquitination requires a sequential and hierarchical reaction of three enzyme classes,

---

the ubiquitin-activating enzyme (E1), the ubiquitin-conjugating enzyme (E2) and the substrate specific ubiquitin ligase (E3) [4]. The glucose-induced degradation deficient (GID)-protein complex is an evolutionarily highly conserved ubiquitin-ligase complex that regulates the metabolic switch from gluconeogenesis to glycolysis in *Saccharomyces cerevisiae* by targeting key enzymes of gluconeogenesis for 26S proteasomal degradation [5–8]. Individual subunits of the yeast GID-complex are conserved throughout the eukaryotic kingdom and Vid30/Gid1, Rmd5/Gid2, Vid24/Gid4, Vid28/Gid5, Gid7, Gid8 and Fyv10/Gid9 have their closest human orthologs in RANBP9 (RAN binding protein 9)-RANBP10, RMND5A (required for meiotic nuclear division 5 homolog A)-RMND5B, GID4 (GID complex subunit 4 homolog), ARMC8 (armadillo repeat containing 8), MKLN1 (muskelin 1) or WDR26 (WD repeat domain 26), GID8 (GID complex subunit 8 homolog) and MAEA (macrophage erythroblast attacher), respectively. These subunits are also part of the human GID-complex [9,10]. RMND5A protein of different species carries a non-canonical RING domain and is critical for ubiquitin ligase activity of the GID-complex *in vivo* and *in vitro* [8,11]. A recent publication describes the transcription factor HBP1 (HMG-box transcription factor 1) as a potential substrate of the murine GID-complex, suggesting a function in cell cycle control [12]. Additionally, the vertebrate GID-complex regulates renal gluconeogenesis via interaction with the protein BICC1 (BicC family RNA binding protein 1), suggesting a function in the regulation of cellular metabolism also in vertebrates [13].

In this context, we describe an ATP/AMP-independent regulation of AMPK activity, which depends on the ubiquitin-ligase function of the murine GID-complex. We found a decreased AMPK ubiquitination in *rmnd5a* knockout cells. These cells display a state of low energy with increased AMPK activity and autophagic flux but decreased MTOR activity. Concluding, we demonstrate that the murine GID-complex negatively regulates AMPK activity by ubiquitination. Consistently, knockdown of *gid*-genes extends both median and total lifespan in *Caenorhabditis elegans*.

Results

The GID-complex regulates autophagic flux and MTOR signaling

We decided to focus on RMND5A, because it is required for the ligase function of the vertebrate GID-complex [8,11]. In *S. cerevisiae*, the GID-complex regulates the metabolic switch from gluconeogenesis to glycolysis [6]. Since the MTOR signaling pathway controls such adaptation [14], we investigated whether the GID-complex affects MTOR signaling in vertebrates. To investigate a potential function of the GID-complex associated with MTOR signaling, we generated a NIH-3T3 *rmnd5a* knockout cell line using a CRISPR/CAS9-approach (*rmnd5a*-KO, hereinafter referred to as KO, and NIH-3T3 as WT). As depicted in Figure 1A, three sgRNA encoding plasmids were simultaneously transfected into WT cells (sense sequence: CATAGCAGTGTTTCTCGAGT; CATAGCCCA AAACAGTTCCT; CTACATCCAGCATTCCTTGT) and FACS sorted to obtain monoclonal cell lines. The collected KO cells have a 343 bp deletion positioned between 243 bp

and 587 bp (Figure 1A,B) leading to a nonsense frame shift mutation and a reduction in mRNA levels (Figure S1A,B). Expression of the *Rmnd5b* paralog was not affected by *rmnd5a* knockout (Figure S1C).

As a functional readout to assess MTOR signaling, we first measured the phosphorylation level of RPS6 (ribosomal protein S6; hereafter p-RPS6). Under nutrient-rich condition (high-glucose DMEM with 10% serum), p-RPS6 protein levels of WT and KO cells were similar (Figure 1C, compare lanes *1* and *2*). However, after starvation for 24 h (starvation condition: DMEM without glucose and serum) KO cells had a significantly decreased p-RPS6 protein level compared to the WT (Figure 1C, compare lanes *3* and *4*; Figure 1D, pink). These data show that a loss in GID-complex activity results in further reduction of MTOR activity when cells are deprived of glucose and serum. Decreased MTOR activity is associated with increased catabolic activity, such as autophagy, which is commonly assessed through detection of phosphatidylethanolamine modified MAP1LC3B (microtubule associated protein 1 light chain 3 beta; hereafter referred to as LC3; the phosphatidylethanolamine modified as LC3-II; the unmodified as LC3-I) level compared to the loading control [15]. Similar to a reduction in MTOR activity we observed higher levels of LC3-II in KO cells when cells were deprived of glucose and serum (Figure 1C,D, blue). In line with this notion, immunostaining of endogenous LC3 illustrated that KO cells contained more autophagosomes than WT cells (Figure 1E,F). As described previously, intracellular distribution of MTOR changes from a lysosome-associated to a cytosolic distribution upon e.g. amino acid starvation [16]. In KO cells, MTOR was mostly cytosolic and also resembled starvation conditions (Figure S4A). SQSTM1 (sequestosome 1) is an autophagic flux marker, which is specifically degraded by autophagy. Figure 1G revealed a lower basal level of SQSTM1 and a significantly faster SQSTM1 turnover in KO cells. The half-life of SQSTM1 in KO cells was reduced from 5.3 h to 1.8 h compared to the WT under starvation conditions (Figure 1H; compare black with red), revealing an enhanced autophagy-dependent degradation in KO cells. This faster turnover of SQSTM1 measured in KO cells was independent of proteasomal degradation but dependent on lysosomal degradation (Figure 1H; blue [MG132] and yellow [BafA1]).

The GID-complex regulates AMPK activity

To identify the trigger for the increased autophagic flux caused by *rmnd5a* knockout, we analyzed the activity of regulatory components in the AMPK-MTOR signaling axis by western blot analysis. Under nutrient-rich and more severe under starvation conditions, the protein levels of phosphorylated PRKAA/AMPKα at Thr172 (hereafter referred to as p-PRKAA) and 2 AMPK-substrates (p-RPTOR and p-TSC2 [Ser1387]; hereafter referred to as p-RPTOR and p-TSC2) were significantly increased in KO cells (Figure 2A; compare lane 2 and 4), suggesting an enhanced AMPK activity caused by RMND5A deficiency (Figure 2A,B), especially under starvation conditions. In contrast, neither PRKAA protein (Figure 2A) nor *Prkaa* mRNA level were severely affected by *rmnd5a* knockout (Figure S2B), indicating that the increase in AMPK activity was not due to an overall increase of PRKAA subunits, but due to a possible GID-dependent modification of PRKAA that regulates its activity.
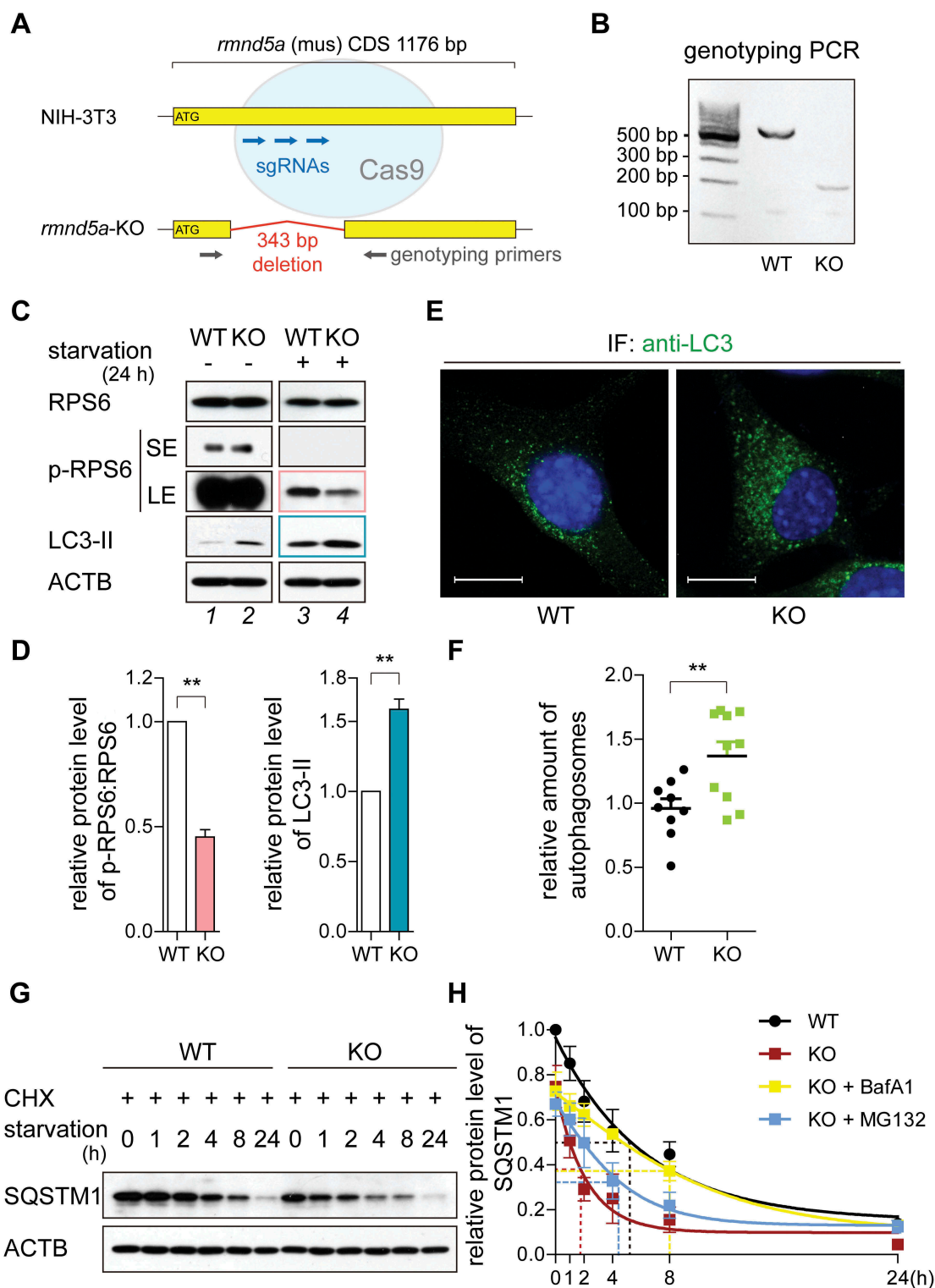
Figure 1. The GID-complex regulates autophagic flux and MTOR signaling. (A) Schematic representation of CRISPR-CAS9 generated *rmnd5a* (NCBI Reference Sequence: NM_024288.2) knockout mutant (*rmnd5a*-KO, hereinafter referred to as KO) in NIH-3T3 cells (hereinafter referred to as WT). Three sgRNA-targeting sites (blue) and a pair of genotyping primers (gray) are depicted. Oligonucleotide sequences are listed in Table 2. (B) genotyping PCR of KO. (C and D) Western blot of MTOR signaling and autophagy markers. Cells were grown on starvation medium (DMEM without glucose and serum; +) or DMEM (-) for 24 h. ACTB/β-actin as loading control. Quantification showing relative protein level of p-RPS6 compared with RPS6 (pink) and LC3-II compared with ACTB (blue). Unpaired t-test n = 3. **, P < 0.01. Abbreviations: p-, phosphorylated; SE, short exposure; LE, long exposure. (E and F) Representative confocal microscope images with autophagosomes (green). Cells were treated with Bafilomycin A1 (BafA1, 100 nM) for 4 h to block autophagosomes fusion with lysosomes. Autophagosomes were stained with anti-LC3B antibody. Scale bars, 10 μm. Quantification showing relative amount of autophagosomes (relative fluorescence area, left). Average values of WT are set to 1. Unpaired t-test n = 15. **, P < 0.01. (G and H) Western blot of SQSTM1 turnover. Cells were treated with cycloheximide (CHX, 100 μg/ml, protein synthesis inhibitor) for 24 h. ACTB/β-actin as loading control. Quantification showing relative protein level of SQSTM1 compared with ACTB. The half-life of SQSTM1 in WT cells (black), KO cells (red), KO cells treated with BafA1 (yellow) and KO cells treated with MG132 (blue) shown by dotted line (supplementary western blot shown in Figure S1D). WT cells at 0 h are set to 1.
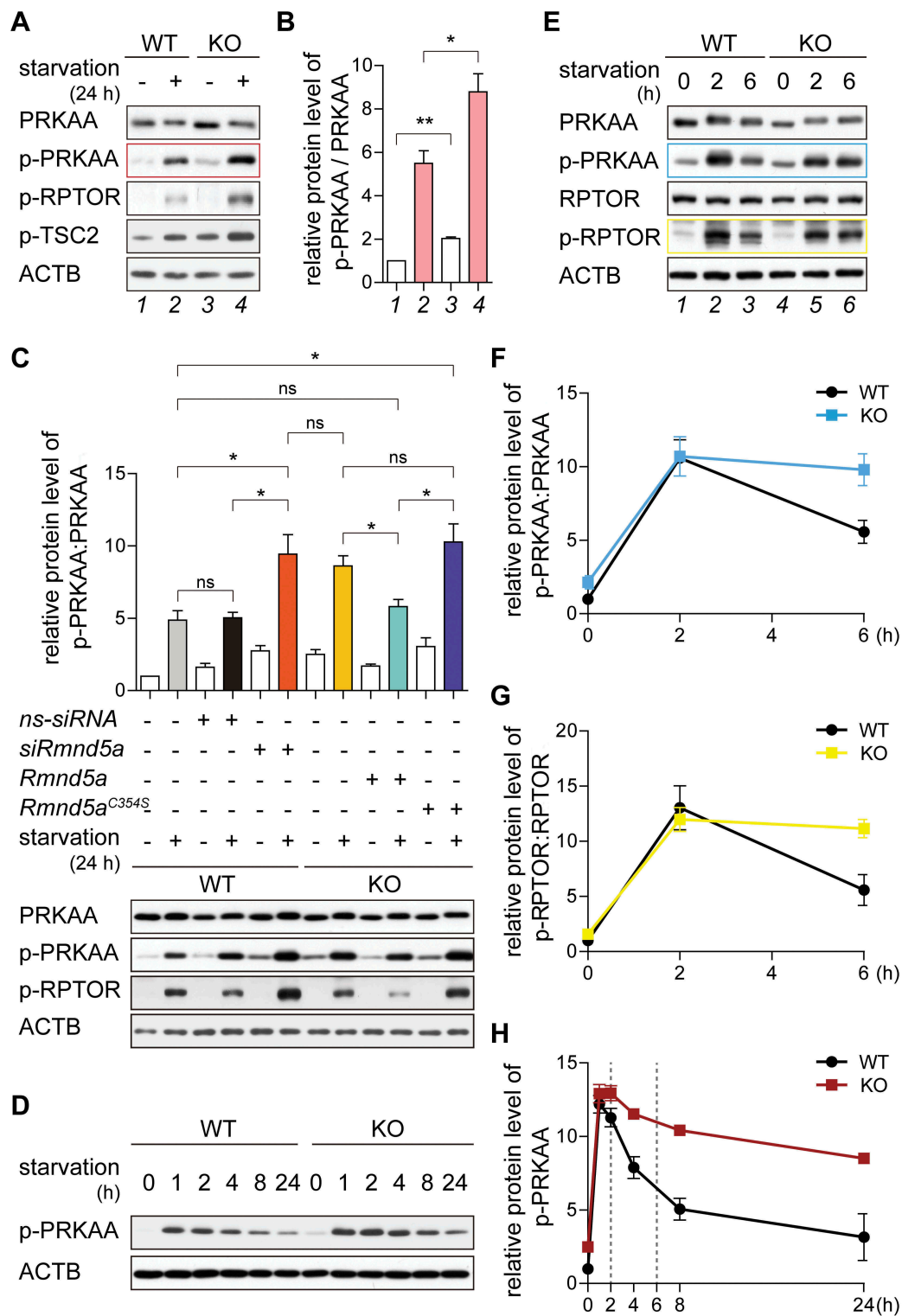
Figure 2. The GID-complex regulates AMPK activity. (A and B) Western blot of AMPK activity markers. Cells were grown on starvation medium (DMEM without glucose and serum; +) or DMEM (-) for 24 h. ACTB as loading control. Long exposure blot shown in Figure S2A. Quantification showing relative protein level of p-PRKAA compared with PRKAA (B). Unpaired t-test n = 3. *, P < 0.05; **, P < 0.01. (C) Western blot of AMPK activity markers. WT cells were transfected with siRNA against *Rmnd5a*. KO cells were transfected with plasmid encoding mouse *Rmnd5a* (NCBI Reference Sequence: NM_024288.2) or *Rmnd5a* RING domain C354S mutant (*Rmnd5a^C354S^*). After 24 h (plasmid) or 48 h (siRNA) of transfection, cells were subsequently starved for additional 24 h (+). ACTB as loading control. Quantification showing relative protein level of p-PRKAA compared with PRKAA. Unpaired t-test n = 3. *, P < 0.05. (D) Western blot of p-PRKAA. Cells were starved for 24 h and samples taken at indicated time points. ACTB as loading control. Quantification shown in (H). (E-G) Western blot of AMPK-MTOR signaling axis markers. Cells were starved for 6 h. ACTB as loading control. Quantification showing relative protein level of p-PRKAA compared with PRKAA (F), and p-RPTOR compared with RPTOR (G). WT cells at 0 h set to 1. Unpaired t-test n = 3. **, P < 0.01. (H) Quantification of (D) showing relative protein level of p-PRKAA compared to ACTB. WT cells at 0 h set to 1. Unpaired t-test n = 3. *, P < 0.05.

RMND5A contains a catalytically active RING domain, which possesses ubiquitin-ligase activity. To test whether RMND5A is a subunit of a *bona fide* ubiquitin ligase catalyzing PRKAA deactivation, we transfected the KO cells with plasmids encoding functional RMND5A (Figure 2C, green) or a functionally inactive RMND5A RING mutant (Figure 2C, purple). While functional RMND5A fully rescued the change in p-PRKAA and p-RPTOR levels (compare gray with green; not significant), the RING mutant failed to do so (compare gray with purple; $P < 0.05$), suggesting that the RING domain of RMND5A is important for AMPK activity regulation especially under starvation conditions. Specificity was further tested with nonspecific control siRNA (*ns-siRNA*) or siRNA to target *Rmnd5a* (*siRmnd5a*) and similar to the KO cells, *Rmnd5a* knockdown resulted in increased p-PRKAA and p-RPTOR levels especially after nutrient starvation (Figure 2C, compare black with red; $P < 0.05$). Together, these results suggest that enhanced AMPK activity is regulated by RMND5A ubiquitin ligase function especially at times of nutrient starvation.

To further experimentally address this time dependent deactivation of AMPK after nutrient starvation, we grew cells under nutrient-rich condition, shifted them to starvation medium and took samples at the indicated time points. In both WT and KO cells, PRKAA was rapidly phosphorylated within 1 h (Figure 2D, between 0 h and 1 h). In WT cells, phosphorylation of PRKAA decreased during further starvation (Figure 2D, WT between 1 h and 24 h), while the level of p-PRKAA was less reduced in KO cells (Figure 2D, KO between 1 h and 24 h). Differences in p-PRKAA levels were subtle in the first 2 h of starvation (Figure 2H; 2 h) but were significantly increased after 6 h of starvation (Figure 2H; compare WT and KO at 6 h). This suggests that the GID-complex plays a major AMPK regulatory function when cells are adapting to starvation conditions to decrease p-PRKAA during long-term starvation. To measure PRKAA activity at these times we focused our western blot analysis on these particular time points and calculated the PRKAA:p-PRKAA ratio (Figure 2E,F). Especially at the 6 h time point the activity of AMPK was significantly increased (Figure 2F, compare blue [KO] with black [WT] at 6 h), suggesting that AMPK activity is reduced especially at times of longer starvation most probably because of faster p-PRKAA turnover between 2 h and 6 h of starvation. This time-dependent change in p-PRKAA also affected its substrates, e.g. p-RPTOR (Figure 2E,G). We thus conclude that GID-activity is required to negatively regulate AMPK activity, especially after a longer period of nutrient starvation. GID-activity was dispensable for rapid deactivation of AMPK by dephosphorylation as a quick response to glucose supplementation (Figure S2D) further supporting a direct GID-dependent regulation of AMPK.

The GID-complex regulates the metabolic adaptation to cellular starvation independent of intracellular ATP levels

The activation of AMPK in response to ATP depletion activates fatty acid oxidation and inhibits biosynthetic pathways such as protein translation to conserve intracellular ATP levels [17]. In order to test whether the *rmnd5a* knockout would be sufficient to induce a similar adaptation, we compared the proteome of WT and KO cells by label-free quantitative mass spectrometry. Hierarchical clustering based on the

correlation between proteome profiles obtained from 3 biological replicates for each cell line revealed a distinct signature induced by the *rmnd5a* knockout (Figure 3A). We thus performed differential protein expression analysis and identified 254 protein groups affected in KO vs. WT cells (adj. $P < 0.01$) (Figure 3B). Consistent with a response to AMPK activation, gene set enrichment analysis revealed increased levels of proteins involved in fatty acid degradation and peroxisomal proteins, and decreased level of the protein synthesis machinery in KO cells (Figure 3C). These phenotypic changes were already measurable under nutrient-rich conditions but seem more pronounced at times of starvation.

AMPK activity is normally regulated by the AMP:ATP ratio in the cell, which depends on the efficiency of respiratory-chain or substrate level phosphorylation. Thus, we investigated whether RMND5A deficiency affected the production of ATP, e.g. by defects in glucose uptake. We assessed mitochondrial respiration and ATP production by measuring the oxygen consumption rate (OCR) (Figure 3E,F) and glycolytic function by measuring extracellular acidification rate (ECAR) (Figure 3G,H). The efficiency of these two major ATP generating pathways was not affected by GID-complex deficiency. Consistently, WT and KO cells contained similar ATP concentrations (Figure 3D). Quantitative metabolomics analysis for a subset of different metabolites further revealed that ATP, GTP and NADH levels were not altered in KO cells. Paradoxically, we also measured reduced AMP/ADP and GMP/GDP levels in KO cells reflecting a high cellular energy status (see Table 7). Concentrations of glucose 6-phosphate, fructose 6-phosphate and other glycolytic metabolites including the previously described allosteric AMPK regulator fructose 1,6-bisphosphate [18] were not significantly changed. Consistent with enhanced branched chain amino acid (BCAA) degradation in KO cells we measured significantly reduced concentrations of different amino acids like leucine, isoleucine and valine (see Table 7).

Together, we show that RMND5A deficiency results in the activation of metabolic pathways normally activated under nutrient deprived conditions. These include the increase of fatty acid and branched chain amino acid degradation, as well as a strong decrease in translational activity. Despite being consistent with increased AMPK activity, AMPK activation is independent of glycolysis and/or mitochondrial respiration, ATP:AMP ratio and fructose 1,6-bisphosphate levels in the cell. Our data strongly support that AMPK activity is directly regulated by the GID-complex independent of the ATP:AMP ratio and previously described allosteric AMPK regulators.

The GID-complex regulates AMPK activity via ubiquitination and proteasomal degradation

Since the RING domain of RMND5A was required for normal AMPK activation (Figure 2C, compare green and purple), we reasoned that p-PRKAA or PRKAA is regulated by GID-dependent ubiquitination and subsequent proteasomal degradation to adjust AMPK activity especially at times of nutrient starvation. To test this, we treated cells with the proteasome inhibitor MG132 and subsequently measured PRKAA and p-PRKAA protein level (Figure 4A). The untreated WT
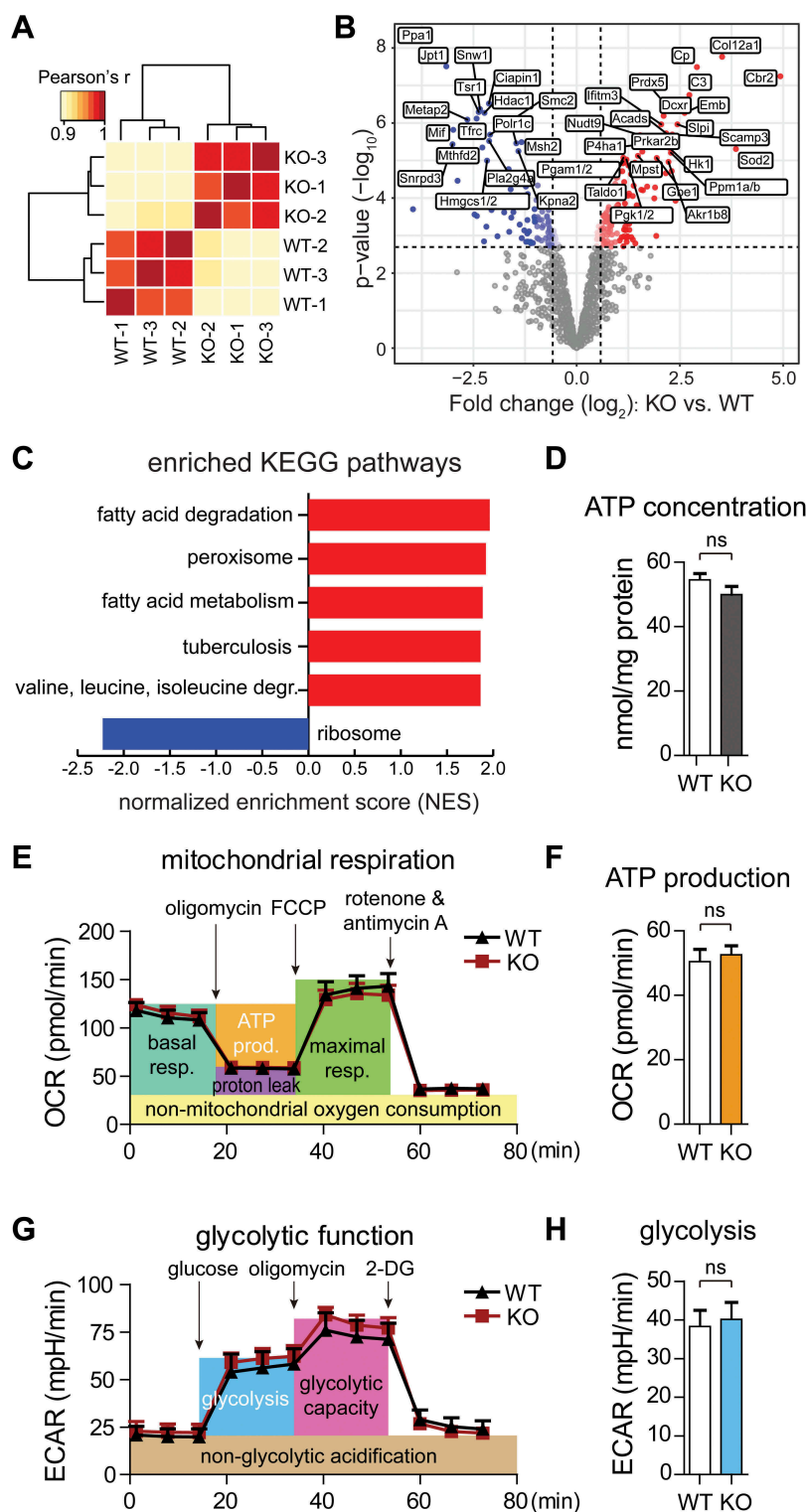
Figure 3. The GID-complex regulates the metabolic adaptation to cellular starvation independent of intracellular ATP levels. (A) Hierarchical clustering based on the correlation between proteome profiles based on 1207 protein groups quantified across the two cell lines. Three biological replicates were analyzed for each cell line. (B) Volcano plot depicting proteins differentially expressed between KO and WT cells. Significantly affected proteins (adj. P < 0.01) are displayed in red or blue according to whether they have higher or lower abundance in KO cells, respectively. Gene names of 40 most affected proteins (sorted by p value) are shown. (C) Gene set enrichment analysis was performed on proteomic data using KEGG pathways. Gene sets are plotted according to the Normalized Enrichment Score (NES) values. Positive and negative values are used for gene sets showing higher and lower abundance in KO cells, respectively. Only pathways significantly enriched (FDR < 0.1) are shown. (D) ATP concentration in WT and KO cells. Unpaired t-test n = 3. P = 0.1761. (E) Seahorse XF Cell Mito Stress Test. Mitochondrial respiration was assessed via oxygen consumption rate (OCR). Abbreviations: resp., respiration; prod., production. (F) Quantification of ATP production (orange area) showing no significant difference between WT and KO cells. Unpaired t-test n = 3. P = 0.3513. (G) Seahorse Glycolysis Stress Test. Glycolytic function was assessed via extracellular acidification rate (ECAR). (H) Quantification of glycolysis (the blue area) showing no significant difference between WT and KO cells. Unpaired t-test n = 3. P = 0.2533.
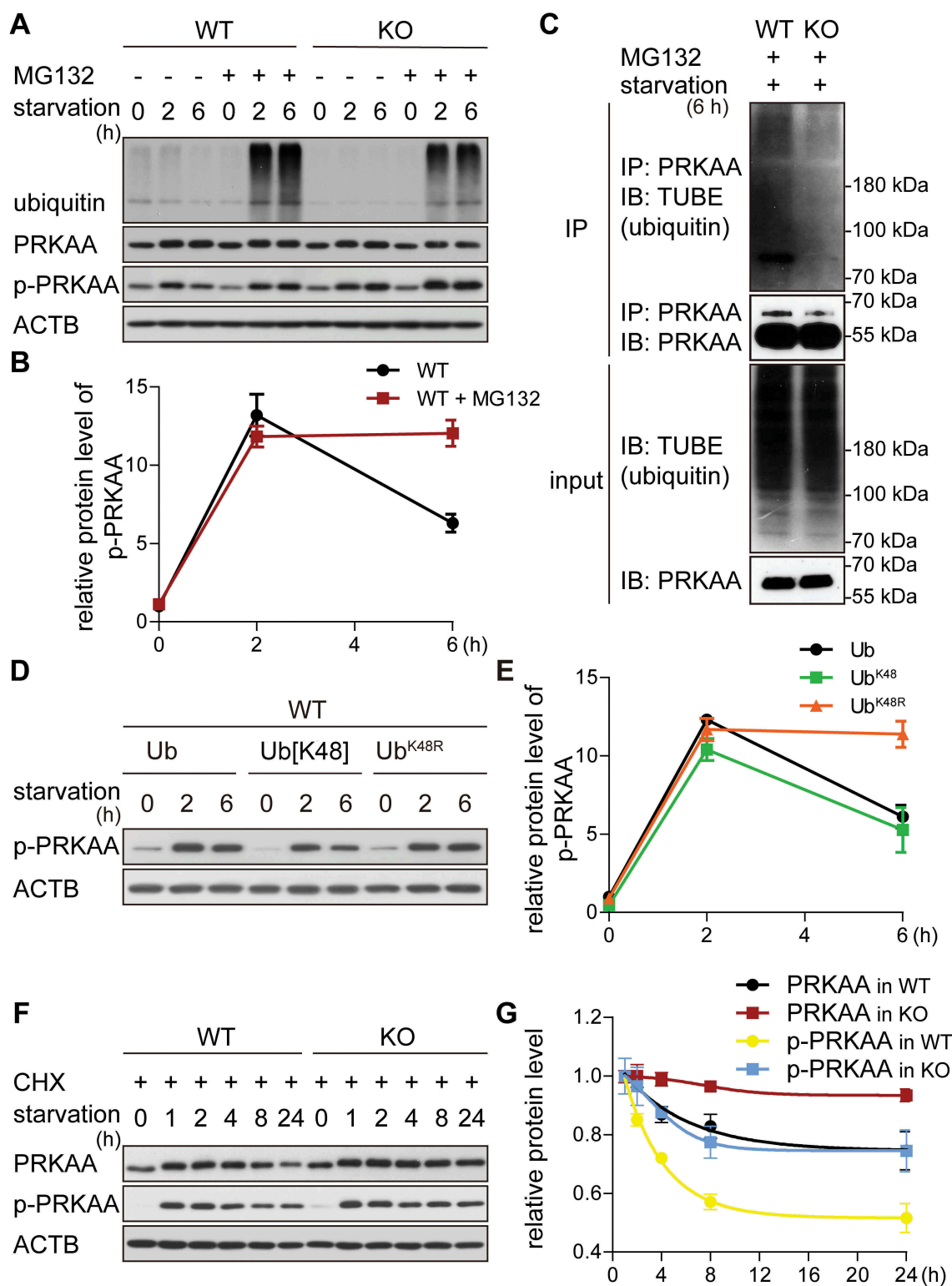
Figure 4. The GID-complex regulates K48-dependent polyubiquitination of AMPK. (A and B) Western blot of p-PRKAA. Cells were starved for 6 h with (+) or without (-) MG132 treatment (10 μM, proteasome inhibitor). ACTB as loading control. Quantification showing relative protein level of p-PRKAA compared to ACTB in WT cells. (C) Western blot of PRKAA ubiquitination. Cells were starved for 2 h, then treated with starvation medium containing MG132 for additional 4 h. Cell lysates were immunoprecipitated by anti-PRKAA antibody and immunoblotted with TUBE (high affinity ubiquitin binding peptide). (D and E) Western blot of p-PRKAA. WT cells transfected with different ubiquitin mutants for 24 h, then starved for 6 h. ACTB as loading control. Quantification showing relative protein level of p-PRKAA compared to ACTB. Abbreviations: Ub, wild-type ubiquitin; Ub[K48], ubiquitin with one lysine residue left at position 48; Ub^{K48R}, ubiquitin with K48R mutation. Plasmids shown in Table 3. (F and G) Western blot of PRKAA and p-PRKAA turnover. Cells were starved for 24 h and simultaneously treated with CHX. ACTB as loading control. Quantification showing relative protein level compared to ACTB. WT cells starved for 1 h are set to 1.

control cells showed decreased p-PRKAA and PRKAA protein levels after 6 h starvation (Figure 4B, DMSO between 2 h and 6 h). However, the inhibition of proteasome prevented this PRKAA:p-PRKAA decline (Figure 4B, MG132 between 2 h and 6 h). In contrast, this effect was not apparent in WT cells treated with the autophagy inhibitor bafilomycin A₁ (BafA1) (Figure S2E). This shows that PRKAA degradation after longer starvation is dependent on proteasomal but not lysosomal degradation, revealing that AMPK deactivation is not only regulated by dephosphorylation, but additionally by proteasomal degradation. It further implies that the degradation of PRKAA is particularly important to adjust AMPK activity at times of prolonged starvation, likely as an adaptation mechanism to reduce energy production via alternative sources e.g. amino acid degradation. Consistent with this hypothesis, both PRKAA and p-PRKAA turnover was significantly slowed down in KO cells compared to WT (Figure 4F,G). The specific reduction of p-PRKAA will affect PRKAA levels and the other way around. To critically test whether PRKAA or p-PRKAA is degraded by the proteasome we first measured PRKAA stability without prior phosphorylation under conventional nutrient rich growth conditions. Under these conditions PRKAA was a stable protein, suggesting that it is not degraded rapidly (Figure S3B). Additionally, we showed that a non-phosphorylatable T183A mutation (corresponds to Thr172 in humans) was stabilized upon longer starvation (Figure S3C). We thus reason that it is indeed p-PRKAA that is targeted by the GID-complex for proteasomal degradation.

To directly test for PRKAA ubiquitination, we immunoprecipitated endogenous PRKAA and subsequently measured ubiquitin modified PRKAA in WT and KO cells starved for 6 h (Figure 4C). Cell lysates (input) showed similar ubiquitination pattern (IB: TUBE) and similar PRKAA levels (IB: PRKAA) in both WT and KO cells. Ubiquitination of immunoprecipitated PRKAA (IP: PRKAA, IB: TUBE) revealed an ubiquitin specific band at around 75 kDa with the typical ubiquitin signal above in WT cells, indicating that PRKAA is indeed ubiquitinated. Interestingly, the ubiquitin pattern was strongly impaired in KO cells, suggesting that ubiquitination of PRKAA is dependent on GID-activity. Similar results were observed when cells were transiently transfected with plasmids encoding HIS-tagged ubiquitin and subsequently used for PRKAA immunoprecipitation (Figure S3A). Moreover, the immunoprecipitation of endogenous PRKAA from WT and KO cells after 6 h starvation resulted in the co-precipitation of at least 2 known subunits of the GID-complex, MKLN1 and RANBP10, specifically in KO cells (see Table 6) suggesting that p-PRKAA is directly ubiquitinated by the GID-complex.

Substrate polyubiquitination via the internal ubiquitin residue K48 is the most common modification that regulates UPS dependent degradation of substrates. To test this for p-PRKAA, we overexpressed different ubiquitin variants in WT cells and followed p-PRKAA protein levels like in previous experiments (Figure 4D). Transfection of wild-type ubiquitin (Ub) and ubiquitin with only one lysine residue located at position 48 (Ub[K48]) did not affect p-PRKAA protein levels at prolonged starvation (Figure 4D, Ub and Ub[K48]

between 2 h and 6 h). In contrast, transfection of ubiquitin with a K48R mutation (Ub^{K48R}) led to stabilization of p-PRKAA at the 6 h time point (Figure 4D, Ub^{K48R}), indicating that p-PRKAA turnover requires K48-dependent polyubiquitination. This treatment clearly phenocopies WT cells treated with MG132 (Figure 4B) and KO cells, suggesting that p-PRKAA turnover is regulated by GID-complex dependent K48 linked polyubiquitination and subsequent proteasomal degradation.

The GID-complex alters primary cilia length by regulating AMPK activity

Several publications describe a functional interplay between the AMPK-MTOR signaling axis and primary cilia length [19–21], e.g. cells treated with the MTOR inhibitor Rapamycin have elongated primary cilia [22]. Measuring primary cilia length can thus be used to assess AMPK-MTOR signaling activity. We started out to measure primary cilia length in WT cells, KO cells and WT cells transfected with *ns-siRNA*, siRNA against *Rmnd5a* (*siRmnd5a*) or siRNA against *Mkln1* (homologous gene of yeast *GID7*) (*siMkln1*). After treating the cells with cilia-inducing medium (high-glucose DMEM with 0.5% serum) for 24 h, we measured an average primary cilium length of 4.6 μm in WT cells and of 4.9 μm in WT cells transfected with *ns-siRNA* (Figure 5B). Consistent with increased AMPK activity, KO cells and WT cells with a *Gid* knockdown had significantly elongated primary cilia (Figure 5A,B) (KO, 5.4 μm; *siRmnd5a*, 5.5 μm; *siMkln1*, 5.6 μm). These data show that the depletion of different GID-subunits results in a significant elongation of primary cilia. To test whether this is dependent on AMPK activity, we mimicked cellular starvation by treating cells with Torin1 (MTOR signaling inhibitor) or *vice versa* mimicked a high energy status with Compound C (AMPK inhibitor) to subsequently measure primary cilia length [23,24]. Inhibition of MTOR signaling in WT cells led to a significant elongation of primary cilia (Figure 5C, compare lanes 1 and 2). On the other hand, inhibition of AMPK with Compound C led to shortened primary cilia (Figure 5C, compare lanes 1 and 3). This data indicates that AMPK and MTOR activity can influence primary cilium length. Similarly, cilia length was also altered in KO cells and treatment with Compound C led to a significant reduction of cilium length, clearly demonstrating that elongated cilia measured in KO cells are due to increased AMPK activity (Figure 5C, compare lanes 4 and 6). Neither the induction (Figure 5D) nor the blockade of ciliogenesis with *Ift88* specific siRNA (Figure 5E) affected AMPK activity, further supporting that AMPK activity is directly regulated by the GID-complex and not by upstream primary cilia dependent sensing and signaling processes.

Gid-complex proteins regulate organismal lifespan

Rapamycin is a specific inhibitor of MTOR activity and is known to alter organismal lifespan [25,26]. Our results show that depletion of GID-complex subunits similarly result in reduced MTOR activity and increased AMPK activity. Therefore, we planned to investigate an influence of reduced GID-complex activity on
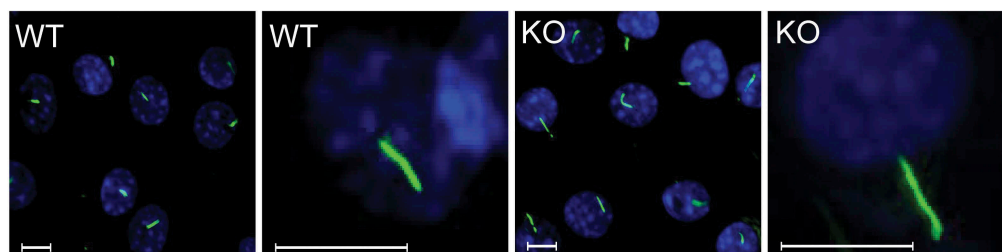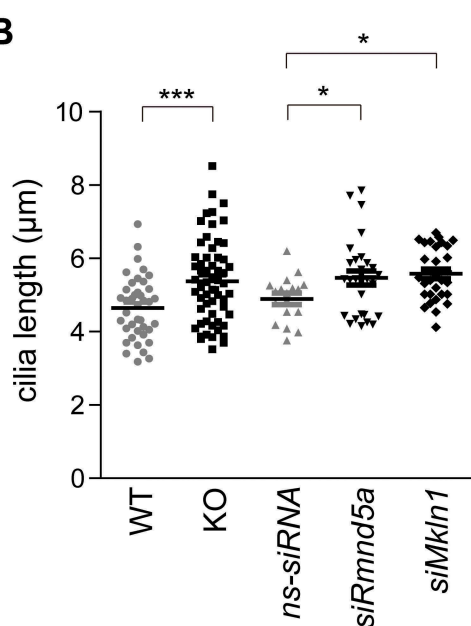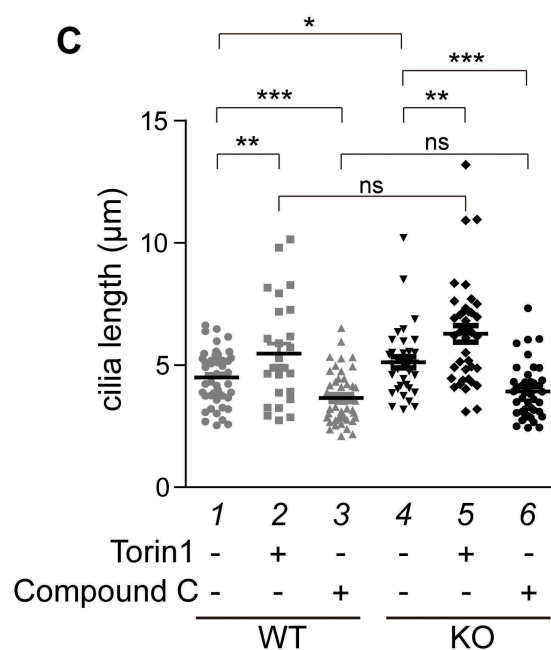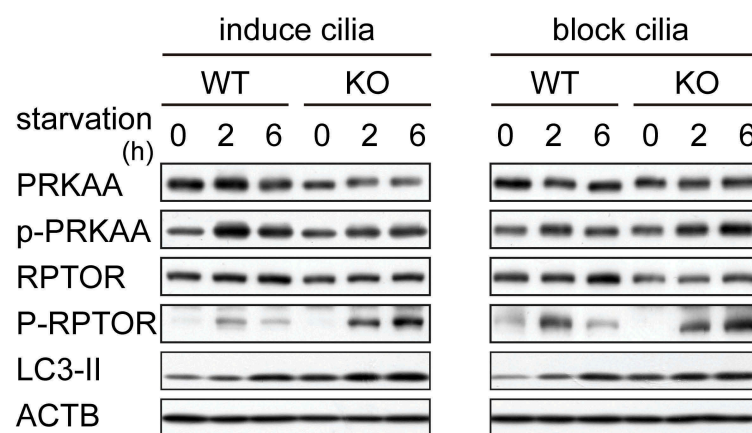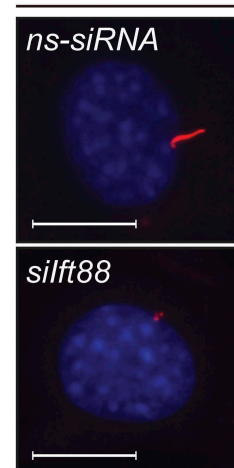
Figure 5. The GID-complex alters primary cilia length by regulating AMPK activity. (A) Representative microscope images of primary cilia. Cells were treated with cilia-inducing medium (high-glucose DMEM with 0.5% serum) for 24 h. Ciliary axoneme were stained with anti-acetylated TUBA4A (ac-tubulin) antibody (green). Scale bars, 10 μm. (B) Quantification of primary cilia length. Cells were transfected with *Rmnd5a* or *Mkln1* siRNA for 24 h, then treated with cilia-inducing medium for 24 h. Knockdown efficiency is shown in Figure S3D. Mean ± SEM of column: WT, 4.643 ± 0.1355 μm (n = 40); KO, 5.375 ± 0.1485 μm (n = 59); *ns-siRNA*, 4.894 ± 0.1559 μm (n = 17); *siRmnd5a*, 5.464 ± 0.1920 μm (n = 29); *siMkln1*, 5.574 ± 0.1325 μm (n = 30). Unpaired t-test, *, P < 0.05; ***, P < 0.001. Oligonucleotide sequences shown in Table 2. (C) Quantification of primary cilia length. Cells were treated with cilia-inducing medium containing Torin1 (1 μM, MTOR signaling inhibitor) or Compound C (10 μM, AMPK inhibitor) for 24 h. Mean ± SEM: WT with DMSO (control) 4.491 ± 0.1566 μm (n = 48); WT with Torin1, 5.472 ± 0.3986 μm (n = 27); WT with Compound C, 3.655 ± 0.1396 μm (n = 51); KO with DMSO 5.133 ± 0.2301 μm (n = 37); KO with Torin1, 6.275 ± 0.3337 μm (n = 40); KO with Compound C, 3.914 ± 0.1652 μm (n = 43). Unpaired t-test, *, P < 0.05; **, P < 0.01; ***, P < 0.001. (D) Western blot of AMPK markers. Cells were treated with cilia-inducing medium for 24 h to induce ciliogenesis, afterward shifted to starvation medium for 6 h. ACTB as loading control. (E) Like (D), with previous transfection of siRNA against *Ift88* (*Mus musculus*, NM_009376.2) for 24 h to block cilia formation. (F) Representative microscope images of primary cilia. WT cells were transfected with siRNA against *Ift88*. Ciliary axoneme was stained by anti-ac-tubulin antibody (red). Scale bars, 10 μm.

Table 1. Proteins of the Gid-complex with accession numbers and protein domains.

S. cerevisiae	H. sapiens	Domains	Accession Nr.	C. elegans
Gid1	RANBP9 RANBP10	SPRY, LisH, CTLH, CRA	NM_005493	Y54E5A.7
Gid2/Rmd5	RMND5A RMND5B	LisH, CTLH, RING	NM_022780	T07D1.2
Gid4	GID4	-	NM_024052	-
Gid5	ARMC8	ARM	NM_213654	-
Gid7	MKLN1	LisH, CTLH, WD40 or Kelch	NM_013225	Y39H10A.6 (Y39H10A_224B)
Gid8	GID8	LisH, CTLH, CRA	NM_017896	F53E2.1
Gid9	MAEA	LisH, CTLH	BC001225	-

organismal lifespan. A classical model organism to investigate organismal lifespan is the nematode *C. elegans*. Since the members of the GID-complex are even conserved in *C. elegans* (Table 1), we knocked down *t07d1.2* (homologous gene of *Gid2/Rmd5a*) and measured lifespan of *C. elegans*. Strikingly, the knockdown of *t07d1.2* led to a significant extension of both the median (50% survival) and maximum (10% survival) lifespan when compared to the empty vector control (Figure 6A, compare red and black curves). The maximum lifespan in the knockdown group was elongated to 24.8 d compared to the control (18.4 d) with an extension of 6.4 d (for statistical details see Table 5 and Table 5 footnote "a,b,c"). Similarly, the individual knockdown of all other conserved GID-subunits in this organism led to a significant extension of both median and maximum lifespan (Figure 6A and Table 5). The knockdown quality was assessed by qPCR and is shown in Figure S3E. Our data strongly suggest that GID-complex deficiency also causes AMPK activation in *C. elegans*, thereby resulting in lifespan extension.

Discussion

In *S. cerevisiae* the GID-complex regulates the metabolic switch from gluconeogenesis to glycolysis by directly targeting key enzymes of gluconeogenesis for polyubiquitination and subsequent proteasomal degradation. Yeast GID-complex substrates include fructose-1,6-bisphosphatase (Fbp1), malate-dehydrogenase (Mdh2) and phosphoenolpyruvat-carboxykinase (Pck1) [8,9]. Recent publications also describe the human GID-complex in the context of regulating renal gluconeogenesis [13]. However, human FBP1 (fructose-bisphosphatase 1) and PCK1 (phosphoenolpyruvate carboxy-kinase 1) are not direct substrates of the GID-complex in vertebrate cell systems and *in vitro* [12]. This suggests a more complex function of the vertebrate GID-complex in the regulation of metabolism, which may be mediated by other well-known regulators. For instance, AMPK is known to control gluconeogenesis by regulating the transcription of PCK1 and G6PC (glucose-6-phosphatase) in the liver [27].

In this manuscript we show that lack of GID-complex activity results in distinct phenotypic changes consistent with a response to AMPK activation. This includes an increase in autophagic flux, branched chain amino acid (BCAA) and fatty acid degradation, a reduction in MTOR activity, longer primary cilia and significant life span extension. We provide strong evidence that these changes are due to direct ubiquitination of PRKAA in a GID-complex dependent manner. We show that the GID-
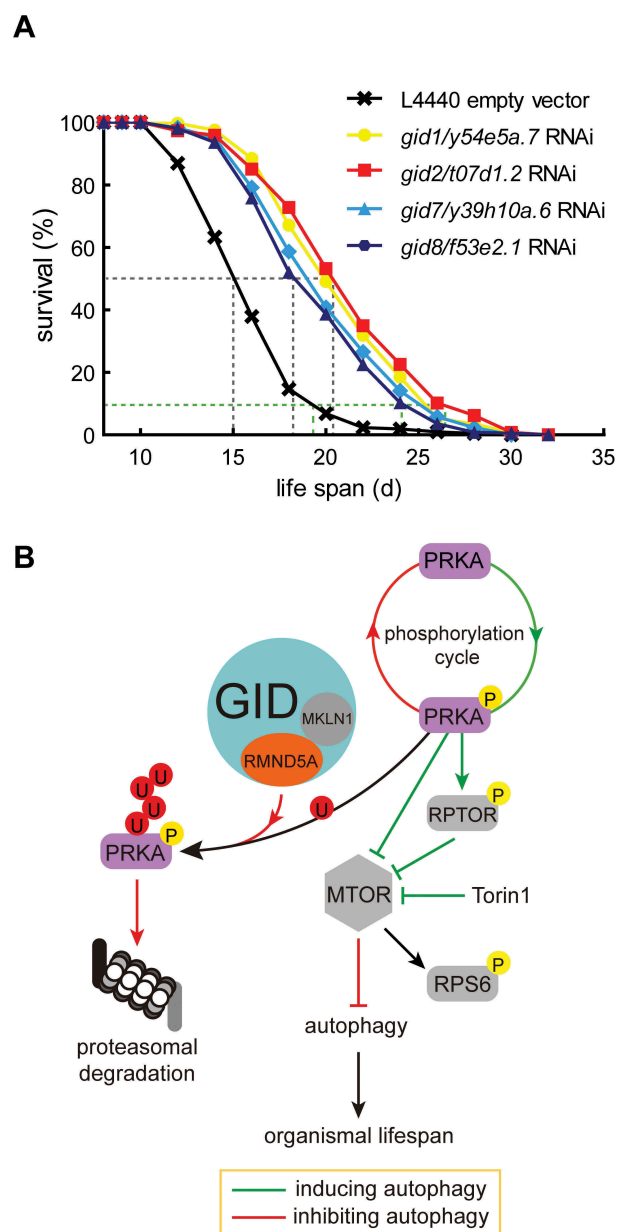
Figure 6. GID-complex proteins regulate organismal lifespan. (A) Survival rates of *C. elegans* depleted of *Gid* orthologs (*gid1/y54e5a.7, gid2/t07d1.2, gid7/y39h10a.6, gid8/f53e2.1*) through RNAi. Experiments were conducted in quintuplicates and were performed two independent times (details in Table 5). One representative experiment is shown. Log-rank test, p < 0.0001. Knockdown efficiency shown in Figure S3E. (B) Model of GID-complex dependent regulation of AMPK activity. The GID-complex as a negative regulator of AMPK activity to adjust AMPK activity at times of prolonged starvation. p-AMPK activity is adjusted by K48-dependent polyubiquitination and subsequent proteasomal degradation. This process is disturbed when cells are lacking GID-complex activity, resulting in increased AMPK activity, reduced MTOR activity and increased autophagic flux.

complex binds PRKAA only in KO cells (see Table 6) and depletion of GID-subunits results in lack of PRKAA ubiquitination and stabilization of p-PRKAA (Figure 4C, S3A and 4F). In *S. cerevisiae* the deletion of Rmd5p allows the association of other Gid-subunits but prevents substrate polyubiquitination and subsequent degradation [28]. Given the high degree of topological conservation [12] we predict that deletion of RMND5A similarly results in an intact GID-complex that binds AMPK but cannot ubiquitinate it for subsequent

degradation ultimately resulting in increased AMPK activity (p-PRKAA levels). This phenomenon was mostly dependent on glucose starvation (Figure S2H and S2F).

Several publications describe AMPK regulation by ubiquitin modification with at least two different functional outcomes. On the one hand, there is evidence that ubiquitination of PRKAA has a negative regulatory function independent of its degradation. The deubiquitinating enzymes USP10 and USP9X are involved in this process [29,30]. On the other hand the MAGEA3/A6-TRIM28 ubiquitin ligase complex downregulates AMPK through ubiquitination and degradation, however only in the context of cancer [31]. Taken together, the existence of several types of ubiquitin modifications on AMPK subunits differing both in linkage type and/or modified AMPK subunits are likely to exist. Our data is consistent with GID-complex catalyzed PRKAA ubiquitination that specifically induced the degradation of p-PRKAA after prolonged glucose starvation. Interestingly, downregulation of p-PRKAA was previously described in rat muscles incubated with glucose or leucine [32]. Together, we like to predict that this process is a response to a shift in energy balance to prevent ongoing autophagy at times of prolonged starvation. We further speculate that similar to MTOR regulation [33] this process constitutes a response to e.g. free amino acids generated by autophagy.

It is difficult to distinguish between GID-complex dependent p-PRKAA and PRKAA turnover. However, our data support that specifically p-PRKAA levels are temporally controlled by glucose starvation. Firstly, the most distinct phenotypes were measured when p-PRKAA levels are high (after 2 h of starvation). Furthermore, non-phosphorylated PRKAA was stable when cells were not starved (Figure S3B). Finally, a T183A mutation of the phosphorylation site (corresponding to T172 in human) resulted in stabilization of PRKAA upon starvation (Figure S3C). Together our results suggest that the GID-complex specifically ubiquitinates p-PRKAA but not unphosphorylated PRKAA for subsequent proteasomal degradation upon long-term starvation.

Several AMPK upstream activators have been described in the literature, e.g. phosphorylation of Thr172 in the activation loop of PRKAA can be mediated by STK11 directly, or in response to calcium flux via CAMKK2 kinase (calcium/calmodulin dependent protein kinase kinase 2) [34]. This phosphorylation step requires high levels of AMP that binds to the γ-subunit of AMPK and subsequently induces a structural change that leads to the exposure of the phosphorylation site. We measured induction of Thr172 phosphorylation upon glucose/serum starvation in both WT and KO cells (Figure 2E, between 0 h and 2 h), suggesting that GID-activity neither affects phosphorylation of PRKAA nor the induction of the active conformational change. Further, we measured similar ATP and decreased AMP levels in KO cells suggesting that AMPK activity is deregulated by different mechanisms (see Table 7 and Figure 3D). Similarly, we can exclude defects in PRKAA dephosphorylation as an explanation for AMPK hyperactivation, because glucose/serum supplementation in both WT and KO cells led to rapid PRKAA dephosphorylation (Figure S2D). These observations suggest that upstream glucose sensing and signaling of AMPK

regulating pathways are still functional in KO cells and further support that the GID-complex directly modifies AMPK activity.

Changes in the AMPK-MTOR signaling axis, like we measured in GID-subunit-depleted cells, are known to alter lifespan in various organisms [35–37]. Consistently, our results showed that individual depletion of all tested GID-subunits resulted in an extended lifespan of *C. elegans*. This observation additionally supports that the GID-complex integrates intracellular signals to regulate AMPK activity in order to adjust cell metabolism to energy expenditure.

Ubiquitin ligases are promising drug targets to treat different pathologies [38]. Thus we like to suggest that inhibition of the GID-complex is a promising strategy for pharmacological manipulation of the AMPK-MTOR signaling axis to treat chronic conditions like polycystic kidney diseases [39], type 2 diabetes [40,41] or to alter organismal longevity [42].

Materials and methods

Organisms and maintenance

NIH-3T3 cells (ATCC, CRL-6442, RRID:CVCL_0594) were maintained in Dulbecco's modified Eagle's medium with 4500 mg/L glucose (high concentration) (Sigma-Aldrich, D6546) or without glucose (no glucose) (Gibco, 11966–025) supplemented with 10% (v:v) fetal calf serum (FCS) (Gibco, 10270–106) if not mentioned otherwise. A *rmnd5a* knockout cell line was constructed as depicted in Figure 1A. Briefly, CRISPR/CAS9 plasmids were ordered from Santa Cruz Biotechnology (sc-427065), transfected with Lipofectamine 2000 (Thermo Fisher Scientific, 11668019) and individual GFP-positive clones sorted into 96-well plates. Positive *rmnd5a* knockout clones were selected by genotyping PCR with primers listed in Table 2. The *C. elegans* strain wild-type Bristol N2 was provided by the Caenorhabditis Genetics Center that is supported by the National Institutes of Health-Office of Research Infrastructure Programs. For RNAi knockdown experiments *E.coli* HT115 *f53e2.1* and *y39h10a.6* clones were derived from an Ahringer RNAi library (Source BioScience [43],). *t07d1.2* and *y54e5a.7* were derived from Vidal ORFeome RNAi libraries (Source BioScience) [44].

Plasmids and oligonucleotides

cDNA of *Rmnd5a* variants (NCBI Reference Sequence: NM_024288.2) were synthesized by BioCat. Transfections were performed using Lipofectamine 2000 for plasmids and Lipofectamine RNAiMAX (Thermo Fisher Scientific, 13778–075) for siRNAs. Site directed mutagenesis was performed as described previously [45]. All other plasmids and oligonucleotides are listed in Tables 2 and 3.

Western blotting and immunoprecipitation

Western blotting was performed as described previously [8]. Cells were lysed with 50 mM Tris-HCl, pH 7.4, 2 mM EDTA, 1 mM EGTA, 50 mM NaF, 1 mM DTT, 10 mM Na4P$_2$O$_7$, 1 mM Na$_3$VO$_4$, 1% Triton X-100 (Serva, 37238), 0.1% SDS,

Table 2. Oligonucleotides used in this study.

Oligonucleotide	Description	Sequence
Rmnd5a (mm) fwd	genotyping PCR	TTGTTCTGACACAGTGCTGC
Rmnd5a (mm) rev	genotyping PCR	ACACGAGGCTTCCCATCAAT
Hprt (mm) fwd	qPCR	TACAGGCCAGACTTTGTTGG
Hprt (mm) rev	qPCR	AACTTGCGCTCATCTTAGGC
Mkln1 (mm) fwd	qPCR	TGTGGATCATTCGGACCCAG
Mkln1 (mm) rev	qPCR	TCTGAAAAGCCTAGAGCTGTGA
Rmnd5a (mm) fwd #1	qPCR	CAGCCAACGGCTTCTCAATG
Rmnd5a (mm) rev #1	qPCR	GACAGACCAGATTCCTGGCA
Rmnd5a (mm) fwd #2	qPCR	GCCTGTCCCATTCTTCGTCA
Rmnd5a (mm) rev #2	qPCR	GGACTCTGTTCCATTGGGCA
Rmnd5b (mm) fwd	qPCR	GTGGGCCAGCTGAGAGC
Rmnd5b (mm) rev	qPCR	AGCACTGGGACATCACAAGG
siMkln1 (mm) #1	siRNA	CACUUCAGACAACAUAACU
siMkln1 (mm) #2	siRNA	AGUUAUGUUGUCUGAAGUG
siRmnd5a (mm) #1	siRNA	CAGGCUGAUGUGAGAAUGAAA
siRmnd5a (mm) #2	siRNA	UUGGUUUGUGGUCAUAUUAUA
siIft88 (mm) #1	siRNA	ACUGGGAGAGUUAUACGAU
siIft88 (mm) #2	siRNA	AUCGUAUAACUCUCCCAGU
sgRmnd5a (mm) seq #1	sgRNA	CATAGCAGTGTTTCTCGAGT
sgRmnd5a (mm) seq #2	sgRNA	ACAAGGAATGCTGGATGTAG
sgRmnd5a (mm) seq #3	sgRNA	CATAGCCCAAAACAGTTCCT
Prkaa1 (mm) fwd	qPCR	GTCAAAGCCGACCCAATGATA
Prkaa1 (mm) rev	qPCR	CGTACACGCAAATAATAGGGGTT
Prkaa2 (mm) fwd	qPCR	AAGATCGGACACTACGTCCTG
Prkaa2 (mm) rev	qPCR	TGCCACTTTATGGCCTGTCAA
tba1 (ce) fwd	qPCR	TCAACACTGCCATCGCCGCC
tba1 (ce) rev	qPCR	TCCAAGCGAGACCAGGCTTCAG
gid1/y54e5a.7 (ce) fwd	qPCR	ACGTAACCTATTCACCGGTTGG
gid1/y54e5a.7 (ce) rev	qPCR	CTCGAGAATCATTTTCCGGACG
gid2/t07d1.2 (ce) fwd	qPCR	TGACGAGCAAGGAAGTAGCTG
gid2/t07d1.2 (ce) rev	qPCR	CAAGCCCGAATTGCGTTGAC
gid7/y39h10a.6 (ce) fwd	qPCR	TTCGTTCATCGCAGTGGACA
gid7/y39h10a.6 (ce) rev	qPCR	CGGTTTCTTTTCCAATCGAGCC
gid8/f53e2.1 (ce) fwd	qPCR	ATCCGAACGAGAACAGACGG
gid8/f53e2.1 (ce) rev	qPCR	GCGAACATCCCGTAAAAGCG
AMPK^{T183A}	Mutagenesis	CAGATGGTGAATTTTTAAGAGCAAGCTGTGGCTCACCCAATTATG

Table 3. Plasmids used in this study.

Name	Source
pPRKAA1/pAMPKα$_1$	Addgene, 27,297
pPRKAA1^{T183A}/pAMPKα$_1$^{T183A}	This work
Flag-HA-USP10	Addgene, 22,543
pcDNA3.1(+)-Rmnd5a (mm)	synthetic construct
pcDNA3.1(+)-Rmnd5a^{C354S} (mm)	synthetic construct
pRK5-HA-Ubiquitin-WT	Addgene, 17,608
pRK5-HA-Ubiquitin^{K48}	Addgene, 17,605
pRK5-HA-Ubiquitin^{K48R}	Addgene, 17,604

Table 4. Antibodies used in this study.

Antibody	Source	Order number
ac-TUBA4A/tubulin	Sigma-Aldrich	T6793
RPS6/S6 Ribosomal Protein	Cell Signaling Technology	2317
p-RPS6/S6 Ribosomal Protein	Cell Signaling Technology	2211
MAP1LC3B	Cell Signaling Technology	2775
ACTB/β-actin	Sigma-Aldrich	A-5441
SQSTM1	Cell Signaling Technology	5114
PRKAA/AMPKα	Cell Signaling Technology	2532
p-PRKAA/AMPKα (T172)	Cell Signaling Technology	2535
RPTOR/Raptor	Cell Signaling Technology	2280
p-RPTOR (Ser792)	Cell Signaling Technology	2083
p-TSC2 (Ser1387)	Cell Signaling Technology	5584
ubiquitin	Thermo Fisher Scientific	PA3-16,717
TUBE	LifeSensors	UM302

0.5 mM PMSF (Roche, 837091), 1× protease inhibitor cocktail (Roche, 11836153001). Protein was determined with the BCA assay (Thermo Fisher Scientific, 23227) and loaded 6 ~ 20 µg per lane. Antibodies are listed in Table 4. For signal quantification, X-ray films were scanned in the transparency mode and saved as 600 dpi tiff images. Densitometry was performed with the ImageJ software (NIH) of short exposure signals (SE) using the rectangular area selection tool. Background signals were subtracted and relative protein levels were compared with the loading control (ACTB/β-actin). For IP experiments, we used µMACS Protein A MicroBeads (Miltenyi Biotec, 130-071-001). For each IP setup, 3 µl of anti-PRKAA/AMPK antibody (Cell Signaling Technologies, 2532) was incubated with 1 ml of cell lysate (1.5 mg/mL) at 4°C overnight then incubated for additional 1 h and eluted according to the protocol provided by the manufacturer.

cDNA synthesis and quantitative PCR (qPCR)

RNA was extracted by using the RNeasy Kit (Qiagen, 74104). 1 µg RNA were reverse transcribed into cDNA in a 10 µl reaction set by using HiScript II Q RT Supermix for qPCR (Vazyme Biotech, R222). A 20 µl qPCR reaction set contained 20 ng cDNA, 1× Maxima SYBR Green/ROX qPCR Master Mix (Thermo Fisher Scientific, K0221), 0.3 µM forward primer, and 0.3 µM reverse primer. A qPCR run on Roche LightCycler 480 II consisted of an UDG pre-treatment for 2 min at 50°C, an initial hot start for 10 min at 95°C, followed by 40 cycles with a denaturation step of 15 s at 95°C and an annealing/extension step of 60 s at 60°C. Afterward, a melt curve was recorded. Each measurement was repeated three times, and each sample was analyzed in triplicate with *Hprt* (hypoxanthine guanine phosphoribosyl transferase) as an internal control. qPCR primers are listed in Table 2. Relative expression was determined using the Abs Quant/2nd Derivative

Table 5. Statistics for RNAi knockdown of Gid orthologs in *C. elegans*.

Exp	Strain/plasmid for RNAi	Effect on Life Span	P (vs. Ctrl)	Mean Life Span (days ± 2SEM)	Mean Life Span (%)	1Max Life Span (days ± 2SEM)	Max Life Span (%)	No of uncensored worms
#1 Figure 6A,B	N2/ L4440			16.4 ± 0.3	100	18.4 ± 0.4	100	210
	N2/ f53e2.1	↑	****	19.9 ± 0.3	121.4	22.8 ± 0.5	123.9	359
	N2/ t07d1.2	↑	****	21.6 ± 0.3	131.4	24.8 ± 0.5	134.8	358
	N2/y39h10a.6	↑	****	20.5 ± 0.3	124.6	23.2 ± 0.5	126.1	347
	N2/y54e5a.7	↑	****	21.3 ± 0.3	129.5	23.6 ± 0.4	128.3	351
#2	N2/ L4440			15.5 ± 0.2	100	17.2 ± 0.8	100	137
	N2/ f53e2.1	↑	****	20.7 ± 0.3	133.3	23.6 ± 0.4	137.2	252
	N2/ t07d1.2	↑	****	22.6 ± 0.2	153.5	26.4 ± 0.7	145.6	267
	N2/y39h10a.6	↑	****	22.1 ± 0.2	142.8	25.5 ± 0.4	148.3	256
	N2/y54e5a.7	↑	****	23.0 ± 0.3	148.1	27.4 ± 0.4	159.3	266

[a] 75% quantile
[b] SEM standard error of the mean of 5 technical replicates
[c] Control: N2/L4440; **** P < 0.0001

Table 6. Peptides and protein IDs of GID-complex subunits identified after PRKAA/AMPK immunoprecipitation in KO cells.

Protein name	MW (kDa)	Peptide	FDR value	Gel mass range (kDa) 30–65	65–100
sp/Q6VN19	67.188	AAATADPGAGNPQAGDSSGGDSGGGLPSPGEQELSR	< 0.1%		*
GID1/RanBP10		ELQALSEQLGR	< 0.1%		*
sp/089050	84.88	WSSFSSTYLPENILVDKPNDQSSR	< 0.1%		*
GID7/MKLN1		ATIDPELNEIHVLSGLSK	< 0.1%		*

Table 7. Absolute concentration of metabolic compounds in WT and KO cells.

Compound name	WT Mean concentration (n = 3) (pmol/10^6 cells) Mean	S.D.	KO Mean concentration (n = 3) (pmol/10^6 cells) Mean	S.D.	KO vs WT Ratio [a]	p-value [b]
Glucose 6-phosphate	34	6.0	38	1.2	1.1	0.340
Fructose 6-phosphate	11	4.5	12	0.7	1.1	0.712
Fructose 1,6-diphosphate	247	127	373	43	1.5	0.221
Glyceraldehyde 3-phosphate	34	25	31	5.9	0.9	0.880
Dihydroxyacetone phosphate	143	78	147	32	1.0	0.933
Glycerol 3-phosphate	69	19	64	6.6	0.9	0.723
2,3-Diphosphoglyceric acid	17	1.4	18	0.4	1.1	0.381
Valine	2541	273	1896	166	0.7	0.034 *
Leucine	2176	211	1581	137	0.7	0.020 *
Isoleucine	2346	260	1681	121	0.7	0.031 *
Tryptophan	182	12	71	6.3	0.4	8.6E-04 ***
Lysine	1041	127	1102	36	1.1	0.497
ATP	5270	547	5336	297	1.0	0.867
ADP	777	67	436	33	0.6	0.005 **
AMP	156	16	64	4.7	0.4	0.006 **
GTP	927	72	906	73	1.0	0.743
GDP	106	6.6	59	2.1	0.6	0.004 **
GMP	25	2.6	12	0.9	0.5	0.008 **
NAD+	722	83	711	74	1	0.871
NADH	64	19	45	6.2	0.7	0.226

[a] The ratio is computed by using averaged detection values. The latter was used as denominator.
[b] The p-value is computed by Welch's t-test (*<0.05, ** <0.01, *** <0.001)

Max analysis method, given as mean ± SEM, statistic analyzed by t-test and measured by two-tailed P value.

Immunofluorescence

Cells were grown on Millicell EZ slide (Merck Millipore, PEZGS0416) pre-treated with 0.1% gelatin solution for 30 min at 37°C, subsequently cells were fixed with 4% paraformaldehyde (PFA) for 10 min at 4°C (or pre-cool methanol for 10 min at −20°C for anti-MAP1LC3B antibody), permeabilized, and blocked with 0.3% Triton X-100, 3% BSA, 1× PBS for 30 min at room temperature. Antibodies are listed in Table 4. We used ImageJ software to quantify the fluorescence intensity.

Seahorse measurements

The oxygen consumption rate (OCR) and extracellular acidification rate (ECAR) in WT and KO cells were measured

with a Seahorse XF96 Extracellular Flux Analyzer (Agilent). Cells were seeded in XF96 cell culture microplates (Seahorse Bioscience, 101085–004) at 15,000 cells per well in 80 μl of DMEM medium and incubated at 37°C in 5% CO₂ for 24 h. Afterward, DMEM was replaced with 180 μl assay medium containing 11 mM glucose, 2 mM pyruvate and 2 mM glutamine to measure OCR or 2 mM glutamine to measure ECAR with the Seahorse XF Glycolysis Stress Test Kit (Agilent, 103020–100). Cells were incubated at 37°C for 60 min to allow temperature and pH equilibration. For OCR measurement with the Mito Stress Test Kit (Agilent, 103015–100), 2 μM oligomycin, 2 μM carbonyl cyanide-4 (trifluoromethoxy) phenylhydrazone (FCCP) and 0.5 μM rotenone & antimycin included in the kit were added respectively to measure the minimum oxygen consumption, the maximal respiration rate and the non-mitochondrial oxygen consumption. For ECAR measurement, 10 mM glucose, 2 μM oligomycin and 50 mM 2-didesoxy-glucose (2DG) also included in the kit were added respectively to measure glycolysis, glycolytic capacity and non-glycolytic acidification.

ATP measurement

Cellular concentration of intracellular ATP was measured with the BioThema ATP Kit SL (BioThema, 144–041). Cells were seeded in 24-well plates and grown to confluency and were fixed by adding 0.5 ml ethanol. Ethanol was evaporated and cells were subsequently resuspended in 250 μl of Tris-EDTA (pH 7.5) (BioThema, 21–103), frozen, scraped off and transferred to a 1.5 ml reaction tube. After centrifugation (1 min at 13 000 rpm), the lysate was used for ATP measurement in a microplate luminometer (CLARIOstar). To do so, 8 μl of sample was further diluted (1:20) in 152 μl of Tris buffer (BioThema, 21–103), mixed with 40 μl ATP reagent SL and light emission was measured before (I_{smp}) and after ($I_{smp+std}$) adding 10 μl of ATP standard diluted (1:5) in Tris-EDTA buffer. The ATP concentration was determined with the following calculation: $ATP_{smp} = 10^{-7} \times I_{smp}/(I_{smp+std} - I_{smp})$.

C. elegans maintenance and lifespan assays

Nematodes were grown and maintained at 20°C; ambient temperatures during handling (transfer) of worms were between 20 and 25°C. Maintenance was on nematode growth medium (NGM) agar plates spotted with E. coli OP50 as food source, as described elsewhere [46]. Synchronization was performed by washing, followed by centrifugation to separate the eggs from the nematodes. Eggs were transferred to fresh NGM agar plates (Carl Roth, 6494) and allowed to hatch and grow for 64 h. Lifespan assays with C. elegans-specific RNA interference were conducted as previously described [47]. Briefly, young adult worms, 64 h after synchronization, were transferred to NGM agar plates containing 1 mM IPTG (Thermo Fisher, R0392), 100 μg/ml ampicillin (Carl Roth, K029) and, if necessary, 12.5 μg/ml tetracycline (AppliChem, A2228). Plates were spotted with E. coli HT115 (DE3) containing L4440 empty vector (Addgene, 1654) or L4440 containing a f53e2.1, y39h10a.6, t07d1.2 or y54e5a.7 DNA fragment. For the first 10 d, nematodes were transferred to

fresh plates daily; thereafter, they were transferred every other day. Experiments were performed in quintuplicates and two independent times. Worms showing no movement, no reaction to gentle stimulation and no pharyngeal pumping were scored as dead. Worms lost or disintegrated due to internal hatchings were censored.

Proteomics data acquisition

Following cell lysis, samples were spun down at 10,000 g for 10 min at 4°C. Protein concentration was assessed using the Biodrop μLite (Serva, 80-3006-51.01) as per manufacturers instructions (using BSA as standard) and 20 μg of protein from each sample was pipetted into a fresh Protein LoBind microcentrifuge tube (Eppendorf, 0030108116). Samples were further centrifuged at 16 000 g for 10 min at 4°C to remove excess DNA and supernatant removed to a fresh tube. Each sample underwent acetone precipitation to remove salts and residual nucleic acids (briefly with the addition of 6 volumes of ice-cold acetone and left at −20°C overnight, samples spun at 16,000 g for 10 min at 4°C, and carefully remove supernatant, and allowing pellet to air-dry). The pellet was subsequently resuspended in 40 μl of 25 mM ammonium bicarbonate (UCB, 1137). Each sample was reduced and alkylated (10 mM DTT (Neofroxx, 1114) for 30 min at 60°C and 55 mM IAA (Sigma, A3221) for 20 min at room temperature in the dark) before being digested with trypsin (Promega, V511A) at 37°C overnight in an air circulated incubator. Finally, peptides were cleaned and concentrated using Pierce Peptide Desalting spin columns (Thermo Fisher, 89,851) as per manufacturers instructions, dried down in a vacuum concentrator and resuspended in 20 μl of 0.1% formic acid (FA) (Biosolve, 069141). Approximately 1 μg of desalted peptides were separated using the nanoAcquity UPLC system (Waters, 176,016,000) fitted with a trapping (nanoAcquity Symmetry C₁₈, 5μm, 180 μm x 20 mm) and an analytical column (nanoAcquity BEH C₁₈, 1.7μm, 75μm x 250mm). The outlet of the analytical column was coupled directly to an Orbitrap Fusion Lumos (Thermo Fisher Scientific, IQLAAEGAAPFADBMBHQ) using the Proxeon nanospray source. Solvent A was water, 0.1% (v:v) formic acid (Roth, 4724.3) and solvent B was acetonitrile (Biosolve, 0001204102BS), 0.1% (v:v) formic acid. The samples were loaded with a constant flow of solvent A at 5 μL/min onto the trapping column. Trapping time was 6 min. Peptides were eluted via the analytical column with a constant flow of 0.3 μL/min. During the elution step, the percentage of solvent B increased in a linear fashion from 3% to 25% in 30 min, then increased to 32% in 5 more min and finally to 50% in a further 0.1 min. Total runtime was 60 min. The peptides were introduced into the mass spectrometer via a Pico-Tip Emitter 360 μm OD x 20 μm ID; 10 μm tip (New Objective) and a spray voltage of 2.2 kV was applied. The capillary temperature was set at 300°C. The RF lens was set to 30%. Full scan MS spectra with mass range 375–1500 m/z were acquired in profile mode in the Orbitrap with resolution of 120,000 FWHM. The filling time was set at maximum of 50 ms with limitation of 2×10^5 ions. The "Top Speed" method was employed to take the maximum number of precursor ions (with an intensity threshold of 5×10^3) from the full scan MS for fragmentation (using HCD collision energy, 30%) and

quadrupole isolation (1.4 Da window) and measurement in the ion trap, with a cycle time of 3 s. The MIPS (monoisotopic precursor selection) peptide algorithm was employed but with relaxed restrictions when too few precursors meeting the criteria were found. The fragmentation was performed after accumulation of 2×10^3 ions or after filling time of 300 ms for each precursor ion (whichever occurred first). MS/MS data were acquired in centroid mode, with the Rapid scan rate and a fixed first mass of 120 m/z. Only multiply charged ($2^+ - 7^+$) precursor ions were selected for MS/MS. Dynamic exclusion was employed with maximum retention period of 60 s and relative mass window of 10 ppm. Isotopes were excluded. Additionally only 1 data dependent scan was performed per precursor (only the most intense charge state selected). Ions were injected for all available parallelizable time. In order to improve the mass accuracy, a lock mass correction using a background ion (m/z 445.12003) was applied. For data acquisition and processing of the raw data, Xcalibur 4.0 (Thermo Scientific) and Tune version 2.1 were employed.

Proteomics data analysis

Raw data were searched using the Andromeda search engine [48] build into MaxQuant (version 1.5.3.28) [49]. The data were searched against the mouse Uniprot database (Swissprot entry only, release 2016_01) together with a list of common contaminants appended. The data were searched with the following modifications: Carbamidomethyl (C) (fixed) and Oxidation (M) and Acetyl (Protein N-term) (variable). The mass error tolerance for the full scan MS spectra was set at 20 ppm and for the MS/MS spectra at 0.5 Da. The reversed sequences of the target database were used as decoy database. Peptide and protein hits were filtered at a false discovery rate of 1% using a target-decoy strategy [50]. Additionally, only proteins identified by at least 2 unique peptides were retained.

Differential protein expression analysis was performed as described in [51]. Briefly, the LFQ intensity values per protein (from the proteinGroups.txt output of MaxQuant) were used for quantitative analysis. The R package MSnbase [52] was used to process proteomics data and perform data imputation using imputeLCMD. Missing values were imputed using a mixed strategy based on the definition of Missing At Random (MAR) and Missing Not At Random (MNAR) values. MNAR were defined for each pairwise comparison as values that were (i) missing in 3 out of 3, or 2 out of 3 biological replicates in one sample group, and (ii) present in all the 3 biological replicates in the second sample group. Because of their nonrandom distribution across samples, these values were considered as underlying biological difference between sample groups. MNAR values were computed using the method "MinDet" by replacing values with minimal values observed in the sample. MAR were consequently defined for each pairwise comparison as values that were missing in 1 out of 3 biological replicates per sample group. MAR values were imputed based on the method "knn" (k-nearest neighbors) [52]. All the other cases (e.g., protein groups that had less than 2 values in both sample groups) were filtered out because of the lack of sufficient information to perform robust statistical analysis. Data were quantile normalized to reduce technical variations. Differential protein abundance was evaluated using the limma package [53]. The mass spectrometry proteomics data have been deposited to the ProteomeXchange Consortium via the PRIDE [54] partner repository with the dataset identifier PXD015170.

Metabolomics analysis

Targeted quantitative analysis was performed as described in manual E-170,602 supplied by "Human Metabolome Technologies (HMG)". Briefly, 5 million cells per sample were washed with 10 mL of 5% mannitol solution in triplicates. Thereafter metabolites were extracted with 800 μL methanol and 550 μL of internal standard supplied by HMG. To remove macromolecules, cell extracts were subjected to an ultrafiltration step using centrifugal filter units supplied by HMG. Metabolites were measured and quantified using capillary electrophoresis mass spectrometry (CE-TOFMS and CE-QqQMS). Details of the setup are provided upon request.

Statistical analysis

Statistic values were calculated using t-test analysis with the GraphPad Prism 5 software as described. Data include values from at least three replicate experiments. For *C. elegans* lifespan analyzes, statistical calculations were performed using JMP software version 9.0 (SAS Institute Inc.), applying the log-rank test.

Disclosure statement

No potential conflict of interest was reported by the authors.

ORCID

Alessandro Ori http://orcid.org/0000-0002-3046-0871
Peter Walentek http://orcid.org/0000-0002-2332-6068

References

[1] Hardie DG, Ross FA, Hawley SA. AMPK: a nutrient and energy sensor that maintains energy homeostasis. Nat Rev Mol Cell Biol. 2012;13(4):251–262. [Cited 2012 March 23]. PubMed PMID: 22436748.

[2] Jansen M, Ten Klooster JP, Offerhaus GJ, et al. LKB1 and AMPK family signaling: the intimate link between cell polarity and energy metabolism. Physiol Rev. 2009;89(3):777–798. [Cited 2009 July 09]. PubMed PMID: 19584313.

[3] Pickart CM, Eddins MJ. Ubiquitin: structures, functions, mechanisms. Biochim Biophys Acta. 2004;1695(1–3):55–72. [Cited 2004 December 02]. PubMed PMID: 15571809.

[4] Sadowski M, Suryadinata R, Tan AR, et al. Protein monoubiquitination and polyubiquitination generate structural diversity to control distinct biological processes. IUBMB Life. 2012;64 (2):136–142. [Cited 2011 December 02]. PubMed PMID: 22131221.

[5] Hämmerle M, Bauer J, Rose M, et al. Proteins of newly isolated mutants and the amino-terminal proline are essential for ubiquitin-proteasome-catalyzed catabolite degradation of fructose-1,6-bisphosphatase of Saccharomyces cerevisiae. J Biol Chem. 1998;273(39):25000–25005. [Cited 1998 September 17]. PubMed PMID: 9737955.

[6] Chen SJ, Wu X, Wadas B, et al. An N-end rule pathway that recognizes proline and destroys gluconeogenic enzymes. Science. 2017;355(6323):eaal3655. PubMed PMID: 28126757.

[7] Francis O, Han F, Adams JC. Molecular phylogeny of a RING E3 ubiquitin ligase, conserved in eukaryotic cells and dominated by homologous components, the muskelin/RanBPM/CTLH complex. PLoS One. 2013;8(10):e75217. PubMed PMID: 24143168; PubMed Central PMCID: PMCPMC3797097.

[8] Santt O, Pfirrmann T, Braun B, et al. The yeast GID complex, a novel ubiquitin ligase (E3) involved in the regulation of carbohydrate metabolism. Mol Biol Cell. 2008;19(8):3323–3333. [Cited 2008 May 30]. PubMed PMID: 18508925; PubMed Central PMCID: PMC2488282.

[9] Liu H, Pfirrmann T. The Gid-complex: an emerging player in the ubiquitin ligase league. Biol Chem. 2019. [Cited 2019 March 21]. PubMed PMID: 30893051. DOI:10.1515/hsz-2019-0139

[10] Texier Y, Toedt G, Gorza M, et al. Elution profile analysis of SDS-induced subcomplexes by quantitative mass spectrometry. Mol Cell Proteomics. 2014;13(5):1382–1391. PubMed PMID: 24563533; PubMed Central PMCID: PMC4014293.

[11] Pfirrmann T, Villavicencio-Lorini P, Subudhi AK, et al. RMND5 from xenopus laevis is an E3 ubiquitin-ligase and functions in early embryonic forebrain development. PLoS One. 2015;10(3): e0120342. [Cited 2015 March 21]. PubMed PMID: 25793641; PubMed Central PMCID: PMC4368662.

[12] Lampert F, Stafa D, Goga A, et al. The multi-subunit GID/CTLH E3 ubiquitin ligase promotes cell proliferation and targets the transcription factor Hbp1 for degradation. Elife. 2018;7. [Cited 2018 June 19]. PubMed PMID: 29911972; PubMed Central PMCID: PMCPMC6037477. DOI:10.7554/eLife.35528

[13] Leal-Esteban LC, Rothe B, Fortier S, et al. Role of bicaudal C1 in renal gluconeogenesis and its novel interaction with the CTLH complex. PLoS Genet. 2018;14(7):e1007487. [Cited 2018 July 12]. PubMed PMID: 29995892; PubMed Central PMCID: PMCPMC6056059.

[14] Snowdon C, Hlynialuk C, van der Merwe G. Components of the Vid30c are needed for the rapamycin-induced degradation of the high-affinity hexose transporter Hxt7p in saccharomyces cerevisiae. FEMS Yeast Res. 2008;8(2):204–216. [Cited 2007 November 08]. PubMed PMID: 17986252.

[15] Klionsky DJ, Abdelmohsen K, Abe A, Abedin MJ, Abeliovich H, Acevedo Arozena A, et al. Guidelines for the use and interpretation of assays for monitoring autophagy (3rd edition). Autophagy. 2016;12(1):1–222. Epub 2016/01/23. doi:10.1080/155486 27.2015.1100356. PubMed PMID: 26799652; PubMed Central PMCID: PMCPMC4835977

[16] Betz C, Hall MN. Where is mTOR and what is it doing there? J Cell Biol. 2013;203(4):563–574. [Cited 2014 January 05]. PubMed PMID: 24385483; PubMed Central PMCID: PMCPMC3840941.

[17] Hardie DG, Corton J, Ching YP, et al. Regulation of lipid metabolism by the AMP-activated protein kinase. Biochem Soc Trans. 1997;25(4):1229–1231. [Cited 1998 February 05]. PubMed PMID: 9449981.

[18] Zhang CS, Hawley SA, Zong Y, et al. Fructose-1,6-bisphosphate and aldolase mediate glucose sensing by AMPK. Nature. 2017;548 (7665):112–116. [Cited 2017 July 21]. PubMed PMID: 28723898; PubMed Central PMCID: PMCPMC5544942. DOI

[19] Pampliega O, Cuervo AM, Autophagy and primary cilia: dual interplay. Curr Opin Cell Biol. 2016;39:1–7. [Cited 2016 January 31]. PubMed PMID: 26826446; PubMed Central PMCID: PMCPMC4733852.

[20] Pampliega O, Orhon I, Patel B, et al. Functional interaction between autophagy and ciliogenesis. Nature. 2013;502 (7470):194–200. [Cited 2013 October 04]. PubMed PMID: 24089209; PubMed Central PMCID: PMCPMC3896125. DOI

[21] Tang Z, Lin MG, Stowe TR, et al. Autophagy promotes primary ciliogenesis by removing OFD1 from centriolar satellites. Nature. 2013;502(7470):254–257. [Cited 2013 October 04]. PubMed PMID: 24089205; PubMed Central PMCID: PMCPMC4075283.

[22] Sherpa RT, Atkinson KF, Ferreira VP, et al. Rapamycin increases length and mechanosensory function of primary cilia in renal epithelial and vascular endothelial cells. Int Educ Res J. 2016;2 (12):91–97. [Cited 2017 May 23]. PubMed PMID: 28529994; PubMed Central PMCID: PMCPMC5436805.

[23] Thoreen CC, Kang SA, Chang JW, et al. An ATP-competitive mammalian target of rapamycin inhibitor reveals rapamycin-resistant functions of mTORC1. J Biol Chem. 2009;284(12):8023–8032. [Cited 2009 January 20]. PubMed PMID: 19150980; PubMed Central PMCID: PMCPMC2658096.

[24] Corton JM, Gillespie JG, Hawley SA, et al. 5-aminoimidazole-4-carboxamide ribonucleoside. A specific method for activating AMP-activated protein kinase in intact cells? Eur J Biochem. 1995;229(2):558–565. [Cited 1995 April 15]. PubMed PMID: 7744080.

[25] Gonzalez A, Hall MN. Nutrient sensing and TOR signaling in yeast and mammals. Embo J. 2017;36(4):397–408. [Cited 2017 January 18]. PubMed PMID: 28096180.

[26] Uno M, Nishida E, Lifespan-regulating genes in C. elegans. NPJ Aging Mech Dis. 2016;2:16010. [Cited 2017 July 20]. PubMed PMID: 28721266; PubMed Central PMCID: PMCPMC5514992.

[27] Lochhead PA, Salt IP, Walker KS, et al. 5-aminoimidazole-4-carboxamide riboside mimics the effects of insulin on the expression of the 2 key gluconeogenic genes PEPCK and glucose-6-phosphatase. Diabetes. 2000;49(6):896–903. [Cited 2000 June 24]. PubMed PMID: 10866040.

[28] Menssen R, Schweiggert J, Schreiner J, et al. Exploring the topology of the gid complex, the E3 ubiquitin ligase involved in catabolite-induced degradation of gluconeogenic enzymes. J Biol Chem. 2012;287(30):25602–25614. [Cited 2012 May 31]. PubMed PMID: 22645139; PubMed Central PMCID: PMC3408164.

[29] Deng M, Yang X, Qin B, et al. Deubiquitination and Activation of AMPK by USP10. Mol Cell. 2016;61(4):614–624. [Cited 2016 February 16]. PubMed PMID: 26876938; PubMed Central PMCID: PMCPMC4836875.

[30] Al-Hakim AK, Zagorska A, Chapman L, et al. Control of AMPK-related kinases by USP9X and atypical Lys(29)/Lys (33)-linked polyubiquitin chains. Biochem J. 2008;411 (2):249–260. [Cited 2008 February 08]. PubMed PMID: 18254724.

[31] Pineda CT, Ramanathan S, Fon Tacer K, et al. Degradation of AMPK by a cancer-specific ubiquitin ligase. Cell. 2015;160 (4):715–728. [Cited 2015 February 14]. PubMed PMID: 25679763.

[32] Coughlan KA, Balon TW, Valentine RJ, et al. Nutrient excess and AMPK downregulation in incubated skeletal muscle and muscle of glucose infused rats. PLoS One. 2015;10(5):e0127388. [Cited 2015 May 23]. PubMed PMID: 25996822; PubMed Central PMCID: PMCPMC4440828.

[33] Yu L, McPhee CK, Zheng L, et al. Termination of autophagy and reformation of lysosomes regulated by mTOR. Nature. 2010;465 (7300):942–946. [Cited 2010 June 08]. PubMed PMID: 20526321; PubMed Central PMCID: PMCPMC2920749.

[34] Mihaylova MM, Shaw RJ. The AMPK signalling pathway coordinates cell growth, autophagy and metabolism. Nat Cell Biol. 2011;13(9):1016–1023. [Cited 2011 September 06]. PubMed PMID: 21892142; PubMed Central PMCID: PMCPMC3249400.

[35] Greer EL, Dowlatshahi D, Banko MR, et al. An AMPK-FOXO pathway mediates longevity induced by a novel method of dietary restriction in C. elegans. Curr Biol. 2007;17(19):1646–1656. [Cited 2007 September 29]. PubMed PMID: 17900900; PubMed Central PMCID: PMCPMC2185793.

[36] Ehninger D, Neff F, Xie K. Longevity, aging and rapamycin. Cell Mol Life Sci. 2014;71(22):4325–4346. [Cited 2014 July 13]. PubMed PMID: 25015322; PubMed Central PMCID: PMCPMC4207939.

[37] Bitto A, Ito TK, Pineda VV, et al. Transient rapamycin treatment can increase lifespan and healthspan in middle-aged mice. Elife. 2016;5. [Cited 2016 August 24]. PubMed PMID: 27549339; PubMed Central PMCID: PMCPMC4996648. DOI:10.7554/eLife.16351

[38] Huang X, Dixit VM. Drugging the undruggables: exploring the ubiquitin system for drug development. Cell Res. 2016;26 (4):484–498. [Cited 2016 March 24]. PubMed PMID: 27002218; PubMed Central PMCID: PMCPMC4822129.

[39] Fantus D, Rogers NM, Grahammer F, et al., Roles of mTOR complexes in the kidney: implications for renal disease and transplantation. Nat Rev Nephrol. 2016;12(10):587–609. [Cited 2016 August 02]. PubMed PMID: 27477490.

[40] Coughlan KA, Valentine RJ, Ruderman NB, et al., AMPK activation: a therapeutic target for type 2 diabetes? Diabetes Metab Syndr Obes. 2014;7:241–253. [Cited 2014 July 16]. PubMed PMID: 25018645; PubMed Central PMCID: PMCPMC4075959.

[41] Zhou G, Myers R, Li Y, et al. Role of AMP-activated protein kinase in mechanism of metformin action. J Clin Invest. 2001;108(8):1167–1174. [Cited 2001 October 17]. PubMed PMID: 11602624; PubMed Central PMCID: PMCPMC209533.

[42] Johnson SC, Rabinovitch PS, Kaeberlein M. mTOR is a key modulator of ageing and age-related disease. Nature. 2013;493 (7432):338–345. [Cited 2013 January 18]. PubMed PMID: 23325216; PubMed Central PMCID: PMCPMC3687363.

[43] Fraser AG, Kamath RS, Zipperlen P, et al. Functional genomic analysis of C. elegans chromosome I by systematic RNA interference. Nature. 2000;408(6810):325–330. [Cited 2000 December 01]. PubMed PMID: 11099033.

[44] Rual JF, Ceron J, Koreth J, et al. Toward improving caenorhabditis elegans phenome mapping with an ORFeome-based RNAi library. Genome Res. 2004;14(10B):2162–2168. [Cited 2004 October 19]. PubMed PMID: 15489339; PubMed Central PMCID: PMCPMC528933.

[45] Pfirrmann T, Lokapally A, Andreasson C, et al. SOMA: a single oligonucleotide mutagenesis and cloning approach. PLoS One. 2013;8(6):e64870. PubMed PMID: 23750217; PubMed Central PMCID: PMC3672168.

[46] Brenner S. The genetics of caenorhabditis elegans. Genetics. 1974;77(1):71–94. [Cited 1974 May 01]. PubMed PMID: 4366476; PubMed Central PMCID: PMCPMC1213120.

[47] Urban N, Tsitsipatis D, Hausig F, et al. Non-linear impact of glutathione depletion on C. elegans life span and stress resistance. Redox Biol. 2017;11:502–515. [Cited 2017 January 14]. PubMed PMID: 28086197; PubMed Central PMCID: PMCPMC5228094.

[48] Cox J, Neuhauser N, Michalski A, et al. Andromeda: a peptide search engine integrated into the MaxQuant environment. J Proteome Res. 2011;10(4):1794–1805. [Cited 2011 January 25]. PubMed PMID: 21254760.

[49] Cox J, Mann M. MaxQuant enables high peptide identification rates, individualized p.p.b.-range mass accuracies and proteome-wide protein quantification. Nat Biotechnol. 2008;26(12):1367–1372. [Cited 2008 November 26]. PubMed PMID: 19029910.

[50] Elias JE, Gygi SP. Target-decoy search strategy for increased confidence in large-scale protein identifications by mass spectrometry. Nat Methods. 2007;4(3):207–214. [Cited 2007 March 01]. PubMed PMID: 17327847.

[51] Mackmull MT, Klaus B, Heinze I, et al. Landscape of nuclear transport receptor cargo specificity. Mol Syst Biol. 2017;13 (12):962. [Cited 2017 December 20]. PubMed PMID: 29254951; PubMed Central PMCID: PMCPMC5740495.

[52] Gatto L, Lilley KS. MSnbase-an R/Bioconductor package for isobaric tagged mass spectrometry data visualization, processing and quantitation. Bioinformatics. 2012;28(2):288–289. [Cited 2011 November 25]. PubMed PMID: 22113085.

[53] Ritchie ME, Phipson B, Wu D, et al. limma powers differential expression analyses for RNA-sequencing and microarray studies. Nucleic Acids Res. 2015;43(7):e47. [Cited 2015 January 22]. PubMed PMID: 25605792; PubMed Central PMCID: PMCPMC4402510. DOI

[54] Perez-Riverol Y, Csordas A, Bai J, et al. The PRIDE database and related tools and resources in 2019: improving support for quantification data. Nucleic Acids Res. 2019;47(D1):D442–D50. [Cited 2018 November 06]. PubMed PMID: 30395289; PubMed Central PMCID: PMCPMC6323896.